# Synthesis and Characterization of Silk-Inspired Thermoplastic Polyurethane Elastomers

by

**Gregory Stewart Pollock**

Bachelor of Science, Chemical Engineering
The University of Texas at Austin, Austin, TX, December 1998

SUBMITTED TO THE DEPARTMENT OF CHEMICAL ENGINEERING IN PARTIAL FULFILLMENT OF THE REQUIREMENTS FOR THE DEGREE OF

DOCTOR OF PHILOSOPHY

AT THE

MASSACHUSETTS INSTITUTE OF TECHNOLOGY

SEPTEMBER 2005

© 2005 Massachusetts Institute of Technology. All rights reserved.

Signature of Author: _____
Department of Chemical Engineering / Program in Polymer Science and Technology
July 8, 2005

Certified by: _____
Paula T. Hammond
Thesis Advisor

Certified by: _____
Gareth H. McKinley
Co-Thesis Advisor, Mechanical Engineering

Accepted by: _____
Daniel Blankschtein
Professor of Chemical Engineering
Chairman, Committee for Graduate Students

MASSACHUSETTS INSTITUTE OF TECHNOLOGY
SEP 12 2005
LIBRARIES

ARCHIVES

# Synthesis and Characterization of Silk-Inspired Thermoplastic Polyurethane Elastomers

by
Gregory Stewart Pollock

Submitted to the Department of Chemical Engineering on July 8, 2005 in Partial Fulfillment of the Requirements for the Degree of Doctor of Philosophy in Chemical Engineering

## ABSTRACT

Segmented polyurethane elastomers containing additional ordered structures within the hard or soft domains were developed to mimic the hierarchical structure and superior properties observed in spider silk fibers. The silk's toughness is related to a fiber morphology that includes β-pleated crystalline sheets within an amorphous matrix, as well as an additional interphase with an orientation and mobility between that of the two microphases. In the polyurethane mimics, bulky aromatic diisocyanates were incorporated between aliphatic hexamethylene diisocyanate (HDI) hard segments and poly(tetramethylene oxide) (PTMO) soft segments, to enhance the size and orientation of the interphase. The mixture of diisocyanates reduces the crystallinity of the HDI hard segments, allowing the polyurethane to form more well-organized domains observed by AFM imaging. The more interconnected hard domains allow the elastomers to deform to higher elongations and absorb more energy without a decrease of initial modulus.

Shearing of the hydrogen-bonded hard domains orients the hard blocks at a preferred tilt angle of ±20° from the strain direction during tensile deformation. While the average spacing of hard domains increases during deformation, the spacing of hard domains aligned with the strain decreases, and the spacing of hard domains at the preferred tilt angle remains constant. Strain-induced crystallization of the PTMO soft segments was observed in all samples; however, hard segments with mixed diisocyanates exhibited non-crystalline alignment of the hard domains.

Several polyurethane nanocomposite structures were also created using particles that preferentially associate with hard or soft segments. HDI-PTMO polyurethane/Laponite nanocomposites provided modest mechanical property improvements (80% increase in modulus and 15% increase in toughness) without any loss of extensibility. The Laponite discs exhibited an exfoliated structure, associating with and reinforcing the hydrophilic polyurethane hard segments. HDI-PTMO polyurethane/MQ siloxane resin nanocomposites also exhibited particle association with the hard segments, providing a 60% increase in modulus with a small loss of toughness. However, composites of isobutyl-POSS dispersed in polyurethanes with mixed hard segments exhibited formation of POSS crystals associated with the soft segments at all loadings, resulting in tensile failure at strains 80-100% lower than the pure polyurethane.

Thesis Supervisor: Paula T. Hammond
Title: Mark Hyman, Jr. Associate Professor of Chemical Engineering

# Acknowledgements

*Soli Deo Gloria*

I would first like to thank my research advisor, Paula Hammond, for all her inspiration, guidance, patience, and support—even in areas unrelated to my research, but no less important to me. I also want to thank my thesis committee members, Gareth McKinley, Ned Thomas, and Ken Beers, for their invaluable insights and encouragement during this long process. Paula and Gareth also deserve my sincere thanks for creating a unique research project with so much room for growth and collaboration, and inviting me to be a part of it.

I have been blessed with many talented collaborators, who have contributed to this thesis and my own growth as a researcher: LaShanda James-Korley and Ryan Waletzko in the Hammond group; Shawna Liff, Nitin Kumar and Nikola Kojic in the McKinley group; Brian Pate and Rachel Pytel in the Thomas group; and Randy Hill from Dow Corning. Many thanks go to all the members of the Hammond research group, past and present, for their expertise and friendship. I specifically want to thank my undergrad researchers, Man Sze Ko, Hanhan Wang and Gul Gurkan for their contributions in the lab, and my predecessors in the Hammond group, Mark Johnson, Bindu Nair, Mitch Anthamatten and Cathy Santini, who taught me so much about synthesis, TEM, SAXS, and block copolymers. This thesis would also not be possible without the tremendous research facilities at the Institute for Soldier Nanotechnologies (ISN) and the Center for Materials Science and Engineering, as well as generous funding from the NSF, NASA, and the ISN.

While in graduate school, my life has been enriched by knowing so many wonderful people and being a part of some exciting groups. Joe, Jon, Colin, Cynthia, Ed and all my friends in the Graduate Christian Fellowship helped me grow in my faith amidst the trials of research. Martin, Nathan, Jason, Tim, Sara and the rest of the Thirsty Ear staff made my time as manager such a rewarding experience. Pete, Welkin, Heather and the rest of the Musical Theatre Guild nurtured my love for the stage and kept my right brain satisfied. All my friends on the Boston Poker Tour (too many to name, and I don't think they want the notoriety) helped me keep my sanity the last few years, while unwittingly teaching me a little about statistics and psychology. And life would not have been the same without Lori, Erika, and Andy, and all our random adventures together.

Finally and most importantly, this thesis would not have been possible without the love and support of my family and closest friends. My parents, Bruce and Robin Pollock, and my sister and brother-in-law, Jennifer and Daniel Dugan, have always been there for me and believed I could do this. Dan and Filicia Davenport never seemed that far away, and were always ready with a word of encouragement or advice when I needed it. Lastly, I want to especially thank Emily Braunstein, who gave me so much support and affection over the last three years; whenever I fell down, she was always there to pick me back up.

# Table of Contents

List of Figures ..... 7
List of Tables ..... 11
**Chapter 1: Introduction ..... 12**
1.1 Project Goal and Outline ..... 12
1.2 Background ..... 13
1.2.1 Spider Silk Structure and Properties ..... 13
1.2.2 Segmented Polyurethane Elastomers ..... 19
1.2.3 Interphases in Semicrystalline Polymers ..... 23
1.2.4 Polyurethane Nanocomposites ..... 24
1.2.5 Liquid Crystalline Polyurethanes ..... 25
1.3 Conclusions ..... 27
1.4 References ..... 28
**Chapter 2: Materials Design ..... 33**
2.1 Introduction ..... 33
2.2 Polyurethane Blocks ..... 34
2.2.1 Soft Segments ..... 34
2.2.2 Hard Segments ..... 35
2.3 Reinforcing Units ..... 38
2.3.1 Layered Silicate Clays ..... 38
2.3.2 Siloxane Cages ..... 39
2.3.3 Liquid Crystalline Soft Segments ..... 42
2.3 Conclusions ..... 43
2.4 References ..... 44
**Chapter 3: Segmented Polyurethanes with Mixed Hard Segments ..... 49**
3.1 Introduction ..... 49
3.2 Experimental ..... 51
3.2.1 Materials ..... 51
3.2.2 Polyurethane Synthesis ..... 51
3.2.3 Polyurethane Film Casting ..... 52
3.2.4 Instrumentation ..... 53

3.3 Polyurethane Characterization ..... 55
3.3.1 Microphase Separation ..... 56
3.3.2 Polyurethane Morphology ..... 62
3.3.3 Mechanical Behavior ..... 69
3.3.4 Effect of Isocyanate Addition Method ..... 72
3.3.5 Annealing Effects on Microphase Separation ..... 74
3.4 Conclusions ..... 75
3.5 References ..... 76
**Chapter 4: Morphology of Segmented Polyurethanes with Mixed Hard Segments under Deformation ..... 78**
4.1 Introduction ..... 78
4.2 Experimental ..... 83
4.2.1 Instrumentation ..... 84
4.2.2 Scattering Analysis ..... 85
4.3 Results and Discussion ..... 86
4.3.1 In-Situ SAXS ..... 86
4.3.2 In-Situ WAXS ..... 91
4.3.3 In-Situ Polarized Optical Microcopy ..... 97
4.4 Conclusions ..... 100
4.5 References ..... 101
**Chapter 5: Polyurethane/Clay Nanocomposites ..... 103**
5.1 Introduction ..... 103
5.2 Experimental ..... 105
5.2.1 Materials ..... 105
5.2.2 Solvent-Exchange Method and Film Casting ..... 106
5.2.3 Instrumentation ..... 107
5.3 Mechanical Behavior ..... 108
5.4 Morphological Behavior ..... 112
5.6 Conclusions ..... 117
5.7 References ..... 117
**Chapter 6: Polyurethane/Siloxane Nanocomposites ..... 118**

6.1 Introduction ..... 118
6.2 Experimental ..... 120
6.2.1 Materials ..... 120
6.2.2 Siloxane Resin Dispersion ..... 120
6.2.3 Instrumentation ..... 121
6.3 Results and Discussion ..... 122
6.3.1 Mechanical Characterization ..... 122
6.3.2 Siloxane Phase Association ..... 128
6.4 Conclusions ..... 131
6.5 References ..... 131
**Chapter 7: Liquid Crystalline Polyurethane Soft Segments ..... 133**
7.1 Introduction ..... 133
7.2 Experimental ..... 134
7.2.1 Materials ..... 135
7.2.2 Biphenyl-PTMO Copolyether Synthesis ..... 135
7.2.3 Biphenyl-PTMO Copolyester Synthesis ..... 136
7.2.4 Segmented Polyurethane Synthesis ..... 137
7.2.5 Instrumentation ..... 138
7.3 Results and Discussion ..... 140
7.3.1 Biphenyl-PTMO Copolyether Soft Segments ..... 140
7.3.2 Biphenyl-PTMO Copolyester Soft Segments ..... 142
7.4 Conclusions ..... 147
7.5 References ..... 148
**Chapter 8: Conclusions and Future Directions ..... 150**
8.1 Summary ..... 150
8.2 Future Directions ..... 152
8.2.1 Polyurethanes with Mixed Hard Segments ..... 152
8.2.2 Polyurethane Nanocomposites ..... 153
8.3 References ..... 155

# List of Figures

Figure 1.1 Amino acid sequence of spider dragline silk protein[2] ..... 15
Figure 1.2 Modeling of spider silk properties on a lattice[11] ..... 17
Figure 1.3 Proposed morphological model of spider silk[3] ..... 19
Figure 1.4 Molecular architecture of segmented polyurethane elastomers ..... 21
Figure 1.5 Cartoon representation of side-chain and main-chain liquid crystalline polymers. ..... 26
Figure 2.1 Two-step solution polymerization of segmented polyurethanes ..... 34
Figure 2.2 Synthesis of polyurethanes with mixed diisocyanates in the hard segments. The macrodiol is first endcapped with the aromatic diisocyanate, then chain extended with an aliphatic diisocyanate and diol. ..... 37
Figure 2.3 Schematic illustration of undispersed Laponite discs.[29] ..... 39
Figure 2.4 Structure of polyhedral oligomeric silsesquioxane (POSS) cages[36] ..... 41
Figure 2.5 Cartoon representation of POSS reinforcement within polyurethane soft segment matrix ..... 41
Figure 2.6 Cartoon representation of main-chain liquid crystalline (LC) mesogens as reinforcing units within the polyurethane soft segment. ..... 43
Figure 3.1 Synthesis of polyurethanes with mixed hard segments. ..... 52
Figure 3.2 DSC traces of polyurethanes with (A) PTMO-2000 soft segments and (B) PTMO-2900 soft segments. The presence of mixed isocyanates in the HT-series and HM-series depresses the hard segment melting point and enthalpy, relative to the H-series. ..... 57
Figure 3.3 DMA Elastic Modulus curves of polyurethanes with (A) PTMO-2000 soft segments and (B) PTMO-2900 soft segments. ..... 60
Figure 3.4 DMA tan(δ) curves of polyurethanes with (A) PTMO-2000 soft segments and (B) PTMO-2900 soft segments. ..... 61
Figure 3.5 WAXS patterns of polyurethanes with mixed hard segments show suppression of the peaks from HDI-BDO crystallites. ..... 63
Figure 3.6 SAXS profiles of polyurethanes with (A) PTMO-2000 soft segments and (B) PTMO-2900 soft segments. ..... 65

Figure 3.7 Tapping-mode AFM phase images of PTMO-2900 based polyurethane films: (A) H-29, (B) HT-29, and (C) HM-29 ..... 67
Figure 3.8 Tapping-mode AFM phase images of PTMO-2000 based polyurethane films: (D) H-20 and (E) HT-20 ..... 68
Figure 3.9 Stress-Strain Behavior of polyurethanes with (A) PTMO-2000 soft segments and (B) PTMO-2900 soft segments. ..... 70
Figure 3.10 DSC comparison of diisocyanate addition methods. Diisocyanates added in one step form hard domains with a lower melting point and melting enthalpy..... 73
Figure 3.11 Tensile comparison of HM-29 polyurethanes synthesized using a one-step or two-step isocyanate addition. ..... 74
Figure 4.1 Model of deformation behavior of a polyurethane with paracrystalline hard segments[1] ..... 79
Figure 4.2 Polyurethane deformation mechanisms based on hard segment rigidity and aspect ratio[4] ..... 81
Figure 4.3 Schematic model for the deformation of MDI-BDO hard domains at intermediate and high strains based upon initial orientation[7] ..... 83
Figure 4.4 Cartoon relationship between hard domain orientations and their corresponding scattering patterns ..... 87
Figure 4.5 Two-dimensional SAXS patterns of H-29 as a function of strain ..... 89
Figure 4.6 Azimuthal plots of H-29 at the average interdomain spacing (17 nm) as a function of strain ..... 90
Figure 4.7 Average interdomain spacing of H-29 integrated in several directions as a function of strain ..... 90
Figure 4.8 Tensile deformation leads to an increase in the isotropic interdomain spacing, while the shearing of hard domains reduces the interdomain spacing along the equator and at ±20°. ..... 91
Figure 4.9 Two-dimensional WAXS patterns of H-29 as a function of strain ..... 93
Figure 4.10 One-dimensional WAXS patterns of H-29 integrated along four directions: (i) all directions (isotropically), (ii) the equator, (iii) the meridian, and (iv) 20° from the meridian ..... 95

Figure 4.11 Azimuthal WAXS plots of H-29 at peak positions A, B, and C indicated in Fig. 4.10 (4.4 Å, 4.1 Å, and 3.7 Å) ..... 96
Figure 4.12 Cartoon summary of the hard segment orientation behavior for H-29 at high strain observed by 2-D WAXS. ..... 97
Figure 4.13 Optical micrographs of H-29 under crossed polarizers as a function of strain ..... 98
Figure 4.14 Optical micrographs of HT-29 under crossed polarizers as a function of strain ..... 99
Figure 4.15 Optical micrographs of HM-29 under crossed polarizers as a function of strain ..... 100
Figure 5.1 Polymer-clay nanocomposite morphologies ..... 104
Figure 5.2 Comparison of the stress-strain behavior of H-20 with and without 10% Laponite loaded ..... 110
Figure 5.3 Dynamic mechanical behavior of H-20 segmented polyurethane with and without 10% Laponite loaded ..... 111
Figure 5.4 TEM images of 10 wt% Laponite/H-20 nanocomposites showing clay exfoliation with some intercalated structure ..... 113
Figure 5.5 WAXD patterns of H-20 polyurethane with and without 10 wt% Laponite loaded. (Laponite and HDI-BDO are included for comparison.) ..... 114
Figure 5.6 DSC traces of H-20 segmented polyurethane with and without 10 wt% Laponite loaded, showing particle association with hard segments ..... 116
Figure 6.1 Segmented polyurethane/POSS nanocomposite structure ..... 119
Figure 6.2 Comparison of the stress-strain behavior of H-20 various with various loadings of MQ-resin ..... 123
Figure 6.3 Comparison of the stress-strain behavior of HT-20 with 3% loadings of MQ-resin and isooctyl-POSS ..... 125
Figure 6.4 Comparison of the stress-strain behavior of HT-20 with various loadings of isobutyl-POSS, cast from THF/DMAc (80%/20%) ..... 127
Figure 6.5 DSC traces of H-29 segmented polyurethane with various loadings of MQ-resin, indicating depression of hard segment crystallization ..... 129

Figure 7.1 Cartoon representation of main-chain liquid crystalline (LC) mesogens as reinforcing units within the polyurethane soft segment..... 133
Figure 7.2 Synthesis of biphenyl-PTMO co-polyether oligomer for use as liquid crystalline polyurethane soft segment..... 136
Figure 7.3 Synthesis of biphenyl-PTMO co-polyester oligomer for use as liquid crystalline polyurethane soft segment..... 137
Figure 7.4 Synthesis of segmented polyurethane with biphenyl-PTMO copolymer soft segment. ..... 138
Figure 7.5 DSC Comparison of a biphenyl-PTMO-250 polyether soft segment to a HDI-polyurethane made with the BP-PTMO soft segment (PU-BP-PTMO) and a HDI-polyurethane made with a pure PTMO-2900 soft segment. ..... 142
Figure 7.6 DSC Comparison of (A) PTMO-650 macrodiol, (B) Biphenyl-PTMO-650 polyester soft segment, and (C) HDI-polyurethane made with the BP-PTMO soft segment. ..... 144
Figure 7.7 DSC Comparison of (A) PTMO-1000 macrodiol, (B) Biphenyl-PTMO-1000 polyester soft segment, and (C) HDI-polyurethane made with the biphenyl-PTMO soft segment. ..... 145
Figure 7.8 DSC Comparison of (A) Polyurethane made with the biphenyl-PTMO soft segment to (B) polyurethane with pure PTMO-2900 soft segment..... 146
Figure 7.9 DMA Comparison of (A) Polyurethane made with the biphenyl-PTMO soft segment to (B) polyurethane with pure PTMO-2900 soft segment..... 147
Figure 8.1 Cartoon representation of covalently linked-POSS cages within a polyurethane soft segment ..... 154

# List of Tables

Table 1.1 Property comparison of silk to other engineering materials[2] ..... 14
Table 3.1 Summary of polyurethane compositions and molecular weights ..... 56
Table 3.2 Summary of DSC and DMA Results—Glass Transition ($T_{g,SS}$), Melting Point ($T_{m,SS}$), and Heat of Melting ($H_{m,SS}$) of Soft Segments, Temperature of Dissociation ($T_{d,HS}$) and Heat of Dissociation ($H_{d,HS}$) of Hard Segments ($1^{st}$ heating after film casting) ..... 58
Table 3.3 Average interdomain spacings of segmented polyurethanes, obtained from SAXS ..... 64
Table 3.4 Summary of mechanical properties of polyurethane films ..... 71
Table 3.5 Hysteresis of polyurethane films stretched to 100% and 300% strain under cyclic loading conditions ..... 72
Table 3.6 Comparison of annealing conditions on selected polyurethane properties..... 75
Table 5.1 Tensile properties of H-20 with and without 10 wt% Laponite loaded..... 110
Table 6.1 Compositions and molecular weights of selected polyurethanes ..... 120
Table 6.2 Tensile properties of H-20 with various loadings of MQ-resin..... 124
Table 6.3 Tensile properties of HT-20 with 3% loadings of MQ-resin and isooctyl-POSS ..... 125
Table 6.4 Tensile properties of HT-20 with various loadings of isobutyl-POSS, cast from THF/DMAc (80%/20%) ..... 127
Table 6.5 Melting temperature and enthalpy of isobutyl-POSS dispersed in PTMO-2900 at various loadings. ..... 130
Table 7.1 Molecular weight buildup of biphenyl-PTMO polyesters and polyurethanes, and hard segment composition of polyurethanes. ..... 143

# Chapter 1: Introduction

## 1.1 Project Goal and Outline

The superior mechanical properties of natural spider silk, specifically its unmatched combination of strength and extensibility, has led to considerable research efforts in the last twenty years to develop silk-inspired materials with similar properties.[1, 2] Natural spider silk is a protein consisting of alternating hard, hydrophilic blocks (β-pleated alanine sheets) and soft hydrophobic blocks (amorphous glycine-rich matrix) that microphase segregate into a network structure. A second level of order has also been observed within the glycine-rich soft domain, and the silk's superior toughness has been attributed to this "oriented amorphous" region.[3, 4] This thesis focuses on the development of segmented polyurethane elastomers that mimic the structure and properties of spider silk through the creation of an oriented amorphous phase. The approach employed here explores two interpretations of the silk's oriented amorphous phase: 1) an expanded interphase between the domains or 2) reinforcing units within the soft domain. In the first part, the hard segments of a polyurethane are modified to incorporate bulky, crystal-disrupting units at the junction between hard and soft segments. In the second part, nanofillers are employed as reinforcing units within the polyurethane, associating with either the hard or soft segments. A further attempt was made to incorporate deformable groups within the soft segment matrix as a covalently attached reinforcing unit. This thesis outlines the design, synthesis, and characterization of segmented polyurethanes and polyurethane nanocomposites that mimic the microstructure of spider silk.

In Chapter 1, the motivation and background material are presented, which underlies the polyurethane design strategies developed in Chapter 2. The first part of our two-part approach examines the modification of the interphase in segmented polyurethanes with mixed hard segments (Chapter 3), including analysis of the deformation of their microstructures (Chapter 4). The second part examines the reinforcement of the polyurethane with clay nanoparticles associated with the hard segments (Chapter 5), siloxane nanoparticles associated with the soft segments (Chapter 6), and liquid crystalline mesogens covalently incorporated into the soft segments (Chapter 7). Research conclusions and potential future directions are discussed in Chapter 8.

## 1.2 Background

The goal of this project is to explore the effects of designed hierarchical structures on the morphology and mechanical properties of segmented polyurethane elastomers, in order to develop high performance materials that mimic the properties of spider silk. The current understanding of the properties, microstructure and morphology of spider silk is presented first, followed by an overview of thermoplastic polyurethane elastomers. Afterward, background material is presented on the selected design features of the polyurethanes, including interphase modification, polyurethane nanocomposites, and liquid crystalline polyurethanes.

### *1.2.1 Spider Silk Structure and Properties*

Spider silk is one of the toughest engineering materials known in nature, capable of spanning large areas and bringing flying insects to a halt by dissipating kinetic energy

without fracturing. The mechanical properties of spider silk are compared with those of several other engineering materials in Table 1. Although spider silk does not match the stiffness (i.e. modulus) or strength of aramid fibers such as Kevlar®, its high elasticity means that its toughness (i.e. energy to break) may be 10-100 times higher than brittle engineering materials such as Kevlar® or steel. Furthermore, its low density ($\rho \sim 1.5$ g/cm3) means that per unit weight, spider silk is in fact stronger than steel.

**Table 1.1 Property comparison of silk to other engineering materials[2]**

| Material | Modulus (GPa) | Tensile Strength (GPa) | Extensibility (%) | Energy to Break (MJ/m3) |
|---|---|---|---|---|
| Dragline Silk | 10 | 1.1 | 27 | 160 |
| Viscid Silk | 0.003 | 0.5 | 270 | 150 |
| Kevlar 49 | 130 | 3.6 | 2.7 | 25 |
| High-tensile Steel | 200 | 1.5 | 0.8 | 6 |
| Synthetic Rubber | 0.001 | 0.05 | 850 | 100 |

The dragline and frame silks of the *Nephila clavipes* spider are both essentially composed of two proteins, termed Spidroin 1 and Spidroin 2, both of which were first characterized by Xu and Lewis.[9] Spidroin 1 is the dominant component in the stronger dragline silk, and its amino acid composition is presented in Figure 1.2[2] This protein may be considered a multiblock copolymer, since it contains several glycine(G)-rich "soft" blocks and alanine-rich "hard" blocks within the same polymer chain. The alanine-rich blocks crystallize to form β-sheet crystals, typically 2 x 5 x 7 nm in size, which are imbedded in a flexible glycine-rich matrix.[1] The polyalanine crystallites serve as physical crosslinks reinforcing the flexible matrix, such that the protein forms a thermoplastic elastomer. Spidroin 2 contains a less blocky arrangement of alanine residues, interrupted by proline-rich sequences that form a less crystalline material.

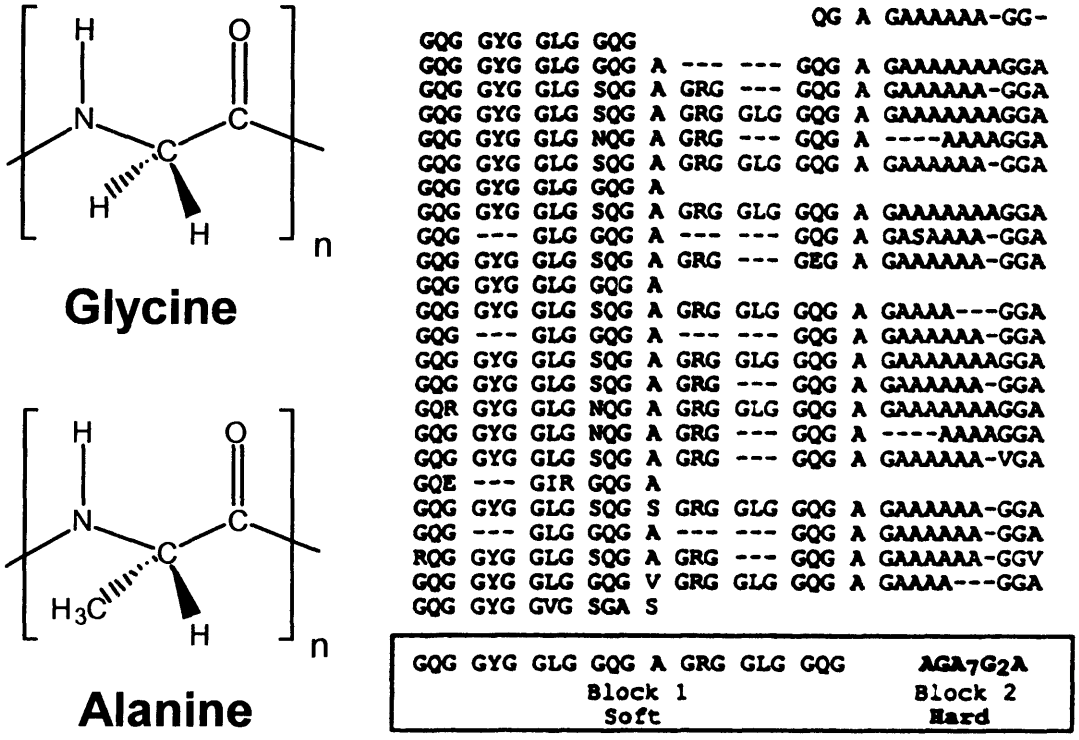


**Figure 1.1 Amino acid sequence of spider dragline silk protein[2]**

The unique molecular architecture of spider silk is responsible for its superior mechanical properties. Two important aspects of the silk's performance are its high *hysteresis*, or ratio of the energy dissipated to the total energy of impact, and *supercontraction*, in which the length of the silk fiber decreases as it is exposed to water, accompanied by a decrease in the mechanical properties.[10] The primary function of natural silk fibers is to bring flying insects to a halt without fracturing. The silk's high hysteresis (65%) allows it to dissipate much of the impact energy as heat, preventing prey from elastically escaping the web and preventing fiber fracture mechanisms. The supercontraction phenomenon seems to indicate that the fiber is pre-stretched during the spinning process, giving it an extra degree of orientation and thus a higher tensile

strength. Experts believe that water causes supercontraction by the breakup of the hydrogen bonds that preserve this extra orientation.[10]

The unique mechanical properties and supercontraction of spider silk have been successfully modeled using an energy-minimization routine on a fixed lattice.[11] Figure 1.2 illustrates both the perceived silk morphology (on the left) and its lattice-based mathematical representation (on the right). The model includes the amorphous chains, β-sheet crystals (15% by volume), entanglements and hydrogen bonds noted in spider silk, clearly labeled on the figure. In addition, the triple lines exiting each crystal represent a higher-modulus constrained amorphous layer immediately adjacent to the crystallites.[12] The stress-strain response of this model is calculated using physical estimates for the moduli of the crystals, amorphous chains, hydrogen bonds, and the high-modulus amorphous layer. To mimic the extra orientation noted in the dry fibers, the lattice is mathematically "pre-stretched" before the hydrogen bonds are inserted. The model of the dry fibers predicts a tensile strength of 1 GPa and an elongation at break of 30%, and the overall form of the stress-strain curve agrees well with experimental observation.[13] When the hydrogen bonds are removed, the model also reproduces the weakened mechanical properties of the wet supercontracted fiber.

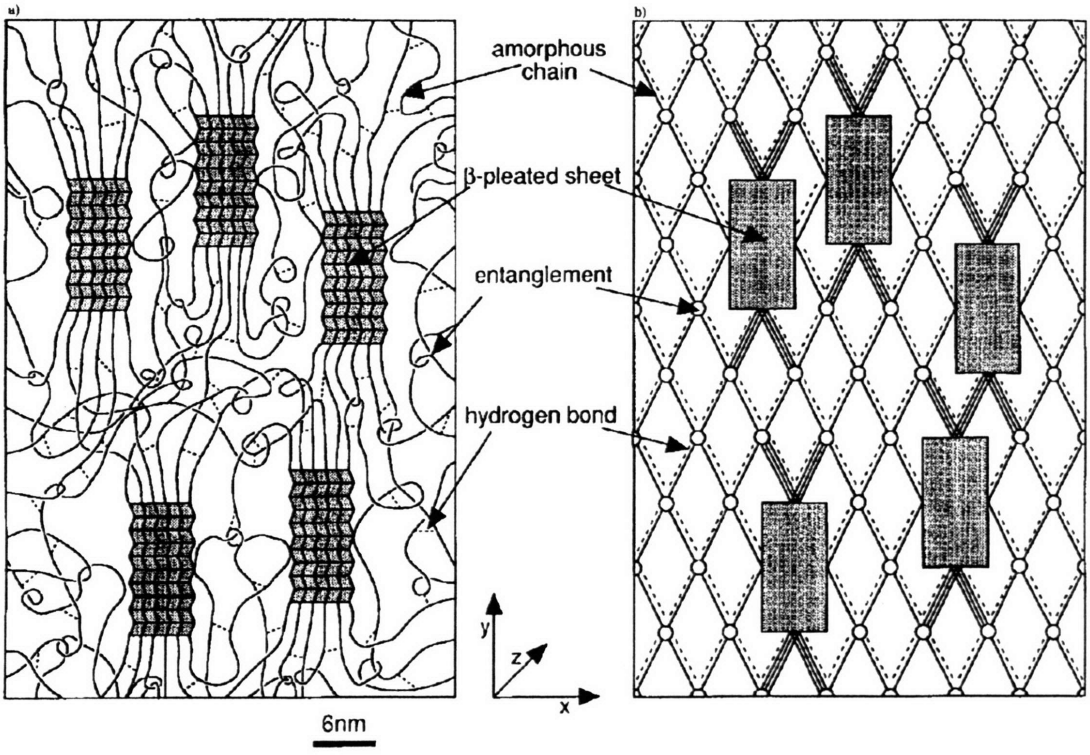


**Figure 1.2 Modeling of spider silk properties on a lattice[11]**

Experimental studies on the morphology of native spider-silk fibers have expanded on the simple two-phase picture presented above. Studies using solid-state nuclear magnetic resonance (NMR) spectroscopy and wide-angle X-ray scattering (WAXS) have demonstrated a third phase which is intermediate of the highly oriented polyalanine crystals and the unoriented amorphous region.[3, 4] Simmons *et al.* found that the $^{2}H$ spectrum of spider silk with deuterated alanine residues could not be fit using a single Gaussian distribution.[3] Instead, the data were well fit by two Gaussian curves, one curve with a very high degree of orientation, comprising ~40% of the alanine population, and another curve with a weaker orientation, comprising ~60% of the alanine population. The percentage of highly oriented alanine residues was also found to decrease upon supercontraction with water.

Grubb and Jelinski demonstrated that the amorphous phase of spider silk was divided between a fully isotropic fraction and a partially oriented fraction.[4] As in the NMR experiment, the WAXS pattern could not be fit with a single distribution. Instead, the pattern was again fit with two Gaussian curves: an amorphous halo and a separate peak with an orientation between that of the crystalline and isotropic fractions. From these WAXS pattern fits, it was determined that ~60% of the amorphous phase is completely isotropic, but ~40% has some higher degree of order.

Combining the two sets of data, the composition of spider silk is estimated to be the following: 15% highly oriented β-sheet crystals, 30% oriented amorphous region, and 55% isotropic amorphous region. Figure 1.3 shows a cartoon of these different types of structures, with the first two oriented regions exaggerated in quantity.[3] The nature of the "oriented amorphous" phase is still unclear in the literature; however, this extra degree of motion during deformation may provide the mechanism for spider silk's superior mechanical properties. The partial orientation is similar to that observed in the interphase around crystallites in semicrystalline polymers, in the interphase around particles or fibers in composite materials, and in liquid crystalline phases. These similarities are the inspiration for the new material design in this research project, which will be introduced in the following sections and developed more fully in Chapter 2.

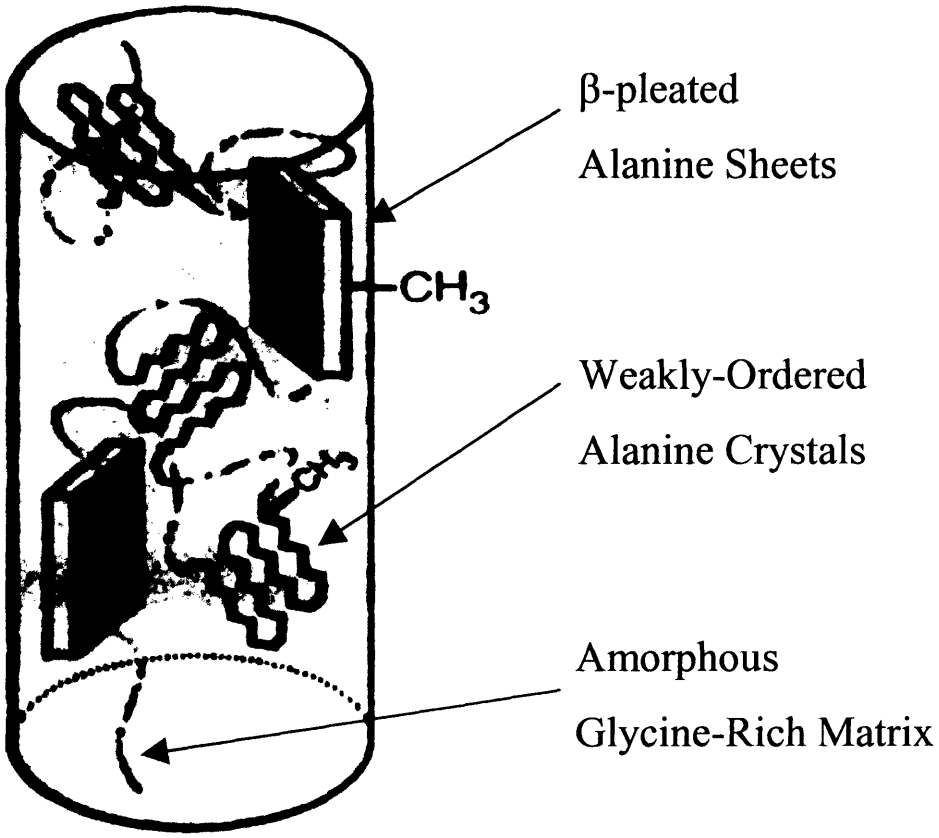


**Figure 1.3 Proposed morphological model of spider silk[3]**

*1.2.2 Segmented Polyurethane Elastomers*

A thermoplastic elastomer is a block copolymer in which each chain contains chemically immiscible blocks or segments that are thermodynamically driven to phase separate.[14] However, the incompatible blocks are covalently linked within the polymer backbone, so they microphase segregate into domains on the length scale of the blocks. Segmented copolymers contain soft segments that are above their glass transition temperature ($T_g$), creating a rubbery, amorphous block, as well as hard segments that are below their $T_g$. The hard segments form crystalline or paracrystalline domains that

behave as rigid reinforcements within the rubbery network.[8] The hard domains serve as physical crosslinks within the rubber to prevent macroscopic flow behavior; however, the domains can be melted or cleared at high temperatures, so that the polymer may be melt processed as an ordinary thermoplastic.[14]

Segmented polyurethanes, the most industrially significant class of thermoplastic elastomer, contain a multiblock structure similar to that found in spider silk protein.[8] The diversity of potential chemical architectures and extensive literature base of segmented polyurethanes make them attractive as a synthetic framework for materials with hierarchical structures. Physically cross-linked segmented polyurethane were first reported in 1958 by Schollenberger[15], which created an alternative to chemically cross-linked polyurethanes and began a multitude of investigations into their mechanical and microstructural behavior as a function of polyurethane composition. Bonart *et al.* confirmed that physical crosslinking was provided by hydrogen bonded urethane hard segments that aggregated to form crystalline or paracrystalline hard domains.[16] These physical crosslinks are reversible above the hard domain melting temperature or in polar solvents. Figure 1.4 presents a simplistic cartoon of the segmented polyurethane architecture.

It is important to distinguish between a segmented copolymer and a triblock copolymer, which also exhibits thermoplastic elastomeric behavior. A triblock copolymer consists of only three blocks, each of which may contain 50-100 repeat units. A segmented copolymer consists of many more blocks, which may have less than 5 repeat units in the hard block and less than 20 repeat units in the soft block.

Consequently, the scale of microphase segregation in a segmented copolymer is very different from that of a triblock copolymer.

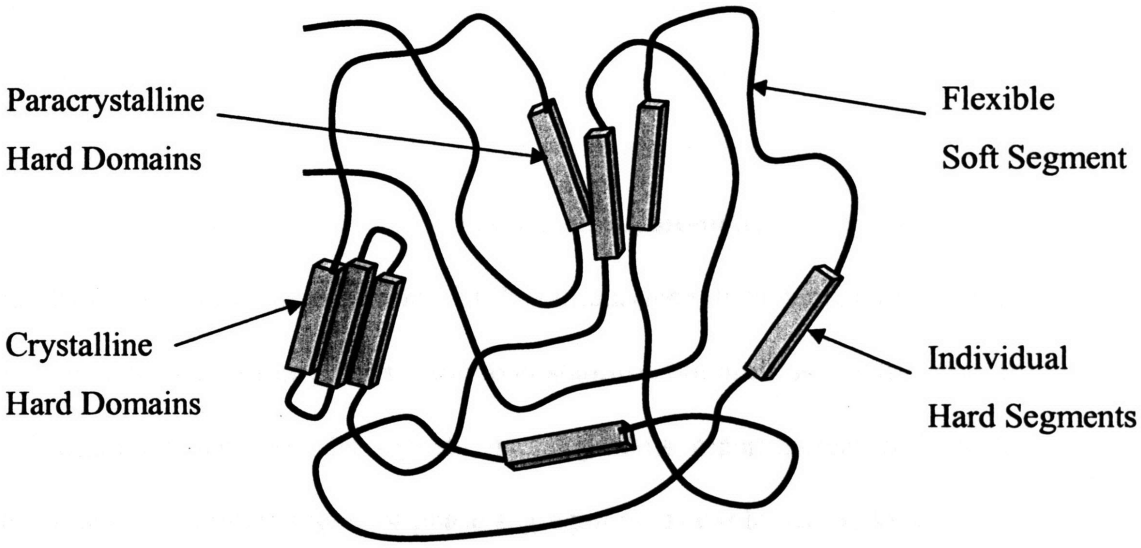


**Figure 1.4 Molecular architecture of segmented polyurethane elastomers**

The method of polyurethane synthesis has considerable effect on the microstructure, and thus the properties of polyurethane elastomers.[17] The one-step method, in which soft segment macrodiol, diisocyanate and chain extender are simultaneously added, is the most common industrial synthetic method. However, this method lacks the control required to produce regular block sequences.[17] In the two-step method, the soft segment macrodiol is first reacted with excess diisocyanates in a slow addition step. The endcapped macrodiol is then reacted with a low molecular weight diol (chain extender), and a stoichiometric quantity of diisocyanate to grow high molecular weight polyurethane. The two-step method produces linear polyurethane elastomers with fewer side reactions and a polydispersity close to 2, as expected for step growth polymers.[18]

Polyurethane hard segments are composed of aromatic or aliphatic diisocyanates with diol or diamine chain extenders. (With diamine chain extenders, the urea linkage is formed instead of the urethane, creating polyurethaneureas.) The most common industrially used diisocyanates 4,4'-methylene bisphenyl diisocyanate (MDI) and toluene diisocyanate (TDI). The rigidity of these aromatic units generally creates polyurethanes with high modulus and tensile strength.[17] However, aromatic diisocyanates are subject to degradation by ultraviolet radiation. 1,6-hexamethylene diisocyanate (HDI) and other aliphatic diisocyanates offer greater ultraviolet stability, but are less reactive than the aromatic diisocyanates.[19] The aliphatic hard segments impart increased flexibility, which can lead to a higher degree of phase segregation, as explained by kinetic arguments.[20, 21]

The polyurethane soft segments are typically a polyester or polyether macrodiol such as poly(ethylene adipate) or poly(tetramethylene glycol) with a glass transition temperature well below the polyurethane's use temperature. Polyester soft segments typically exhibit higher modulus, tensile strength and thermal stability, in part because of the ability of the ester linkages to hydrogen bond with urethanes in the hard segments.[19] Polyether soft segments have better flexibility and hydrolytic stability than polyesters, and undergo less hydrogen bonding with hard segments.[22] Mechanical properties of the polyurethanes are also dependent on the crystallinity or ordering of the soft segments, which is dependent on the molecular weight that typically ranges from 400-6000 g/mol.[17] As the soft segment molecular weight decreases, the modulus and tensile strength of the polyurethane generally increases.

### *1.2.3 Interphases in Semicrystalline Polymers*

Semicrystalline polymers have long been understood to consist of a mixture of crystalline structures such as chain-folded lamellae or pleated sheets within a matrix of amorphous chains.[23] In typical semicrystalline polymers, that is, those that do not exhibit any block sequences limiting the size of the crystallizable regions, the crystalline regions are long, capable of forming larger superstructures such as spherulites. In these cases, the polymer morphology is well modeled as a two-component system, consisting of crystalline and amorphous polymer chains. However, in all semicrystalline polymers, there exists a small "interphase" between the crystalline structures and the amorphous polymer chains in which the orientation and mobility of the chain segments are restricted by the crystalline structure.[24] The dimensions of this interphase are fixed for a given polymer system, typically several nanometers in thickness. For most semicrystalline polymers the contribution of this interphase to the mechanical properties is negligible, due to its low volume fraction within the bulk polymer. However, as the dimensions of the crystalline regions within the polymer shrink to a few nanometers, such as in spider silk or crystalline segmented copolymers, the interphase represents a larger volume fraction of the polymer matrix, and strongly contributes to the mechanical behavior of the polymer.

A variety of experimental and theoretical techniques have been used in the literature to characterize the interphase of semicrystalline polymers.[12] Models fit to wide-angle X-ray scattering (WAXS) data from polyethylene fibers[25], liquid crystalline polyesters[26], Nylon-6[27] and spider silk[4] all required an additional ordering phase beyond the two-component crystalline and amorphous phases to fully describe the data.

Multiple-pulse nuclear magnetic resonance (NMR) spectroscopy has been used to observe magnetization decay in polyethylene terephthalate fibers[28], and spider silk protein[3]. In these cases the decay was fit to three domain species of different mobility, generally termed mobile noncrystalline, constrained noncrystalline, and crystalline domains. TEM has also been used to directly observe the interphase in poly(ethylene terephthalate).[29] Theoretical models of the interphase have included Monte Carlo simulations of polyethylene[30] and atomistic models of spider silk.[12] Small-angle X-ray scattering (SAXS) has also been used to characterize the interfacial size between blocks in block copolymers[31], blends[32], and many segmented copolymers such as polyamides[33], polyesters and polyurethanes.[34, 35] Although the characterization of the interfacial thickness in segmented copolymers is relatively common, designed synthetic efforts to alter the nature of the interphase are relatively uncommon. Huy *et al.* altered the composition between blocks within a styrene-butadiene-styrene triblock copolymer, creating an asymmetric morphology in which the shorter polystyrene chains were intermixed into the softer butadiene phase.[36] This led to an increase in the $T_g$ of the soft phase and more effective stress transfer at the interface, leading to higher orientation of both phases during deformation.

### *1.2.4 Polyurethane Nanocomposites*

The properties of segmented polyurethane elastomers have been improved by the reinforcing effects of nanoscale filler particles.[37] The improved properties include tensile modulus and strength, elongation, thermal stability and barrier properties. The enhancement of properties is a function of the high surface to volume ratio of well-dispersed nanofillers, which promotes greater interaction between the nanofillers and

polyurethane matrix, as well as changes in chain dynamics and crystallinity induced by the particles.[38] The strength of the interfacial bond between the nanofillers and polyurethane matrix may be modified through the use of surfactants, modification of the nanofiller surface, or polarity of the polyurethane block.[39] By creating chemical compatibility between the nanofillers and polyurethane block, the maximum level of nanofillers dispersion is obtained, providing the most significant improvement in polyurethane nanocomposite properties.

Polyurethane nanocomposites have been developed with several methods of nanoparticle dispersion. A common method is the *in situ* polymerization of a soft segment macrodiol in which the nanoscale filler particles have already been dispersed.[40, 41] Nanocomposites have also been prepared by post-processing polyurethanes with nanofillers, via melt compounding[38] or solution processing.[42] The method of nanofillers dispersion has been shown to have little effect on the mechanical properties as long as compatibility between the nanofillers and matrix is maintained.[38]

### *1.2.5 Liquid Crystalline Polyurethanes*

Studies of the orientation mechanisms of polyurethanes have shown that the application of a stress induces orientation in both the hard and soft segments.[43] Upon removal of that stress, the hard segments retain their orientation, while the soft segments relax back to an isotropic state. The addition of a liquid crystalline (LC) mesogen within the soft segment may prevent this total relaxation to an isotropic state, instead leaving a partial orientation within the soft segment, similar to the orientation observed in spider silk. The liquid crystalline phase of matter represents the partial ordering of molecules

between a solid and liquid state.[44] LC materials have the flow behavior of an isotropic liquid, but retain some directional and/or positional ordering, though less than that of a true crystalline state. LC groups can be incorporated directly within a polymer backbone, creating a main-chain liquid crystalline polymer, or as pendant groups to the polymer backbone, creating a side-chain liquid crystalline polymer, as shown in Figure 1.5.[18]

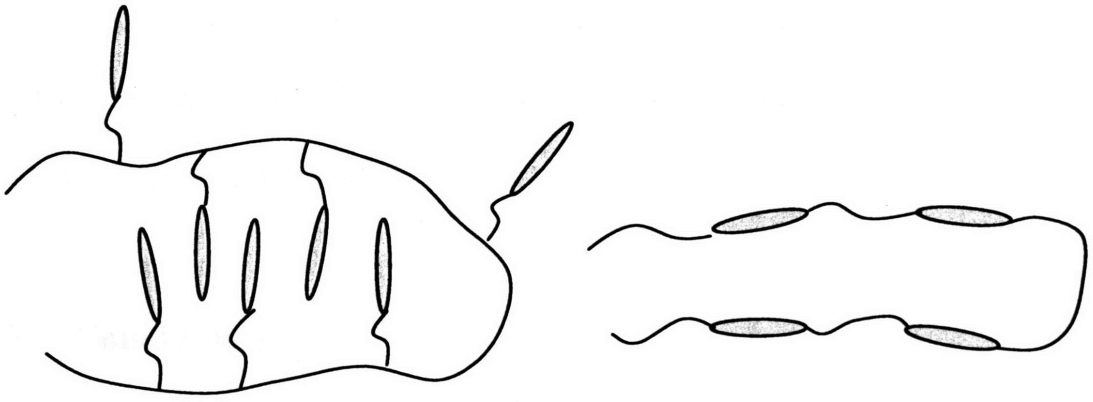

**Side-Chain Liquid Crystalline Polymer** **Main-Chain Liquid Crystalline Polymer**

**Figure 1.5 Cartoon representation of side-chain and main-chain liquid crystalline polymers.**

Several groups have investigated the synthesis and properties of liquid crystalline (LC) polyurethanes that incorporate mesogenic units as diisocyanates or chain extenders within the hard segment.[45-49] These novel segmented polyurethanes combine the mechanical integrity and processability of thermoplastic polyurethane elastomers with the electro-optical, mechano-optical and ferroelectric properties of liquid crystalline materials. However, these polyurethanes do not contain any additional units that provide reinforcement during deformation; the liquid crystalline hard segments remain the only reinforcing structure. Previous research in our group studied the properties of polyurethanes with a LC mesogen attached as a pendant group to a polysiloxane soft

segment backbone.[50] To the author's knowledge, this is the only known modification of a polyurethane soft domain with liquid crystalline groups. This system was studied using infrared dichroism, which allows one to investigate the orientation of functional groups within a sample as it is placed under tension. With this technique, Nair *et al.* observed different modes of motion in the hard segments and the LC mesogens.[51] From this observed cooperation between hard segments and LC mesogens, it is apparent that the hard segments of polyurethanes may play a key role in determining how the LC mesogens respond to applied fields.

## 1.3 Conclusions

This chapter introduced the motivation for this thesis research and offered background material relevant to the design and synthesis of segmented polyurethanes as spider silk analogs. The mechanical behavior, protein architecture, and morphological models of spider silk were discussed, with particular emphasis on the presence of an oriented amorphous third phase within the silk fiber. Design considerations of thermoplastic polyurethane elastomers were considered, including hard segment and soft segment type and synthetic route. The critical role of the interphase in semicrystalline polymers and block copolymers was discussed; as the crystal or microdomain size decreases, the effect of the interphase becomes increasingly important. Progress in the creation of polyurethane nanocomposites was presented, including a review of the various methods of nanoparticle dispersion. Finally, the synthesis and properties of liquid crystalline segmented polyurethanes was reviewed as a potential design framework for the incorporation of rigid reinforcing units within the soft domain. This background

material facilitates the design of polyurethanes with ordered structures at the interphase and in the soft segment.

## 1.4 References


1. Gosline, J.M., et al., *The Mechanical Design of Spider Silks: From Fibroin Sequence to Mechanical Function.* Journal of Experimental Biology, 1999. **202**: p. 3295-3303.
2. O'Brien, J.P., et al., *Nylons from Nature: Synthetic Analogs to Spider Silk.* Advanced Materials, 1998. **10**(15): p. 1185-1195.
3. Simmons, A.H., C.A. Michal, and L.W. Jelinski, *Molecular Orientation and Two-Component Nature of the Crystalline Fraction of Spider Dragline Silk.* Science, 1996. **271**: p. 84-87.
4. Grubb, D.T. and L.W. Jelinski, *Fiber Morphology of Spider Silk: The Effects of Tensile Deformation.* Macromolecules, 1997. **30**: p. 2860-2867.
5. Lazaris, A., et al., *Spider silk fibers spun from soluble recombinant silk produced in mammalian cells.* Science, 2002. **295**: p. 5554.
6. Hest, J.C.M.v. and D.A. Tirrell, *Protein-based materials, toward a new level of structural control.* Chemical Communications, 2001. **19**: p. 1897-1904.
7. Rathore, O. and D.Y. Sogah, *Nanostructure Formation through β-sheet Self-Assembly in Silk-Based Materials.* Macromolecules, 2001. **34**(5): p. 1477-1486.
8. Meckel, W., W. Goyert, and W. Wieder, *Thermoplastic Polyurethane Elastomers*, in *Thermoplastic Elastomers*, G. Holden, et al., Editors. 1996, Hanser: Munich.
9. Xu, M. and R.V. Lewis, *Structure of a Protein Superfiber - Spider Dragline Silk.* Proceedings of the National Academy of Sciences of the United States of America, 1990. **87**(18): p. 7120-7124.
10. Fornes, R.E., R.W. Work, and N. Morosoff, *Molecular Orientation of Spider Silks in the Natural and Supercontracted States.* Journal of Polymer Science, Part B-Polymer Physics, 1983. **21**(7): p. 1163-1172.

11. Termonia, Y., *Molecular Modeling of Spider Silk Elasticity.* Macromolecules, 1994. **27**: p. 7378-7381.
12. Fossey, S.A. and S. Tripathy, *Atomistic modeling of interphases in spider silk fibers.* International Journal of Biological Macromolecules, 1999. **24**(2-3): p. 119-125.
13. Gosline, J.M., M.W. Denny, and M.E. DeMont, *Spider Silk as Rubber.* Nature, 1984. **309**(5968): p. 551-552.
14. Holden, G., et al., eds. *Thermoplastic Elastomers.* 1996, Hanser: Munich.
15. Schollenberger, C.S., H. Scott, and G.R. Moore, Rubber World, 1958. **137**: p. 549.
16. Bonart, R., L. Morbitzer, and G. Hentze, *X-Ray Investigations Concerning the Physical Structure of Cross-Linking in Urethane Elastomers. II. Butanediol as Chain Extender.* Journal of Macromolecular Science - Physics, 1969. **B3**(2): p. 337-356.
17. Szycher, M., *Szycher's Handbook of Polyurethanes.* 1999, New York: CRC Press.
18. Odian, G., *Principles of Polymerization.* 1991, New York: Wiley & Sons.
19. Gogolewski, S., Colloid and Polymer Science, 1989. **267**(9): p. 757.
20. Chu, B., et al., *Microphase Separation Kinetics in Segmented Polyurethanes: Effects of Soft Segment Length and Structure.* Macromolecules, 1992. **25**: p. 5724-5729.
21. Li, Y., et al., *Multiphase Structure of Segmented Polyurethanes: Effects of Hard-Segment Flexibility.* Macromolecules, 1993. **26**: p. 612-622.
22. Bruins, P.F., *Polyurethane Technology.* 1969, New York: Interscience Publishers.
23. Flory, P.J., *Principles of Polymer Chemistry.* 1953, Ithaca: Cornell Univ. Press.
24. Flory, P.J., *On the Morphology of the Crystalline State in Polymers.* Journal of the American Chemical Society, 1962. **84**(15): p. 2857-2867.
25. Baker, A.M.E. and A.H. Windle, *Evidence for a partially ordered component in polyethylene from wide-angle X-ray diffraction.* Polymer, 2001. **42**: p. 667-680.
26. Oda, D.C. and G.C. Rutledge, *Molecular structure and orientation in processed polymers 1. Analysis of X-ray scattering data.* Polymer, 1999. **40**: p. 4635-4646.

27. Murthy, N.S., et al., *Drawing and annealing of nylon-6 fibres: studies of crystal growth, orientation of amorphous and crystalline domains and their influence on properties.* Polymer, 1995. **36**(20): p. 3863-3873.

28. Havens, J.R. and D.L. VanderHart, *Morphology of Poly(ethylene terephthalate) Fibers As Studied by Multiple-Pulse 1H NMR.* Macromolecules, 1985. **18**: p. 1663-1676.

29. Ivanov, D.A., et al., *Direct observation of crystal-amorphous interphase in lamellar semicrystalline poly(ethylene terephthalate).* Macromolecules, 2002. **35**(26): p. 9813-9818.

30. Balijepalli, S. and G.C. Rutledge, *Conformational statistics of polymer chains in the interphase of semi-crystalline polymers.* Computational and Theoretical Polymer Science, 2000. **10**(1-2): p. 103-113.

31. Richards, R.W. and J.L. Thomason, *Small-angle neutron scattering measurement of block copolymer interphase structure.* Polymer, 1983. **24**(9): p. 1089-1096.

32. Hsiao, B.S. and B.B. Sauer, *Glass Transition, Crystallization, and Morphology Relationships in Miscible Poly(aryl ether ketones) and Poly(ether imide) Blends.* Journal of Polymer Science: Part B: Polymer Physics, 1993. **31**(8): p. 901-915.

33. Yu, Y.C., W.H. Jo, and M.S. Lee, *Segmented Block Copolyetheramides Based on Nylon 6 and Polyoxypropylene. III. SAXS Analysis.* Journal of Applied Polymer Science, 1997. **64**: p. 2155-2163.

34. Koberstein, J.T. and R.S. Stein, *Small-Angle X-Ray Scattering Measurements of Diffuse Phase-Boundary Thicknesses in Segmented Polyurethane Elastomers.* Journal of Polymer Science - Polymer Physics, 1983. **21**: p. 2181-2200.

35. Tyagi, D., J.E. McGrath, and G.L. Wilkes, *Small Angle X-ray Studies of Siloxane-urea Segmented Copolymers.* Polymer Engineering and Science, 1986. **26**(20): p. 1371-1398.

36. Huy, T.A., et al., *Influence of interfacial structure on morphology and deformation behavior of SBS block copolymers.* Polymer, 2003. **44**: p. 1237-1245.

37. Tien, Y.I. and K.H. Wei, *High-Tensile-Property Layered Silicates/Polyurethane Nanocomposites by Using Reactive Silicates as Pseudo Chain Extenders.* Macromolecules, 2001. **34**(26): p. 9045-9052.

38. Finnigan, B., et al., *Morphology and properties of thermoplastic polyurethane nanocomposites incorporating hydrophilic layered silicates.* Polymer, 2004. **45**: p. 2249-2260.

39. Thostenton, E.T., C. Li, and T.-W. Chou, *Nanocomposites in context.* Composites Science and Technology, 2005. **65**: p. 491-516.

40. Petrovic, Z.S., et al., *Structure and Properties of Polyurethane-Silica Nanocomposites.* Journal of Applied Polymer Science, 2000. **76**: p. 133-151.

41. Petrovic, Z.S. and W. Zhang, *Glassy and Elastomeric Polyurethanes with Nano-Silica Particles.* Materials Science Forum, 2000. **352**: p. 171-176.

42. Kumar, N., S. Liff, and G.H. McKinley, To Be Submitted, 2005.

43. Seymour, R.W., A.E. Allegrezza, and S.L. Cooper, *Segmental Orientation Studies of Block Copolymers: 1. Hydrogen-Bonded Polyurethanes.* Macromolecules, 1973. **6**(6): p. 896-902.

44. Collings, P.J., *Liquid Crystals: Nature's Delicate Phase of Matter.* 1990, Princeton: Princeton University Press.

45. Lee, T.J., D.J. Lee, and H.D. Kim, *Synthesis and Properties of Liquid Crystalline Polyurethane Elastomers.* Journal of Applied Polymer Science, 2000. **77**: p. 577-585.

46. Jeong, H.M., B.K. Kim, and Y.J. Choi, *Synthesis and Properties of Thermotropic Liquid Crystalline Polyurethane Elastomers.* Polymer, 2000. **41**: p. 1849-1855.

47. Lin, C.K., J.F. Kuo, and C.Y. Chen, *Synthesis and Properties of Novel Polyurethanes Containing the Mesogenic Moiety of α–methylstilbene Derivatives.* European Polymer Journal, 2001. **37**: p. 303-313.

48. Jia, X., X. He, and X. Yu, *Synthesis and Properties of Main-Chain Liquid Crystalline Polyurethane Elastomers with Azoxybenzene.* Journal of Applied Polymer Science, 1996. **62**: p. 465-471.

49. Hsu, T.-F. and Y.-D. Lee, *Properties of thermoplastic polyurethane elastomers containing liquid crystalline chain extender (I) synthesis and properties of hard segments.* Polymer, 1999. **40**: p. 577-587.

50. Nair, B.R., M.A.R. Osbourne, and P.T. Hammond, *Synthesis and Characterization of New Segmented Copolymers with Side Chain Liquid Crystalline Soft Segments.* Macromolecules, 1998. **31**(25): p. 8749-8756.

51. Nair, B.R., V.G. Gregoriou, and P.T. Hammond, *FT-IR Studies of Side Chain Liquid Crystalline Thermoplastic Elastomers.* Polymer, 2000. **41**(8): p. 2961-2970.

# Chapter 2: Materials Design

## 2.1 Introduction

As explained in Chapter 1, spider silk is a multiblock copolymer consisting of flexible glycine-rich soft blocks alternating with crystalline alanine-rich hard blocks that microphase segregate into a network structure. The superior properties of silk have been partially attributed to an additional ordered phase within the soft matrix or at the interphase between the hard and soft blocks. Through careful selection of the polyurethane soft segments and hard segments, as well as orientable nanoparticles or liquid crystalline units, it is possible to create synthetic structures with this third phase and its enhanced mechanical properties. Synthetic segmented copolymers, such as polyurethanes, polyamides or polyesters exhibit the multiblock structure observed in spider silk protein. For this work, segmented polyurethanes were chosen as the synthetic template to mimic the unique morphology of spider silk, primarily due to the ease and variability of component selection and incorporation. In addition, the extensive literature base covering synthetic issues and structure-property relationships[1-18] suggest that segmented polyurethanes would make excellent candidate materials for spider silk analogs. Through careful selection of the polyurethane soft segments and hard segments, as well as orientable nanoparticles or liquid crystalline units, it is possible to create synthetic structures with this third phase enhanced mechanical properties observed in spider silk.

## 2.2 Polyurethane Blocks

The thermoplastic polyurethane elastomers used in this study are synthesized using a two-step solution polymerization illustrated in Figure 2.1. The two-step method provides consistent control over average block lengths and maintains a well-defined microstructure.[7]

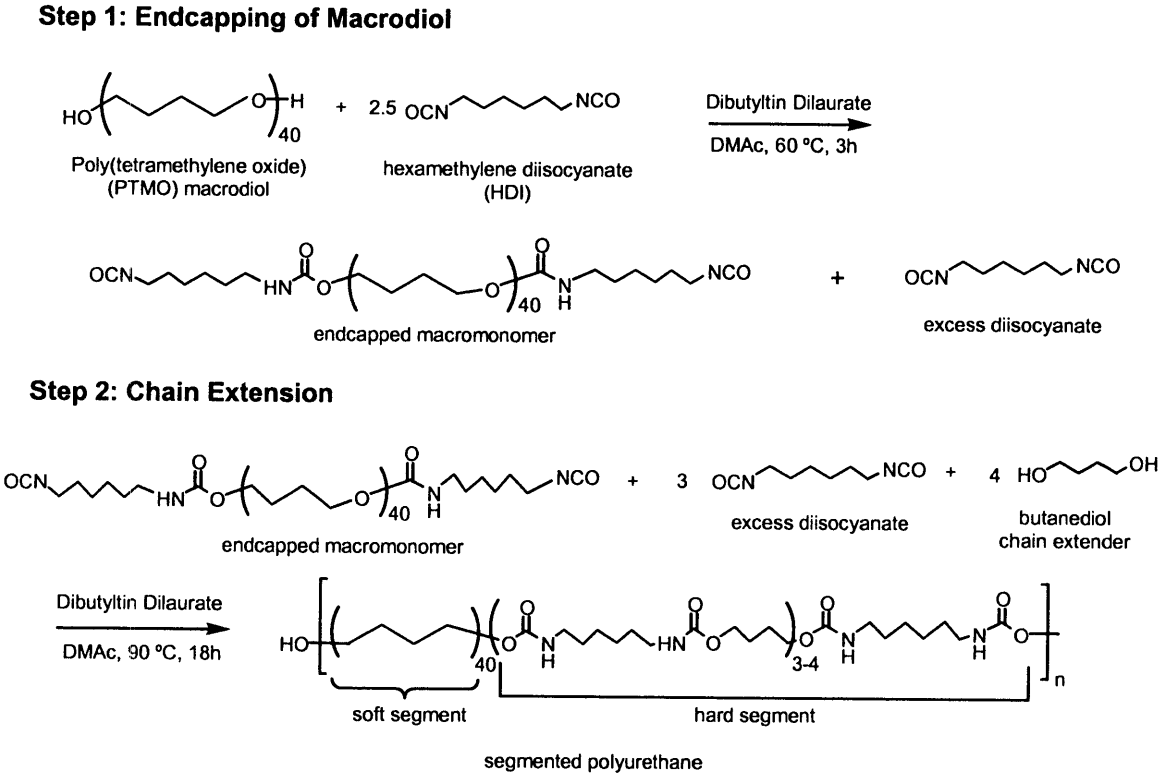


**Figure 2.1 Two-step solution polymerization of segmented polyurethanes**

### *2.2.1 Soft Segments*

The principal requirements for the choice of polyurethane soft segment include its flexibility, incompatibility with the hard segment, and chemical functionality. The soft segment glass transition temperature ($T_g$) must be far below room temperature. As rigid liquid crystalline groups or nanofillers are incorporated into the soft segment, its $T_g$

increases; therefore, the $T_g$ of the pure soft segment must be low enough to remain elastomeric after these other structures are added.[19, 20] The soft segment should also be hydrophobic, to promote phase segregation with the polar, hydrogen bonding urethane groups within the hard segment. Finally, the soft segment must be alcohol terminated to react with the urethane chemistry. Poly(tetramethylene oxide) (PTMO) was chosen as the soft segment material because it has a $T_g$ of -84 °C, is relatively hydrophobic with weak hydrogen bonding, is readily available as a macrodiol of various molecular weights, and is well-studied in segmented polyurethanes.[8]

PTMO is the most common soft segment choice for industrial polyurethane elastomers. It is made through the cationic ring-opening polymerization of tetrahydrofuran, which produces oligomers with a most probable (Flory) distribution of molecular weights.[21] Since some randomness has been observed in spider silk amino acid sequences, [22] this polydispersity was acceptable to the material design. PTMO is readily available with number-average molecular weights ranging from 250 to 2900 g/mol. In order to mimic the relatively long block sequences in spider silk, the two longest chain lengths ($M_n$ = 2000 and $M_n$ = 2900) were chosen for polyurethanes with no synthetic modifications to the soft segment. Shorter chain lengths ($M_n$ = 650 and $M_n$ = 1000) were chosen for soft segments in which liquid crystalline mesogens would be copolymerized, in order to keep the molecular weight of the copolymerized oligomer below 5000 g/mol. This design is explored further in Section 2.2.4.

### *2.2.2 Hard Segments*

The hard segments selected for the basic polyurethanes synthesized in this work consist of an aliphatic diisocyanate, 1,6-hexamethylene diisocyanate (HDI), chain–

extended with an aliphatic diol, 1,4-butanediol (BDO), as indicated in Figure 2.1. HDI is highly crystalline, capable of forming spherulitic crystalline structures at room temperature in an order of minutes.[14] HDI-BDO hard segments also impart significant flexibility to the hard domains, which promotes microphase segregation.[15] The selection of an aliphatic diisocyanate such as HDI also prevents degradation from exposure to ultraviolet radiation typical for aromatic diisocyanates.

Native spider silk exhibits a strong degree of ordering at the intersection of the hard and soft domains. To mimic this behavior, an additional diisocyanate was selected to be introduced at the intersection of the hard and soft segments, allowing it to self-assemble in the interphase between the domains. This additional diisocyanate should be bulkier than HDI and more miscible with the PTMO soft segment than HDI to promote interphase growth. 4,4'-methylenebisphenyl diisocyanate (MDI) and toluene diisocyanate (TDI) are two aromatic diisocyanates that fit these characteristics, and are commonly used in industry. The aromatic diisocyanates should be preferentially located at the junction between the soft segment and the HDI-BDO hard segments. This positioning can be accomplished with the synthetic outline shown in Figure 2.2, in which the aromatic diisocyanate is used to endcap the macrodiol, and the polyurethane is chain-extended with HDI and BDO in the second step. This mixture of diisocyanates also has potential for the partial disruption of HDI-BDO crystalline structures while creating a hard segment that is more stable to UV radiation than pure MDI or TDI hard segments.

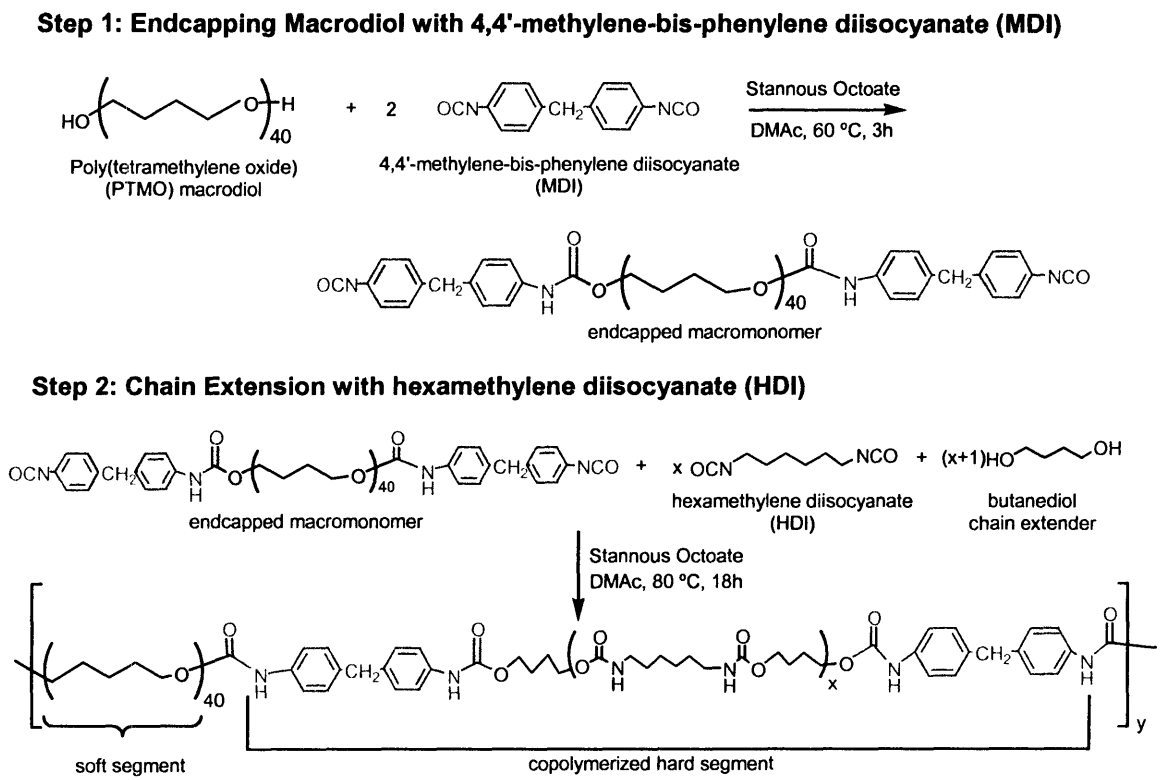


**Figure 2.2 Synthesis of polyurethanes with mixed diisocyanates in the hard segments. The macrodiol is first endcapped with the aromatic diisocyanate, then chain extended with an aliphatic diisocyanate and diol.**

The literature on polyurethanes with a mixture of diisocyanates in the hard segment is relatively limited.[8, 23] Prisacariu *et al.* used a mixture of MDI and 4,4'-dibenzyl diisocyanate (DBDI) with both PTMO and poly(ethylene adipate) soft segments.[23] They found that DBDI's ability to create a linear conformation allowed for greater crystallinity within the hard segments and an improvement of mechanical properties. While their approach did consider the effects of the different order of addition of the various diisocyanates, they did not consider the effects of mixed diisocyanates in terms of the interphase around crystalline hard domains.

## 2.3 Reinforcing Units

### *2.3.1 Layered Silicate Clays*

Polyurethane nanocomposites created from fillers such as nanotubes[24], nanoclays[20, 25] and nanosilica[26, 27] have shown considerable improvements in mechanical and barrier properties. The properties of these segmented polyurethane nanocomposites are heavily dependent on the phase to which the nanofillers associate. The interfacial bond between the filler particle and polyurethane matrix tends to restrict motion of the polymer chains bonded to the particles.[20] Therefore, in most polyurethane nanocomposites, it is desired to have nanofiller particles associate with the hard segment, to avoid restricting the elastic motion of the flexible soft segment. However, if the nanoparticle were on the length scale of other small reinforcing units observed within the soft segment of spider silk, it could potentially reinforce the soft segment during deformation, and provide the desired third phase of ordering in the segmented polyurethane silk analog. This thesis investigates the incorporation of two different classes of nanoparticles into segmented polyurethanes: hydrophilic disc-shaped nanoclays with an affinity for the hard segments, and hydrophobic siloxane nanocages with an affinity for the soft segments.

Thermoplastic polyurethane elastomers have been reinforced with natural and synthetic clays, such as Montmorillonite and Laponite, respectively.[25, 28] Montmorillonite is a natural smectic layered silicate with a high aspect ratio, high layer spacing, and non-uniform platelet size.[29] Polyurethane/Montmorillonite nanocomposites have exhibited significant improvements in mechanical properties; however, the uniform platelet size, smaller layer spacing, and hydrophilic nature of

synthetic Laponite make it an even more attractive candidate for association with HDI-BDO hard segments in polyurethanes. Using a novel solvent-exchange method for Laponite dispersion, collaborators have demonstrated the exfoliation of Laponite in other segmented polyurethanes, providing improvements in initial modulus without a reduction of tensile stress or ultimate elongation.[28] An illustration of the Laponite clay particles is presented in Figure 2.3.

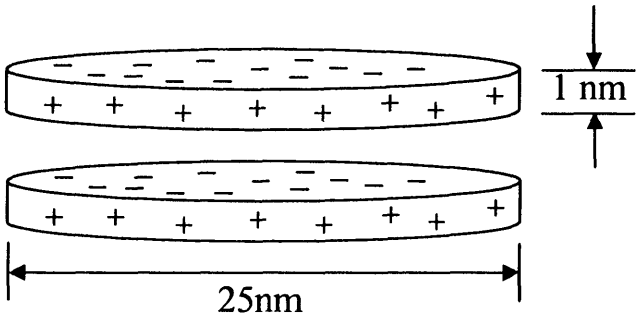


**Figure 2.3 Schematic illustration of undispersed Laponite discs.[29]**

*2.3.2 Siloxane Cages*

Polyhedral oligomeric silsesquioxanes (POSS) are a class of siloxanes with the general repeat structure $SiO_{1.5}R$.[30] They are capable of forming random, ladder or cage structures and can be functionalized at the corners of the cages with non-reactive or reactive groups, the latter enabling their grafting onto polymer matrices. The first oligomeric organosilsesquioxanes were isolated by Scott in 1946,[31] but interest in them increased drastically when a large scale process for POSS monomer synthesis was developed by a group at Edwards Air Force Base in the late 1990s.[32] POSS monomers are now available in a multitude of structures and functionalities from Hybrid Plastics Company in Fountain Valley, CA. At 1-4 nm in diameter (depending on the functional groups), POSS cages have an intermediate size between that of plasticizer molecules and

most nanoparticles. For this reason, POSS has been tested as a nanoscale filler in many polymer matrices, both covalently attached and non-covalently dispersed.[33-40] The chemical structure of a generic POSS cage with seven non-reactive groups (R) and one reactive group (Y) is illustrated in Figure 2.3. Fu *et al.* covalently tethered cyclohexyl-POSS into the hard segments of a polyurethane with MDI and bisphenol A, and found significant mechanical reinforcement of the polyurethane due to the formation of nanoscale POSS crystals within the hard domain.[33, 34] However, there is no literature currently available on the dispersion of POSS cages within a polyurethane soft segment. While the dispersion of many nanoparticles within the soft matrix of a polyurethane may lead to undesired restriction of the soft segment elasticity, it is believed that if the nanofillers are small enough, they could provide the soft segment reinforcement desired for the spider silk analogs. The dispersion of POSS cages and other POSS-like siloxane resins into the polyurethane soft segment can be accomplished through either covalent tethering to the soft segment backbone or non-covalent association with the soft segment matrix. The non-covalent dispersion of POSS cages in PTMO soft segments is the subject of Chapter 6; the covalent tethering of POSS cages was not attempted in this thesis, but will be discussed in Chapter 8.

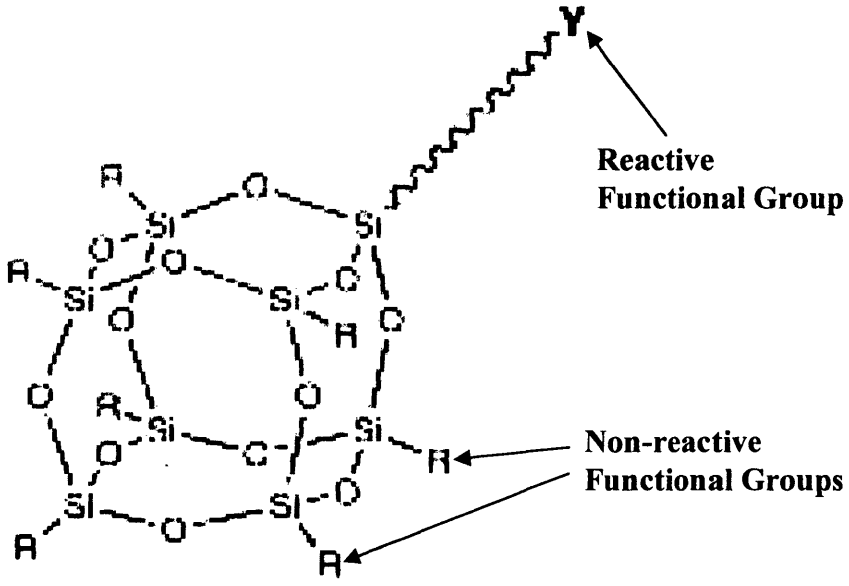


**Figure 2.4 Structure of polyhedral oligomeric silsesquioxane (POSS) cages[36]**

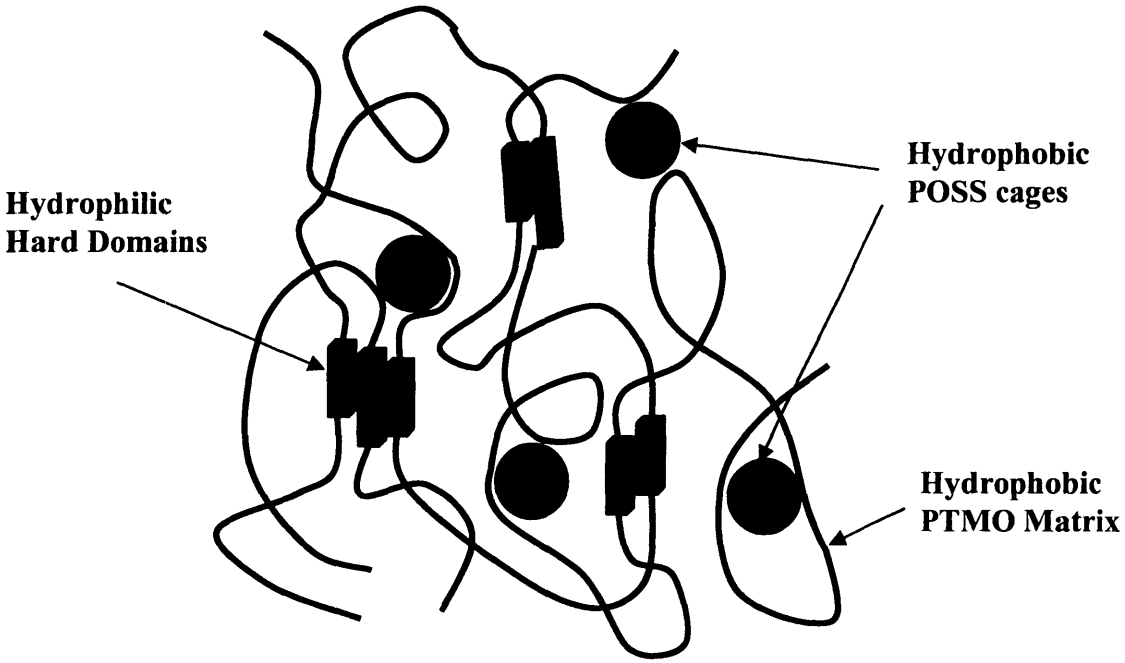


**Figure 2.5 Cartoon representation of POSS reinforcement within polyurethane soft segment matrix**

### *2.3.3 Liquid Crystalline Soft Segments*

As introduced in Section 1.2.5, the incorporation of a liquid crystalline mesogen into a segmented polyurethane can create an orientable unit, capable of cooperative motion with the hard segment during the deformation process. For this work, we propose to incorporate a basic LC mesogen into the soft segment of a polyurethane. This LC mesogen should have a degree of orientation intermediate between the polyurethane hard segment and soft segment, just as spider silk contains sequences that are of intermediate order between the alanine-rich crystals and the glycine-rich amorphous matrix. A cartoon of the polyurethane design is drawn in Figure 2.6. Although previous studies in our group have focused on side-chain LC polyurethanes, we choose to focus now on main-chain LC polyurethanes, where the mesogens are allowed to be more load bearing. This design decision is also made in light of the superior mechanical properties of other main-chain LC polymers.[41]

There is a considerable variety of candidate mesogens and chemical architectures for a main-chain liquid crystalline soft segment. For this initial investigation into the feasibility of soft segment ordering, a simple mesogen with well-known chemistry is desired. 4,4'-biphenyl is the simplest difunctional aromatic mesogen, has been well-documented in the literature, and thus was selected for the initial studies into LC soft segment synthesis.[42-45] In order to be successfully incorporated into a polyurethane, the liquid crystalline soft segment must remain oligomeric. Therefore, shorter segments of PTMO are required between the LC mesogens, while maintaining enough length to ensure flexibility upon the addition of load-bearing mesogens. For this study, intermediate PTMO weights ($M_n$ = 650 and $M_n$ = 1000) were selected. The overall

molecular weight of the copolymer soft segment is controlled through the addition of excess PTMO; this also creates primary alcohol functionalities at the soft segment endgroups, enabling reaction with the polyurethane hard segment. The biphenyl mesogen can be incorporated into the soft segment through an ester or ether linkage. The advantage of the ether linkage is suppressed hydrogen bonding with the hard segment, to maintain polyurethane microphase segregation, as explained in Section 1.3.2. The advantage of the ester linkage is the ease of synthetic addition to the PTMO soft segment. Both approaches to LC incorporation will be explored in Chapter 7.

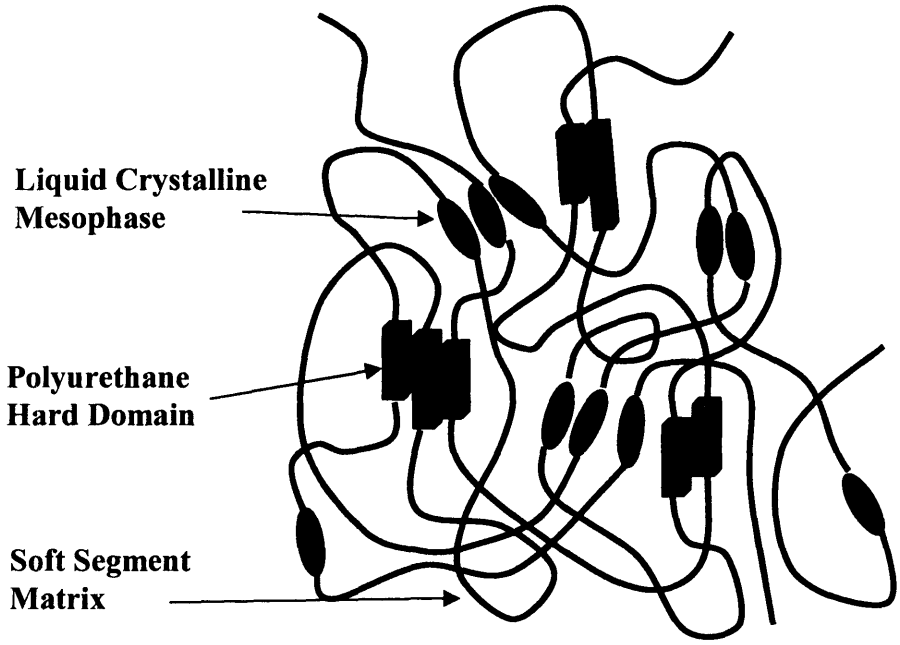


**Figure 2.6 Cartoon representation of main-chain liquid crystalline (LC) mesogens as reinforcing units within the polyurethane soft segment.**

## 2.3 Conclusions

This chapter considers the design of segmented polyurethane materials that contain an oriented amorphous component at the interphase between hard and soft

domain or within the soft phase, in order to mimic the microstructure of spider silk. A mixture of aromatic and aliphatic diisocyanates will be copolymerized within the polyurethane hard segments to promote the growth of the oriented interphase between the hard and soft domains. Laponite, a synthetic layered silicate clay, will be dispersed into the segmented polyurethane, to provide reinforcement of the hard domains. POSS cages and other siloxane resins will also be non-covalently dispersed into the polyurethane soft segment to provide reinforcement of the soft matrix during deformation. Finally, liquid crystalline mesogens will be covalently attached within the soft segment to create an orientable soft segment structure, capable of forming a third phase that contributes to the deformation process.

## 2.4 References


1. Seymour, R.W., A.E. Allegrezza, and S.L. Cooper, *Segmental Orientation Studies of Block Copolymers: 1. Hydrogen-Bonded Polyurethanes.* Macromolecules, 1973. **6**(6): p. 896-902.
2. Allegrezza, A.E., et al., *Segmental orientations studies of block copolymers: 2. Non-hydrogen bonded polyurethanes.* Polymer, 1974. **15**: p. 433.
3. Chang, Y.-J.P. and G.L. Wilkes, *Superstructure in Segmented Polyether-Urethanes.* Journal of Polymer Science - Polymer Physics, 1975. **13**: p. 455-476.
4. Koberstein, J.T. and R.S. Stein, *Small-Angle X-Ray Scattering Measurements of Diffuse Phase-Boundary Thicknesses in Segmented Polyurethane Elastomers.* Journal of Polymer Science - Polymer Physics, 1983. **21**: p. 2181-2200.
5. Bonart, R., L. Morbitzer, and G. Hentze, *X-Ray Investigations Concerning the Physical Structure of Cross-Linking in Urethane Elastomers. II. Butanediol as Chain Extender.* Journal of Macromolecular Science - Physics, 1969. **B3**(2): p. 337-356.

6. Bonart, R., L. Morbitzer, and E.H. Muller, *X-Ray Investigations Concerning the Physical Structure of Crosslinking in Urethane Elastomers. III. COmmon STructure Principles for Extensions with Aliphatic Diamines and Diols.* Journal of Macromolecular Science - Physics, 1974. **B9**(3): p. 447-461.
7. Szycher, M., *Szycher's Handbook of Polyurethanes.* 1999, New York: CRC Press.
8. Oertel, G., *Polyurethane Handbook.* 1985, Munich: Hanser Publishers.
9. Ng, H.N., et al., *Effect of segment size and polydispersity on the properties of polyurethane block polymers.* Polymer, 1973. **14**: p. 255-261.
10. Wilkes, C.E. and C.S. Yusek, *Investigation of Domain Structure in Urethan Elastomers by X-Ray and Thermal Methods.* Journal of Macromolecular Science - Physics, 1973. **B7**(1): p. 157-173.
11. Bruins, P.F., *Polyurethane Technology.* 1969, New York: Interscience Publishers.
12. Velankar, S. and S.L. Cooper, *Microphase Separation and Rheological Properties of Polyurethane Melts. 1. Effect of Block Length.* Macromolecules, 1998. **31**: p. 9181-9192.
13. Velankar, S. and S.L. Cooper, *Microphase Separation and Rheological Properties of Polyurethane Melts. 2. Effect of Block Incompatibility on the Microstructure.* Macromolecules, 2000. **33**: p. 382-394.
14. Li, Y., et al., *Multiphase Structure of Segmented Polyurethanes: Effects of Hard-Segment Flexibility.* Macromolecules, 1993. **26**: p. 612-622.
15. Li, Y., et al., *Effect of Hard Segment Flexibility on Phase Separation of Segmented Polyurethanes.* Macromolecules, 1994. **27**: p. 612-614.
16. Nair, B.R., M.A.R. Osbourne, and P.T. Hammond, *Synthesis and Characterization of New Segmented Copolymers with Side Chain Liquid Crystalline Soft Segments.* Macromolecules, 1998. **31**(25): p. 8749-8756.
17. Nair, B.R., *Synthesis, Characterization, and Infrared Dichroism of Novel Side-Chain Liquid Crystalline Polyurethane Systems*, in *Materials Science and Engineering*. 2000, Massachusetts Institute of Technology: Cambridge.
18. Nair, B.R., V.G. Gregoriou, and P.T. Hammond, *FT-IR Studies of Side Chain Liquid Crystalline Thermoplastic Elastomers.* Polymer, 2000. **41**(8): p. 2961-2970.

19. Collings, P.J., *Liquid Crystals: Nature's Delicate Phase of Matter.* 1990, Princeton: Princeton University Press.
20. Thostenton, E.T., C. Li, and T.-W. Chou, *Nanocomposites in context.* Composites Science and Technology, 2005. **65**: p. 491-516.
21. Odian, G., *Principles of Polymerization.* 1991, New York: Wiley & Sons.
22. O'Brien, J.P., et al., *Nylons from Nature: Synthetic Analogs to Spider Silk.* Advanced Materials, 1998. **10**(15): p. 1185-1195.
23. Prisacariu, C., et al., *The effect of hard segment ordering in copolyurethane elastomers obtained by using simultaneously two types of diisocyanates.* Polymer, 2003. **44**: p. 5407-5421.
24. Koerner, H., et al., *Remotely actuated polymer nanocomposites--stress recovery of carbon-nanotube-filled thermoplastic elastomers.* Nature Materials, 2004. **3**(2): p. 115-120.
25. Tien, Y.I. and K.H. Wei, *High-Tensile-Property Layered Silicates/Polyurethane Nanocomposites by Using Reactive Silicates as Pseudo Chain Extenders.* Macromolecules, 2001. **34**(26): p. 9045-9052.
26. Petrovic, Z.S., et al., *Structure and Properties of Polyurethane-Silica Nanocomposites.* Journal of Applied Polymer Science, 2000. **76**: p. 133-151.
27. Petrovic, Z.S. and W. Zhang, *Glassy and Elastomeric Polyurethanes with Nano-Silica Particles.* Materials Science Forum, 2000. **352**: p. 171-176.
28. Kumar, N., S. Liff, and G.H. McKinley, To Be Submitted, 2005.
29. Fossum, J.O., *Physical phenomena in clays.* Physica A, 1999. **270**: p. 270-277.
30. Li, G., et al., *Polyhedral Oligomer Silsesquioxane (POSS) Polymers and Copolymers: A Review.* Journal of Inorganic and Organometallic Polymers, 2001. **11**(3): p. 123-154.
31. Scott, D.W., *Thermal Arrangement of Branched-Chain Methylpolysiloxanes.* Journal of the American Chemical Society, 1946. **68**: p. 356.
32. Lichtentan, J.D., et al., *Method of functionalizing polycyclic silicones and the resulting compounds.* 1999: U.S. Patent 5942638.

33. Fu, B.X., et al., *Structural development during deformation of polyurethane containing polyhedral oligomeric silsesquioxane (POSS) molecules.* Polymer, 2001. **42**: p. 599-611.

34. Fu, B.X., et al., *Nanoscale reinforcement of polyhedral oligomeric silsesquioxane (POSS) in polyurethane elastomer.* Polymer International, 2000. **49**: p. 437-440.

35. Fu, B.X., et al., *Physical gelation in ethylene-propylene copolymer melts induced by polyhedral oligomeric silsesquioxane (POSS) molecules.* Polymer, 2003. **44**: p. 1499-1506.

36. Romo-Uribe, A., et al., *Viscoelastic and Morphological Behavior of Hybid Styryl-Based Polyhderal Oligomeric Silsesquioxane (POSS) Copolymers.* Journal of Polymer Science: Part B: Polymer Physics, 1998. **36**: p. 1857-1872.

37. Mather, P.T., et al., *Mechanical Relaxation and Microstructure of Poly(norbornyl-POSS) Copolymers.* Macromolecules, 1999. **32**: p. 1194-1203.

38. Pan, G., J.E. Mark, and D.W. Schaefer, *Synthesis and Characterization of Fillers of Controlled Structure Based on Polyhedral Oligomeric Silsesquioxane Cages and Their Use in Reinforcing Siloxane Elastomers.* 2003.

39. Waddon, A.J., et al., *Nanostructured Polyethylene-POSS Copolymers: Control of Crystallization and Aggregation.* Nano Letters, 2002. **2**(10): p. 1149-1155.

40. Zhang, W., et al., *Effect of Methyl Methacrylate/Polyhedral Oligomeric Silsesquioxane Random Copolymers in Compatabilization of Polystyrene and Poly(methyl methacrylate) Blends.* Macromolecules, 2002. **35**: p. 8029-8038.

41. Northholt, M.G. and D.J. Sikkema, *Lyotropic Main Chain Liquid Crystal Polymers.* Advances in Polymer Science, 1990. **98**: p. 115-177.

42. Meurisse, P., et al., *Polymers with Mesogenic Elements and Flexible Spacers in the Main Chain: Aromatic-Aliphatic Polyesters.* The British Polymer Journal, 1981. **13**: p. 55-63.

43. Hong, K.-C., J. Kim, and J.-Y. Bae, *Synthesis and characterization of oxyethylene copolymers with phenyl and/or 4,4'-biphenyl structural units in the backbone.* Polymer Bulletin, 2000. **44**: p. 115-122.

44. Chang, S. and C.D. Han, *A Thermotropic Main-Chain Random Copolyester Containing Flexible Spacers of Differing Lengths. Synthesis and Characterization.* Macromolecules, 1996. **29**: p. 2383-2391.

45. Lai, W.W. and T.C. Chang, *Studies on the Thermotropic Liquid Crystalline Polymer. XII. Synthesis and Properties of Crosslinkable Thermotropic Liquid Crystalline Homo- and Copoly(ether-ester)s.* Journal of Polymer Science: Part A: Polymer Chemistry, 1995. **33**: p. 1075-1083.

# Chapter 3: Segmented Polyurethanes with Mixed Hard Segments

## 3.1 Introduction

Thermoplastic polyurethane elastomers are a technologically important class of materials consisting of alternating hard and soft segments within the same polymer backbone.[1] At use temperatures, the hard and soft segments microphase separate into a variety of structures, depending on the composition of the two segments. The hard segments arrange into hard domains that serve as physical crosslinks within the matrix of soft segment chains; these hard domains can be crystalline, para-crystalline, or amorphous, depending on the chemical structure of the hard segment.

As explained in Chapter 1, spider silk is a naturally occurring thermoplastic elastomer, consisting of poly(alanine) hard segments that microphase segregate from glycine-rich soft segments.[2] The β-pleated poly(alanine) sheets form physical crosslinks that anchor the silk's network structure. However, some research has speculated that silk's superior mechanical properties are due to an oriented 'interphase' between the poly(alanine) hard segments and the soft matrix.[3] The existence of this interphase has been demonstrated experimentally for semicrystalline polymers such as polyethylene terephthalate (PET)[4] and polyethylene (PE).[5],[6] The role of the interphase becomes more important as the average size of the crystallites decreases, even though the dimensions of the interphase remain constant, since a larger volume fraction of the polymer is represented by the interphase material. The importance of the interphase has also been demonstrated for amorphous block copolymers, such as

between the PS and PB blocks in a PS-PB-PS triblock permitted a more effective stress transfer between the two blocks.[7]

In order to mimic the superior properties of spider silk, we devised a synthetic design strategy to expand the interphase of a segmented polyurethane elastomer. With this strategy, two different diisocyanates were polymerized within the hard segment of the polyurethane. A bulkier, aromatic diisocyanate (MDI or TDI) was preferentially located at the junction between the hard and soft segment, while the aliphatic diisocyanate (HDI) was preferentially located in the interior of the hard segment. This aliphatic diisocyanate along with the aliphatic chain extender (1,4-butanediol, BDO) tends to crystallize, similar to the polyalanine crystallites in spider silk, while the bulky diisocyanates interrupt the crystallinity near the interphase. The HDI-BDO hard segments also exhibit a strong microphase separation with poly(tetramethylene oxide) (PTMO) soft segments.

In this manner, we have designed a segmented polyurethane with two different diisocyanates in the hard segment, which will be referred to as "mixed hard segments" throughout the remainder of this thesis. The mixed hard segments are designed to alter the crystallization and microphase separation characteristics of the segmented polyurethane and to create a more well-connected hard domain structure, which in turn leads to improved mechanical performance.

## 3.2 Experimental

### *3.2.1 Materials*

Poly(tetramethylene oxide) (PTMO, $M_n$ = 2900) was purchased from Polysciences, and Terethane® 2000 (PTMO, $M_n$ = 2000) was purchased from Sigma-Aldrich. All other materials were purchased from Sigma-Aldrich. Both PTMO samples were dried under vacuum for 4-5 days at 80 °C. 1,4-butanediol was dried over calcium hydride ($CaH_2$) overnight and then vacuum distilled. 1,6-diisocyanatohexane (HDI), 2,4-tolylene diisocyanate (TDI), and 4,4'methylene-bis-phenylene diisocyanate (MDI) were all vacuum distilled. N,N'-dimethylacetamide (DMAc) and stannous octoate were used as received. All materials were transferred to a glove box after purification to control water content and enable the development of high molecular weight polymer.

### *3.2.2 Polyurethane Synthesis*

A series of polyurethanes with two different diisocyanates in the hard segment was polymerized in a glove box with the two-step approach outlined in Figure 3.1. In the first step, the PTMO soft segment was endcapped with two equivalents of TDI or MDI in DMAc under a $N_2$ atmosphere with a stannous octoate catalyst, and the solution was held at 60 °C for 3 hours. (Only TDI is shown in Figure 3.1, for simplicity.) In the second step, the endcapped macromonomer was polymerized to high molecular weight through the stoichiometric addition of HDI and 1,4-butanediol at 90 °C for 12-18 hours. The concentration of polyurethane in DMAc was kept below 10% to avoid gelation or early precipitation of the polyurethane solution. Progress of the reaction was monitored via FTIR by observing the free isocyanate peak at 2250 $cm^{-1}$, and adding extra charges of

1,4-butanediol until the isocyanate peak disappeared. Finally, the polyurethane was precipitated into a ten-fold excess of methanol, collected via filtration, and dried under vacuum at room temperature for >24 hours.

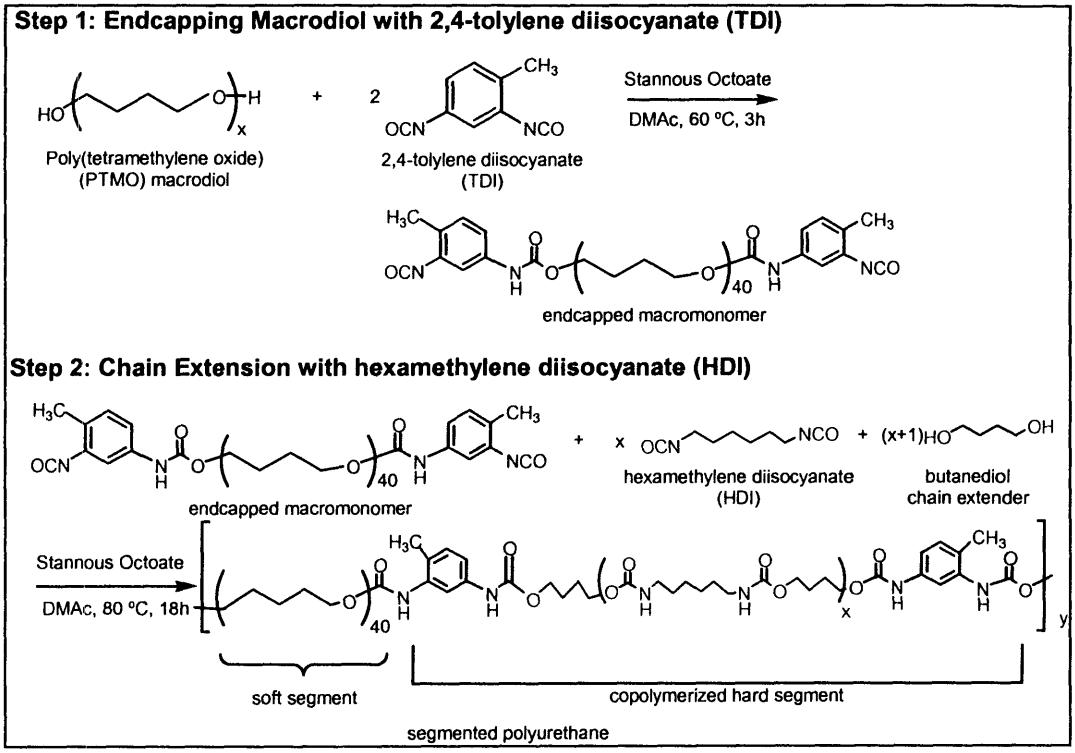


**Figure 3.1 Synthesis of polyurethanes with mixed hard segments. The macrodiol is first endcapped by the aromatic diisocyanate, and then chain extended with HDI and butanediol in a second step.**

### *3.2.3 Polyurethane Film Casting*

Films of the synthesized polyurethanes were prepared for characterization by free casting from solutions in DMAc. 280-300 mg of polyurethane was dissolved in DMAc to a concentration of 5 wt%. The solution was refluxed at 100-120 °C for 1-2 hours, cooled to room temperature, and transferred to custom-made Teflon® dishes 4 cm x 6 cm x 4 cm deep. DMAc was allowed to evaporate in a fume hood at room temperature for 2-3 days until the film appeared completely dry, after which the films were placed in a vacuum oven at 60 °C and annealed for 1 hour. Final film thicknesses varied from 0.08

mm to 0.12 mm, depending on the total amount of the sample. Strips of polyurethane film for tensile testing were cut from the cast film using a custom-built cutter consisting of 2 straight razors held at a fixed width of 5.4 mm.

### *3.2.4 Instrumentation*

#### 3.2.4.1 Gel Permeation Chromatography

Molecular weights and molecular weight distributions of segmented polyurethanes were determined relative to poly(ethylene oxide) standards by a Waters Gel Permeation Chromatograph (GPC) equipped with a refractive index detector, two PL Gel 5μm MIXED-C columns from Polymer Laboratories, and a DMAc eluent.

#### 3.2.4.2 Differential Scanning Calorimetry

Thermal phase behavior was examined with a TA Instruments Q1000 Differential Scanning Calorimeter (DSC), operated at a heating rate of 10°C/min under a 50 mL/min nitrogen purge. Polyurethane films cast as described in Section 3.2.3 were subjected to two heating and cooling cycles from -90 to 200 °C. Transitions were recorded from the first heating and cooling scans, to observe phase behavior in the cast films, using a linear extrapolation method for $T_m$ and midpoint inflection method for $T_g$.

#### 3.2.4.3 Dynamic Mechanical Analysis

Dynamic mechanical analysis (DMA) was performed on a TA Instruments Q800 DMA equipped with a film/fiber clamp, operated at a frequency of 1 Hz and heating rate of 3 °C/min from -100 to 160 °C.

#### 3.2.4.4 Small-angle X-Ray Scattering (SAXS)

Small-angle X-ray scattering experiments were performed on a Molecular Metrology SAXS equipped with CuKα radiation and a two-dimensional, gas proportional multi-wire Gabriel detector. Variations in beam intensity were corrected by normalizing with a photodiode placed on the beam stop when subtracting background radiation.

#### 3.2.4.5 Wide-Angle X-ray Diffraction

The semicrystalline character of polyurethane hard segments was investigated using a Rigaku RU300 rotating anode X-ray generator with a 185 mm diffractometer and a scintillation counter. Scattered CuKα radiation with wavelength of 1.54 Å was detected at a scan rate of 1°/min and a 0.05° sample interval.

#### 3.2.4.6 Atomic Force Microscopy (AFM)

Atomic Force Microscope images were taken on a Dimension D3100 with a Nanoscope IIIa controller. Polyurethane films for AFM imaging were free cast onto glass slides from 1 wt% solutions in DMAc. Phase images of the sample surface were collected in tapping mode using Veeco Nanoprobe tips (130 μm, 280-361 kHz).

#### 3.2.4.7 Tensile Testing

The tensile properties of the segmented polyurethanes were determined using a Zwick/Roell Z010 with a 500N load cell and convex jaw grips with aluminum and flat polyurethane faces to minimize tearing at the grips. All polyurethane films were prepared as described in Section 3.2.3, and cut into strips with a 5.4 mm width, a 40 cm gauge length, and a film thickness of 0.08 mm to 0.12 mm.

## 3.3 Polyurethane Characterization

The segmented polyurethanes examined in this study were designed to include two different diisocyanates within the hard segment, with the bulkier aromatic diisocyanate preferentially located at the interphase between hard and soft domains. To examine the effect of this architecture on polymer morphology and properties, a series of six principal samples were synthesized, using HDI, HDI and TDI, or HDI and MDI as hard segments, and PTMO-2000 or PTMO-2900 as soft segments. The matrix of these samples, including composition and molecular weights is summarized in Table 3.1. For the remainder of this chapter, H will refer to polyurethanes with only HDI in the hard segment, while HT will refer to a mixture of HDI and TDI, and HM will refer to a mixture of HDI and MDI. The number in the sample name indicates the molecular weight of the soft segment in that polyurethane. It should be noted that the hard segment wt% varies greatly between the PTMO-2000 and PTMO-2900 series, since the polyurethanes were designed to have the same number of diisocyanates in the hard segments, specifically three HDI units toward the hard segment interior, and two HDI, TDI or MDI units at the hard segment exterior. Two additional samples were synthesized with HDI and MDI in the hard segment; however, their addition order was varied to further examine the role of the prepolymer synthesis technique described in the previous section. The characterization of these two samples, HM-29-T and HM-29-S, are included in the following tables for comparison, but will be described separately in Section 3.3.4.

**Table 3.1 Summary of polyurethane compositions and molecular weights (GPC data taken in DMAc relative to PEO standards.)**

| Sample | Soft Segment | Hard Segment | HS wt% | Mw (kDa) | Mw/Mn |
|---|---|---|---|---|---|
| H-20 | PTMO-2000 | HDI-BDO | 37 | 233 | 2.13 |
| H-29 | PTMO-2900 | HDI-BDO | 29 | 79 | 2.11 |
| HT-20 | PTMO-2000 | HDI-TDI-BDO | 38 | 140 | 2.97 |
| HT-29 | PTMO-2900 | HDI-TDI-BDO | 34 | 41 | 2.21 |
| HM-20 | PTMO-2000 | HDI-MDI-BDO | 41 | 96 | 5.12 |
| HM-29 | PTMO-2900 | HDI-MDI-BDO | 32 | 75 | 3.50 |
| HM-29-T* | PTMO-2900 | HDI-MDI-BDO | 32 | 28 | 2.64 |
| HM-29-S* | PTMO-2900 | HDI-MDI-BDO | 32 | 25 | 2.62 |

* HM-29-S was synthesized by adding both diisocyanates in the same step, while HM-29-T was synthesized using the usual 2-step addition.

### *3.3.1 Microphase Separation*

The DSC traces for polyurethanes with PTMO-2000 and PTMO-2900 soft segments are presented in Figure 3.2, and the relevant thermal properties of all samples are summarized in Table 3.2. The segmented polyurethanes all exhibit two major transitions in DSC—an endotherm at 5-20 °C, corresponding to the melting of crystallites of PTMO, and an endotherm at 145-175 °C, corresponding to the melting of hard domains. The glass transition of the soft segment is not observable in DSC due to limitations on the temperature range of the instrument; however, the soft segment $T_g$, which ranges from -60 to -67 °C, is observable in DMA and is included in Table 3.2. The glass transition of the hard segment is not observable in DSC or DMA, and is likely suppressed by the partial crystallinity of these hard segments or thermally masked by the melting of the soft segments.

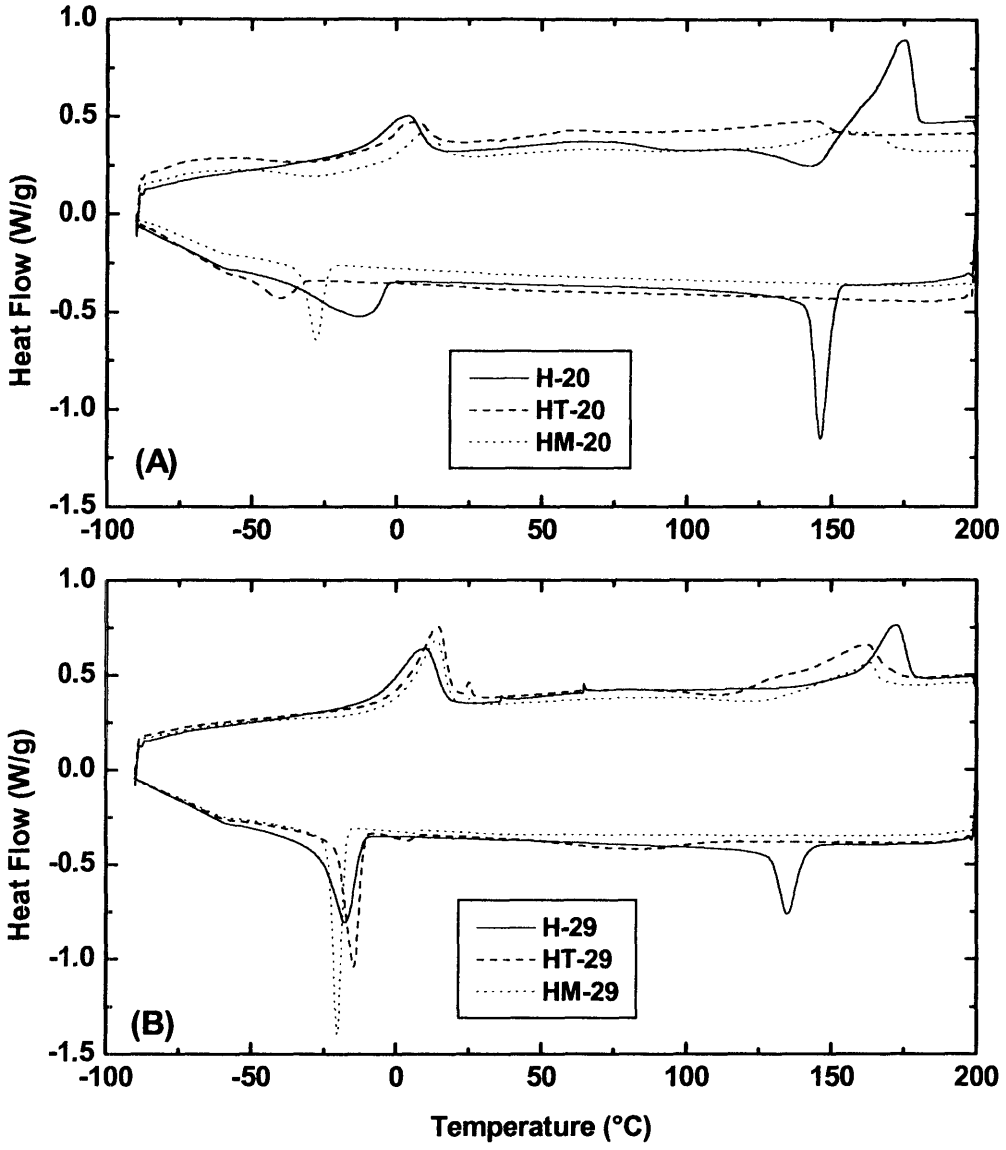


**Figure 3.2 DSC traces of polyurethanes with (A) PTMO-2000 soft segments and (B) PTMO-2900 soft segments. The presence of mixed isocyanates in the HT-series and HM-series depresses the hard segment melting point and enthalpy, relative to the H-series.**

From the data in Table 3.2, we observe that the melting temperatures and enthalpies of melting were higher for hard domains containing only HDI than for hard domains containing mixtures of HDI and TDI or MDI. In addition, the hard domains in

the HT and HM polyurethanes did not re-crystallize as readily upon cooling as H polyurethanes, probably due to kinetic limitations during cooling of the sample at 10 °C/min. The diminished reversibility and melting enthalpy in the HT and HM polyurethanes indicates a disruption of hard domain crystallinity by the bulkier TDI and MDI units. Comparing the soft segment transitions, PTMO-2900 soft segments all exhibit higher $T_m$ and $\Delta H_m$ than PTMO-2000 soft segments, since the longer chain segments are less constrained and can form larger crystallites, as predicted by Flory for any semicrystalline polymer.[8] In addition, the soft segment melting points are elevated by the presence of mixed hard segments in the HT and HM polyurethanes. This effect is likely due to increased phase segregation between the hard and soft domains, which reduces the interruption of soft segment crystallites by dissolved hard segments. This increased phase segregation of mixed hard segments is also indicated by DMA results.

**Table 3.2 Summary of DSC and DMA Results—Glass Transition ($T_{g,SS}$), Melting Point ($T_{m,SS}$), and Heat of Melting ($H_{m,SS}$) of Soft Segments, Temperature of Dissociation ($T_{d,HS}$) and Heat of Dissociation ($H_{d,HS}$) of Hard Segments (1st heating after film casting)**

| Sample | $T_{g,SS}$ (°C) | $T_{m,SS}$ (°C) | $H_{m,SS}$ (J/g SS) | $T_{d,HS}$ (°C) | $H_{d,HS}$ (J/g HS) |
|---|---|---|---|---|---|
| H-20 | -60 | 4 | 29 | 174 | 92 |
| H-29 | -63 | 10 | 41 | 173 | 76 |
| HT-20 | -69 | 6 | 19 | 144 | 26 |
| HT-29 | -67 | 14 | 48 | 161 | 72 |
| HM-20 | -65 | 11 | 19 | 155 | 39 |
| HM-29 | -66 | 14 | 42 | 163 | 34 |
| HM-29-T | -66 | 19 | 54 | 157 | 28 |
| HM-29-S | N/A | 18 | 44 | 137 | 18 |
| PTMO-2000 | -84 | 25 | 105 | - | - |
| PTMO-2900 | -84 | 27 | 103 | - | - |
| HDI-BDO HS | - | - | - | 175 | 105 |

The DMA storage modulus curves obtained from the six polyurethane samples are overlaid in Figure 3.3. The first inflection of the storage modulus curve is taken as the soft segment $T_g$, which ranges from -60 to -67 °C for all samples and is listed in Table

3.2. In PTMO-polyurethanes of similar composition, it has been observed that MDI and TDI are more miscible with the soft segment, resulting in an elevation of the soft segment $T_g$ by 20 °C.[9] However, the HT and HM samples containing MDI and TDI at the interphase do not exhibit this phase mixing, and are even more phase segregated than the H polyurethanes with a pure HDI hard segment. The second inflection around 20 °C corresponds to the melting of the soft segments; above this temperature, the modulus remains higher for the samples based on PTMO-2000, presumably due to the higher hard segment content and greater hard segment connectivity.

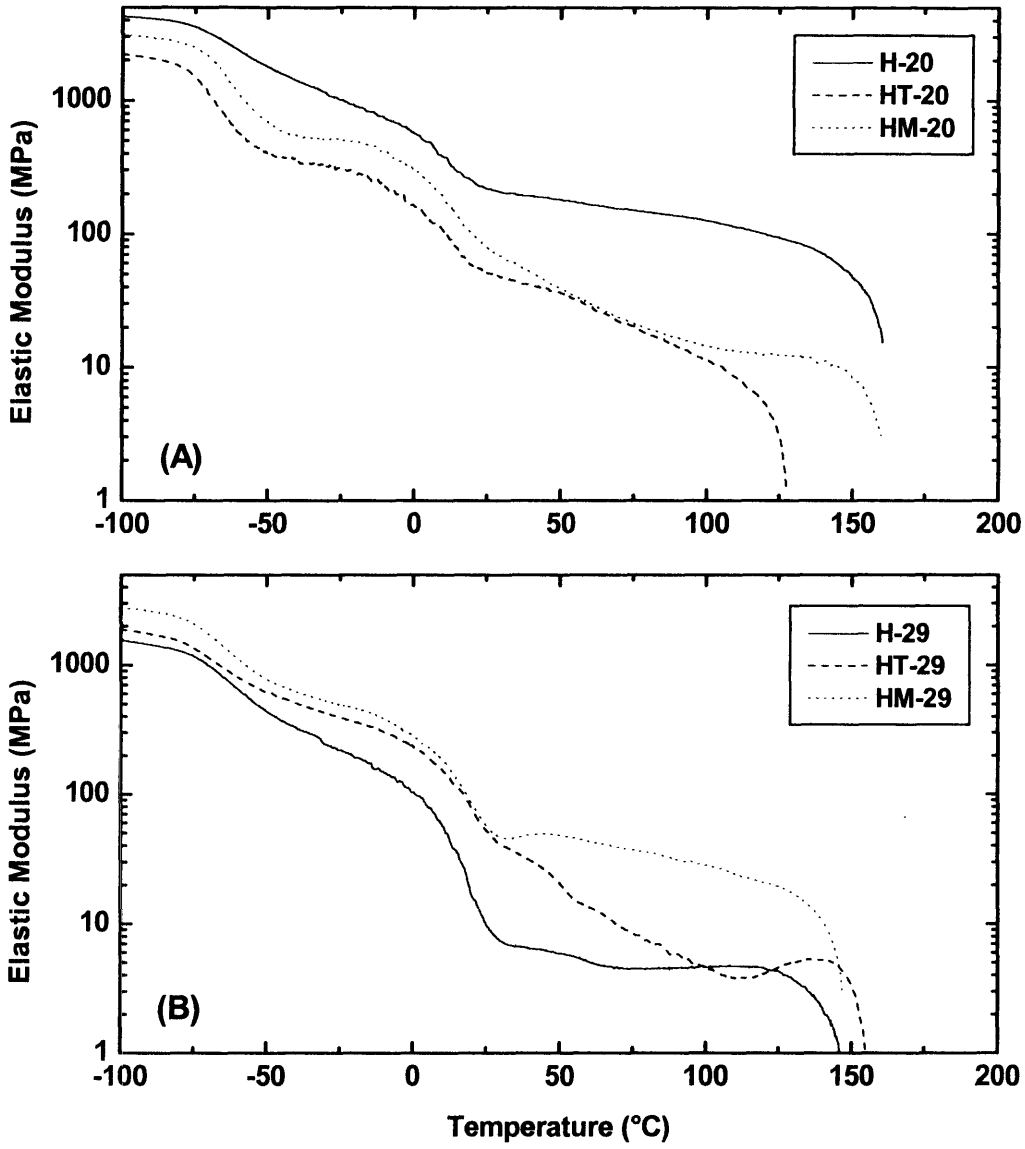


**Figure 3.3 DMA Elastic Modulus curves of polyurethanes with (A) PTMO-2000 soft segments and (B) PTMO-2900 soft segments.**

The tan(δ) curves for all six samples are overlaid in Figure 3.4. The polyurethanes based on PTMO-2000 all show a higher damping peak around -60 °C than the samples based on PTMO-2900. As shown previously in the DSC results, the longer soft segment lengths of PTMO-2900 form more crystallites which in turn damp the glass

transition of the soft segment. This effect has been shown with other polyurethanes with crystallizable soft segments.[10]

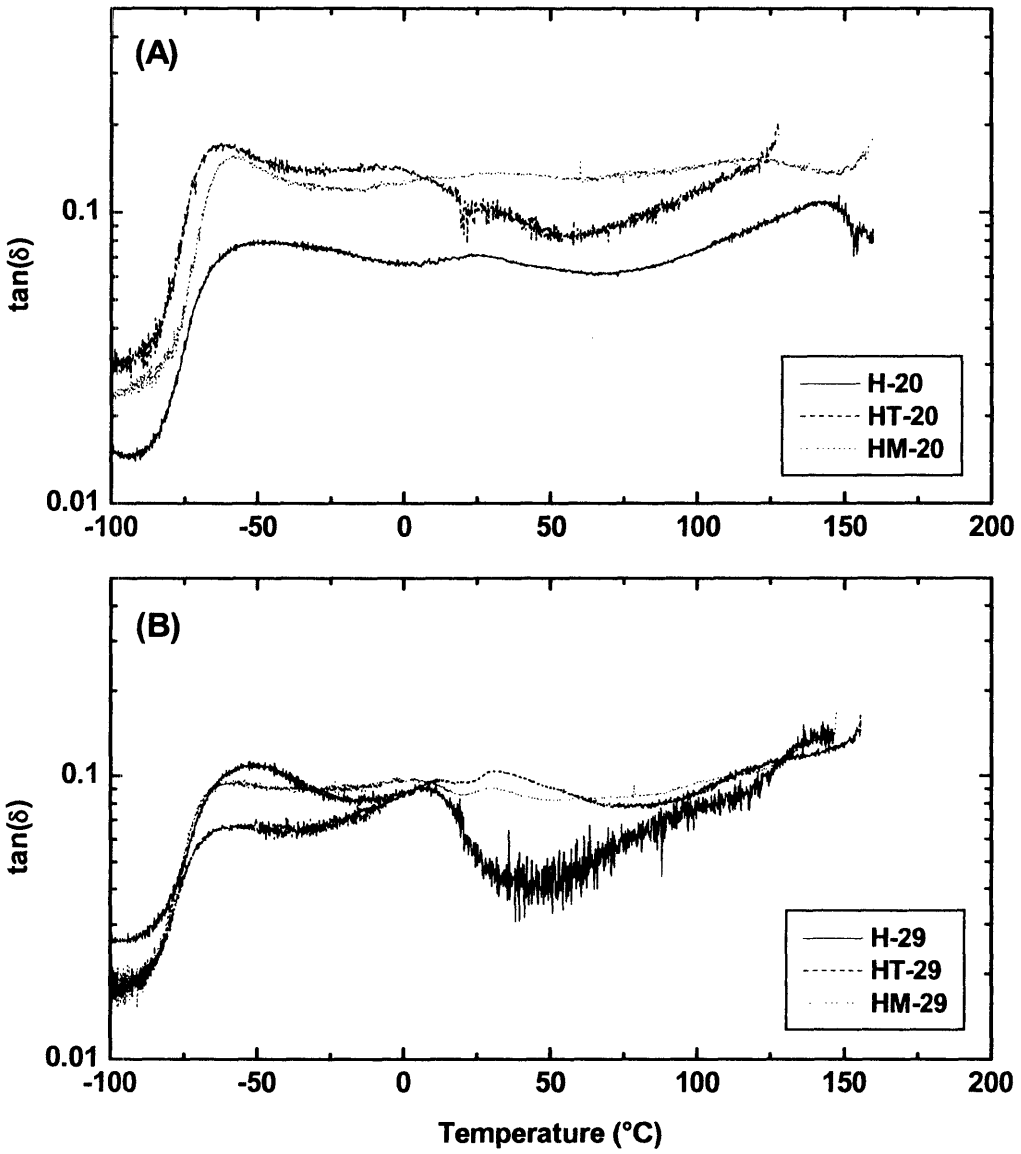


**Figure 3.4 DMA tan(δ) curves of polyurethanes with (A) PTMO-2000 soft segments and (B) PTMO-2900 soft segments.**

### *3.3.2 Polyurethane Morphology*

Small-angle and wide-angle X-ray scattering (SAXS and WAXS) have long been established as a good technique for the morphology characterization of segmented polyurethanes.[11] WAXS provides information about the semicrystalline character of polymers through Bragg's Law scattering between coordinated polymer segments. While these semicrystalline peaks are not as sharp as those for pure crystalline materials, they still provide considerable insight into the crystalline structure with a polyurethane phase. In SAXS, the periodic spacing of the two polyurethane microphases leads to Bragg's Law-type scattering at lower angles. The contrast mechanism for this scatter is the electron density difference between the hard and soft phases. To simplify analysis in this work, the scattering vector s for both SAXS and WAXS is defined using the following relationship:

$$s = 2\sin\theta/\lambda$$

where $2\theta$ is the diffraction angle and $\lambda$ is the radiation wavelength. The crystalline spacing and average interdomain spacing are thus given by the reciprocal of the scattering vector at peak intensity in WAXS and SAXS, respectively.

The thermal analysis described in the Section 3.3.1 suggests a partial disruption of hard segment crystallinity due to the presence of aromatic diisocyanates in the HT and HM samples. This result was confirmed through the use of WAXS to examine the correlation distances between semicrystalline hard segments. Figure 3.5 shows the isotropic WAXS patterns from H-29, HT-29 and HM-29, along with a specially synthesized pure HDI-BDO hard segment. The three crystalline peaks for HDI-BDO labeled A, B, and C correspond to d-spacings of 4.4 Å, 4.1 Å, and 3.7 Å, and are clearly

reproduced in the pattern for H-29. However, peaks A and B are suppressed in both HT-29 and HM-29, due to the interruption of HDI crystal structures by the aromatic TDI and MDI units.

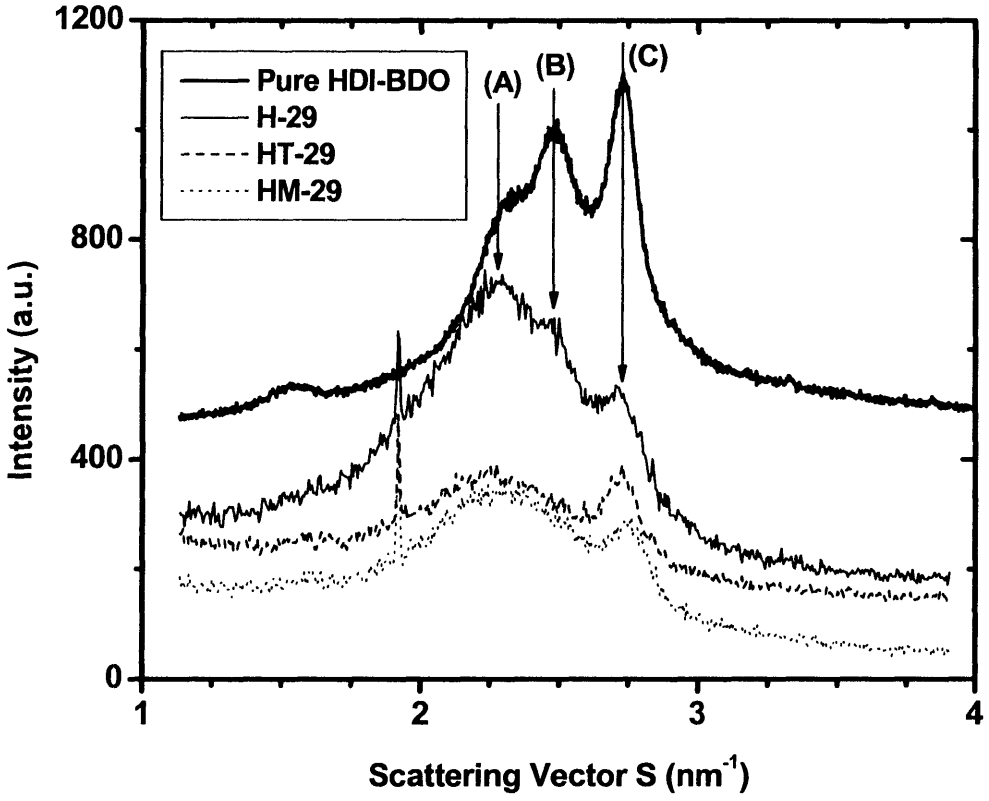


**Figure 3.5 WAXS patterns of polyurethanes with mixed hard segments show suppression of the peaks from HDI-BDO crystallites.**

The isotropic SAXS profiles for the synthesized polyurethanes are presented in Figure 3.6, and broken into two panels based on the soft segment length. The average interdomain spacings corresponding with each of the scattering peaks are tabulated in Table 3.3. As expected, the polyurethanes with PTMO-2900 soft segments exhibit larger interdomain spacings than those with PTMO-2000 soft segments. All polyurethanes

were designed with hard segments of similar size, using a 5:4:1 ratio of diisocyanates to chain extender to macrodiols. However, the polyurethanes containing two TDI units exhibit a larger interdomain spacing than those with just HDI, and the polyurethanes with two MDI units exhibit the largest interdomain spacing. The more flexible aliphatic HDI unit has the ability to fold back on itself, so the contracted domain spacing likely indicates a more compact hard domain structure.[12]

**Table 3.3 Average interdomain spacings of segmented polyurethanes, obtained from SAXS**

| Sample | Average Interdomain Spacing (nm) |
|---|---|
| H-20 | 14 |
| H-29 | 16 |
| HT-20 | 17 |
| HT-29 | 20 |
| HM-20 | 18 |
| HM-29 | 25 |
| HM-29-T | 24 |
| HM-29-S | 21 |

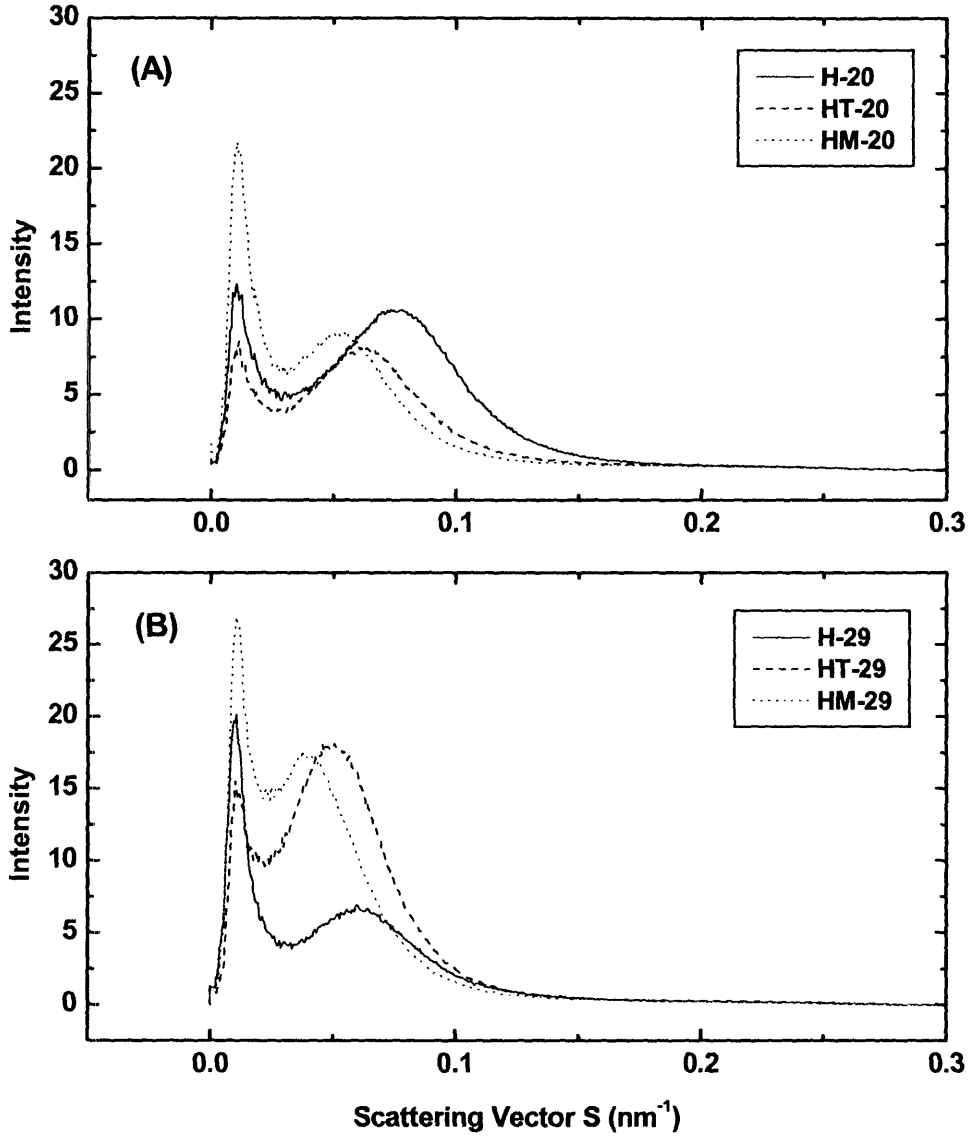


**Figure 3.6 SAXS profiles of polyurethanes with (A) PTMO-2000 soft segments and (B) PTMO-2900 soft segments.**

Tapping-mode atomic force microscopy (AFM) has also been demonstrated to be a good technique for observing the morphology of polyurethane films.[13],[14] The phase image provides contrast based on the difference in moduli of the hard and soft domains. Segmented polyurethane films typically form a layer of soft segment on the

film surface; however, if the tapping force is elevated, it is possible to image the bulk morphology underneath. By testing several different microphase-separated polymers, McLean and Sauer demonstrated that the higher phase signal, or the brighter region of the phase image, corresponds with the hard domains of segmented polyurethanes.[13] The phase images of H-29, HT-29 and HM-29 films are shown together in Figure 3.7, while the phase images of H-20 and HT-20 are shown in Figure 3.8. The resolution of the hard domains is limited by the AFM tip size, which has a diameter of ~10 nm. However, it is possible to measure the interdomain spacings of each sample, which correspond well to the spacings determined earlier by SAXS. In addition, AFM phase images also provide a method to observe the connectivity of the hard domains, which is not observable by SAXS. Comparing the images of H-29 to HT-29 in Figure 3.7, we observe that HT-29 forms larger, more continuous domains, 300-600 nm in length, while the H-29 films from shorter domains, only 50-100 nm in length. This trend is duplicated in the PTMO-2000 based polyurethanes in Figure 3.8, with H-20 forming shorter domains than HT-20, although the difference is less dramatic.

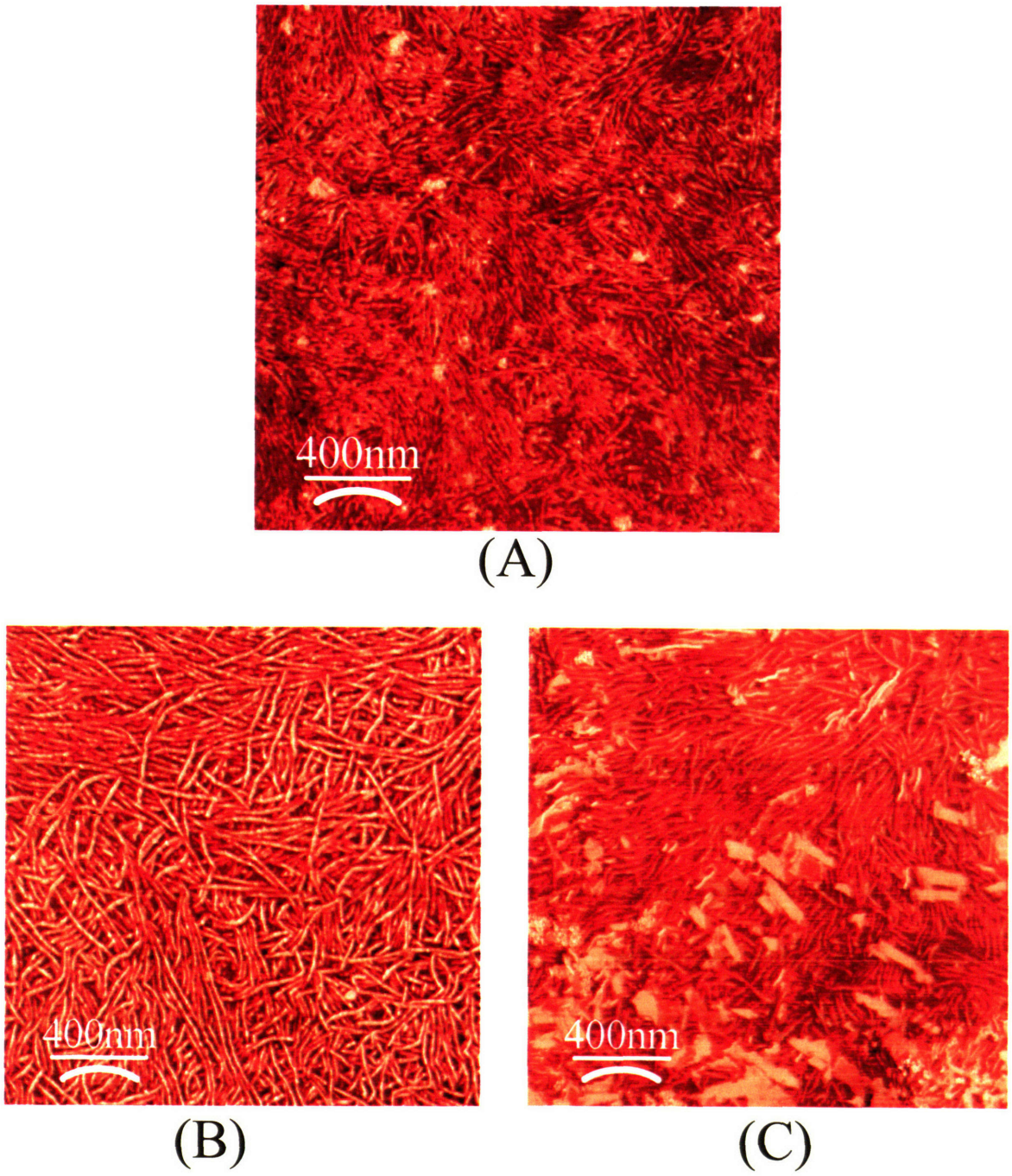


**Figure 3.7 Tapping-mode AFM phase images of PTMO-2900 based polyurethane films: (A) H-29, (B) HT-29, and (C) HM-29**

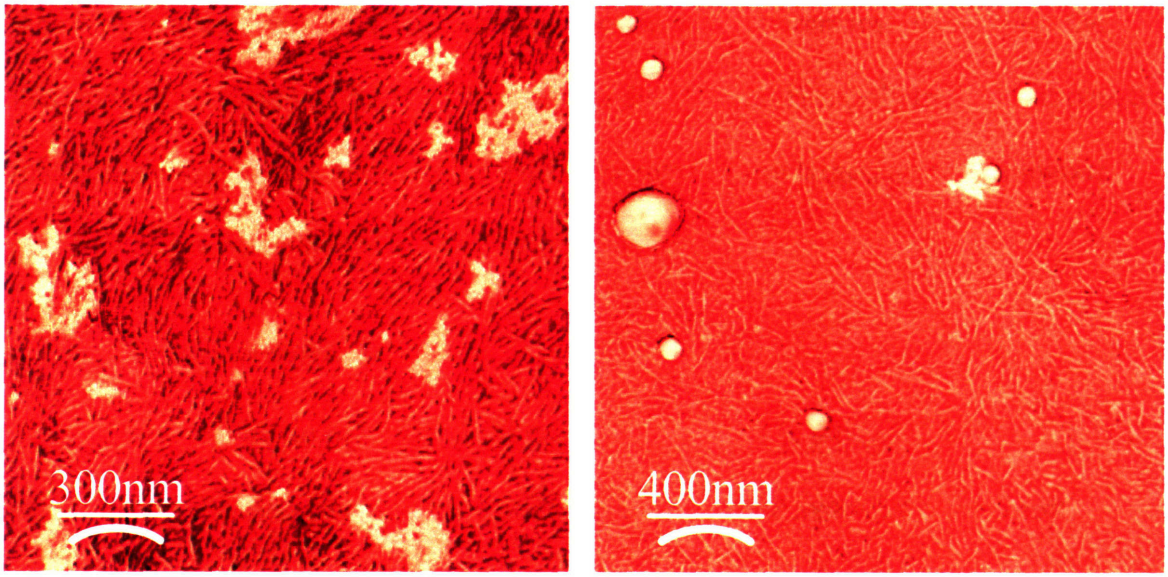


(D) (E)

**Figure 3.8 Tapping-mode AFM phase images of PTMO-2000 based polyurethane films: (D) H-20 and (E) HT-20**

The suppressed crystallinity of HT-29 and HM-29 observed by DSC and WAXS is likely responsible for their better hard domain organization. When cooling below the hard segment melting point or casting a film from solution, a competition exists between the thermodynamic incompatibility of the two phases and the crystallization of the hard segments. Register *et al.* studied the competition between these modes of microphase segregation in semicrystalline diblock copolymers containing a highly crystalline ethylene block and an amorphous methylbutylene or styrene-ethylene-butylene block.[15, 16] In these asymmetric diblocks, it is possible to confine the crystallization of ethylene within spherical or cylindrical microdomains. However, as the interblock segregation becomes too weak, the ethylene crystallization disrupts the microdomain structure and alters the crystallization kinetics. In the H-series of polyurethanes studied here, the microphase segregation appears to be driven by the fast crystallization of HDI-BDO hard segments. The hard domains formed in this manner are already locked into a crystal

structure, limiting their ability to rearrange and form larger domains. In contrast, the thermodynamic incompatibility of the phase in the HT- and HM-polyurethanes drives the microphase segregation, allowing the hard segments to form larger, more continuous domains before being locked in by a crystal structure.

### *3.3.3 Mechanical Behavior*

The stress-strain behavior of the polyurethane films is plotted in Figure 3.9, with plots (A) and (B) each comparing the different hard segment types for a fixed soft segment length. Each curve represents the average of three tested samples, and the averages and standard deviations of the mechanical properties are listed in Table 3.4. In general, the H-series polyurethanes exhibit an initial modulus typical of segmented polyurethanes, then begin to yield around 25% strain, after which they maintain a very linear profile until breaking at 400-500% strain. In contrast, the polyurethanes with mixed hard segments (HT and HM series) generally exhibit lower yield strengths, but have higher initial moduli, higher ultimate tensile strengths and higher extensibility than pure HDI polyurethanes. Polyurethane HM-20 had the poorest mechanical properties, although this is explained by synthetic problems that led to the broad molecular weight distribution observed in GPC. The broad distribution of polymer chain lengths is likely accompanied by a broad distribution of hard segment sizes, which do not as readily form a well-connected polyurethane network structure.

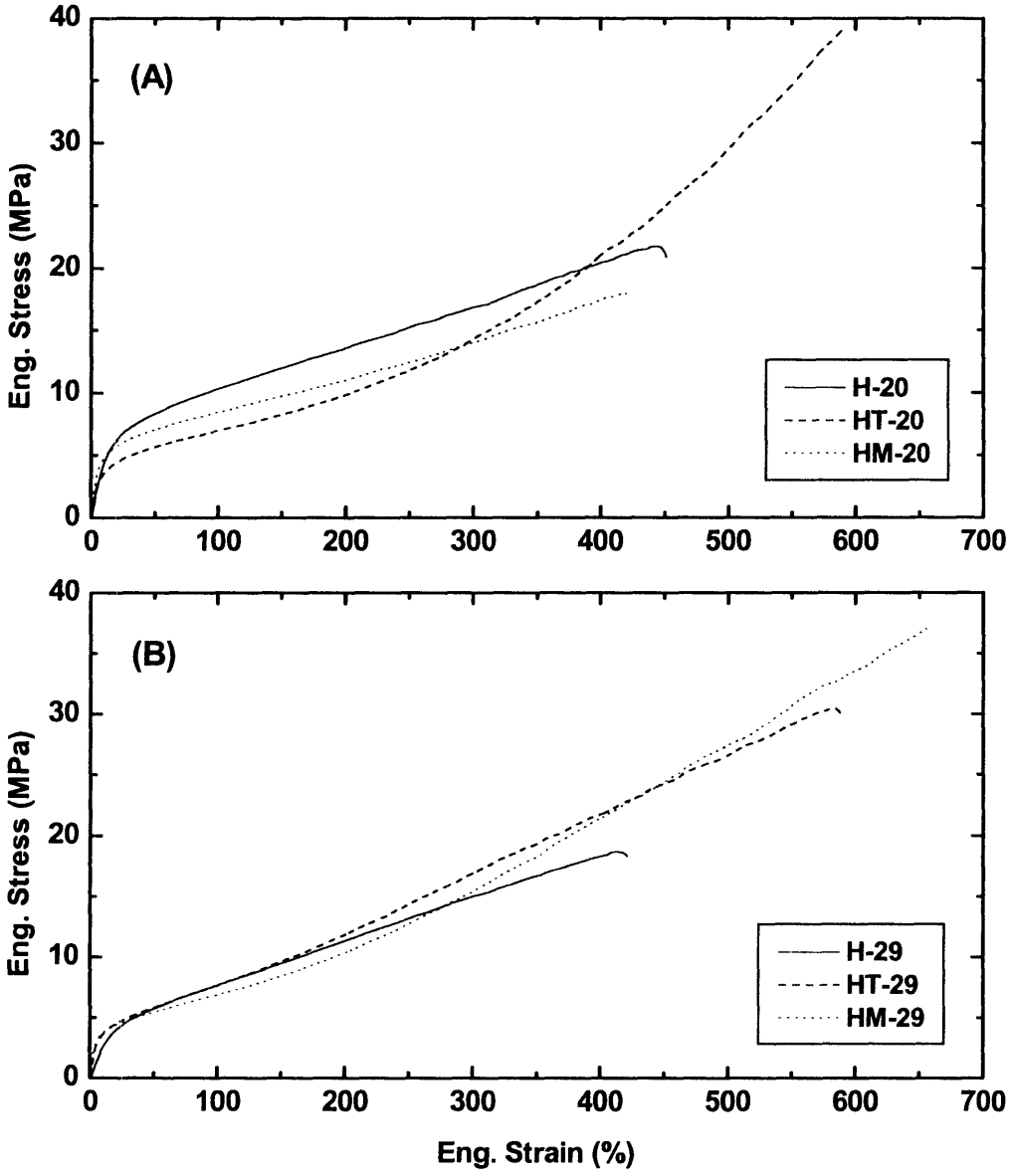


**Figure 3.9 Stress-Strain Behavior of polyurethanes with (A) PTMO-2000 soft segments and (B) PTMO-2900 soft segments.**

Samples HT-29 and HM-29 exhibit a small amount of strain hardening above 300% strain, while HT-20 exhibits pronounced strain hardening from 300% to 600% strain. This strain hardening is also observed in polyurethanes with pure MDI and TDI hard segments,[9] but the presence of strongly hydrogen-bonding HDI in the mixed hard

segments increases the initial modulus relative to these other pure hard segments. The combination of two diisocyanates appears to be a potential method for disrupting the crystallinity of HDI hard domains while retaining its strong phase segregation and hard domain integrity, leading to better tensile properties.

**Table 3.4 Summary of mechanical properties of polyurethane films**

| Sample | Modulus (MPa) | Tensile Strength (MPa) | Extensibility (%) | Toughness (MPa) |
|---|---|---|---|---|
| H-20 | 50 ± 2 | 21 ± 2 | 456 ± 26 | 64 ± 8 |
| H-29 | 29 ± 5 | 19 ± 3 | 443 ± 30 | 51 ± 7 |
| HT-20 | 57 ± 12 | 41 ± 2 | 612 ± 19 | 107 ± 8 |
| HT-29 | 57 ± 5 | 30 ± 2 | 577 ± 11 | 96 ± 7 |
| HM-20 | 77 ± 7 | 17 ± 1 | 421 ± 29 | 45 ± 6 |
| HM-29 | 66 ± 4 | 37 ± 2 | 652 ± 37 | 121 ± 12 |
| HM-29-T | 26 ± 2 | 12 ± 1 | 506 ± 13 | 33 ± 1 |
| HM-29-S | 47 ± 9 | 13 ± 2 | 481 ± 41 | 36 ± 7 |

Polyurethane samples were also deformed using a hysteresis loop, to compare the energy dissipation by the various hard segment types. Films were deformed in tension to 100% strain, relaxed to zero stress, deformed to 300% strain, and relaxed again. The percent hysteresis was calculated as the difference in area between the loading and unloading curves for each cycle. The hysteresis values for all the synthesized polyurethanes are presented in Table 3.5. The hysteresis at high extensions is similar for all studied samples, with a large amount of plastic deformation due to the strain-induced crystallization of PTMO soft segments. However, there is a distinct difference in the hysteresis at 100% strain between the samples with mixed hard segments and HDI hard segments. The polyurethanes containing MDI units undergo a more pronounced hysteresis as the rigid diisocyanates deform in a less reversible manner, strongly aligning with the direction of strain. These deformation mechanisms are examined in more detail by X-ray scattering and optical microscopy in Chapter 4.

**Table 3.5 Hysteresis of polyurethane films stretched to 100% and 300% strain under cyclic loading conditions**

| Sample | Hysteresis at 100% | Hysteresis at 300% |
|---|---|---|
| H-20 | 68% | N/A |
| H-29 | 65% | 84% |
| HT-20 | 65% | 80% |
| HT-29 | 76% | 86% |
| HM-20 | 77% | 85% |
| HM-29 | 73% | 83% |
| HM-29-T | 76% | 84% |
| HM-29-S | 73% | 81% |

### *3.3.4 Effect of Isocyanate Addition Method*

Two additional samples were synthesized in order to examine the role of the prepolymer synthesis technique described in the previous section. Prisacariu *et al.* synthesized segmented polyurethanes with a mixture of MDI and 4,4'-dibenzyl diisocyanate (DBDI) and found that the properties improved when the isocyanates were added together in a random fashion, rather than in a separate prepolymer stage.[17] HM-29-T was synthesized in the two-step method by endcapping with MDI and then chain extending with HDI and 1,4-butanediol. HM-29-S was synthesized by adding HDI and MDI in a single step, and then chain extending with 1,4-butanediol. Both samples were smaller in molecular weight than the rest of the series, but similar enough to each other to enable comparison.

The DSC traces for these comparison samples are shown in Figure 3.10, and their melting points and enthalpies are included in Table 3.2. Sample HM-29-S, which had a mixture of HDI and MDI units added at once, exhibited a hard segment melting point 20 °C lower than HM-29-T, the sample made by the two-step prepolymer method. HM-29-S also had a hard segment melting enthalpy 30% lower than HM-29-T. This decreased

hard domain ordering is also reflected by the interdomain spacing observed in SAXS and listed in Table 3.3. HM-29-S has a smaller interdomain spacing, indicating that as the two diisocyanates are added in the same step, a broader distribution of hard segment sizes occurs, creating a weaker periodic structure.

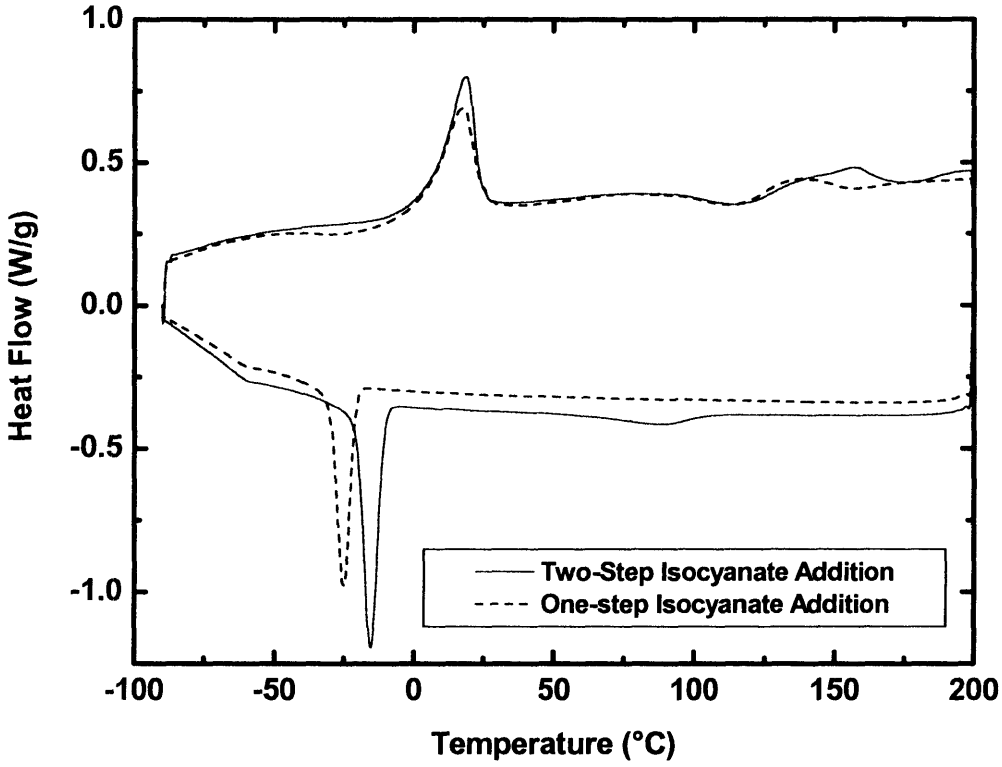


**Figure 3.10 DSC comparison of diisocyanate addition methods. Diisocyanates added in one step form hard domains with a lower melting point and melting enthalpy.**

The reduction of hard domain ordering created by the simultaneous addition of HDI and MDI results in improved polyurethane mechanical properties, as shown in Figure 3.11 and listed in Table 3.4. HM-29-S has a slightly reduced elongation at break, but a distinctly higher modulus and ultimate tensile strength. While these mechanical properties are below the higher molecular weight polymers listed in Table 3.4, they still

show that the addition of diisocyanates in one step results in an improved modulus and tensile strength without a loss of extensibility.

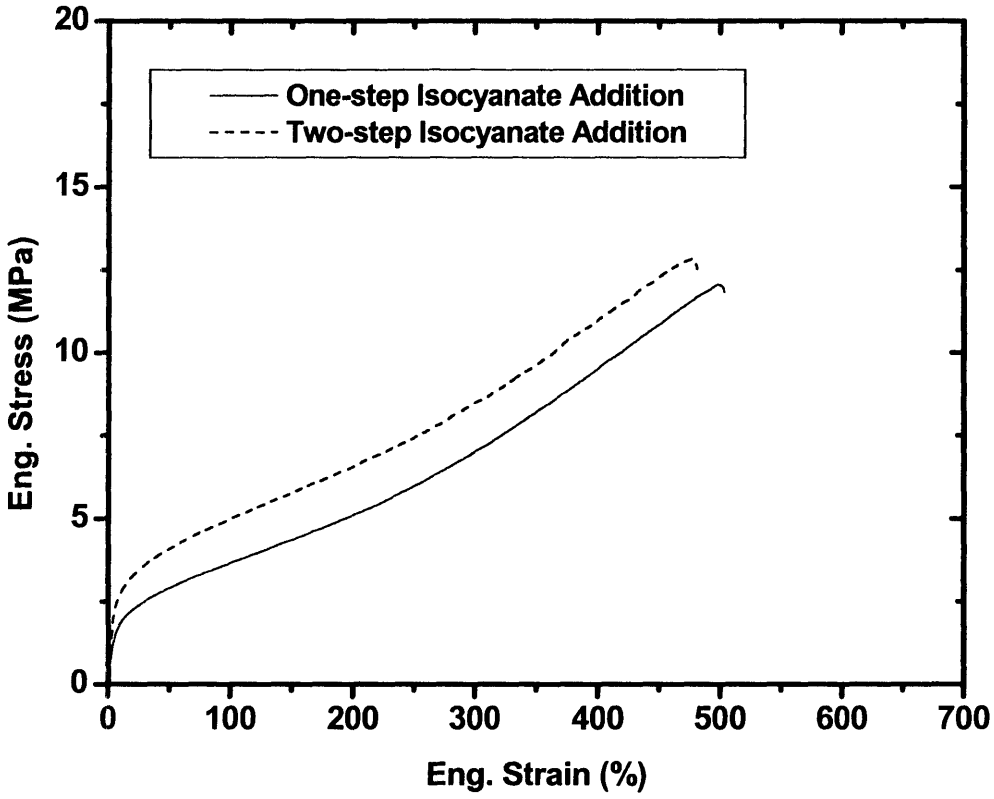


**Figure 3.11 Tensile comparison of HM-29 polyurethanes synthesized using a one-step or two-step isocyanate addition.**

### *3.3.5 Annealing Effects on Microphase Separation*

Polyurethanes containing HDI hard segments have been shown to be relatively insensitive to annealing, since the hard segments quickly organize into hard domains and microphase segregate during film casting.[18] A small study of annealing conditions was performed on the HT and HM polyurethanes to confirm the lack of importance of annealing on these particular samples. Several samples were annealed at 130 °C under

vacuum for 1 hour and then slowly cooled to room temperature over several more hours. The annealed films were then compared to unannealed films by DSC, SAXS, and mechanical testing. A comparison of selected properties from these techniques is presented in Table 3.6. The melting point and enthalpy of melting of the hard domains, as well as the interdomain spacings are all relatively insensitive to the annealing, indicating that the hard domains are well-formed upon initial casting, without a subsequent annealing step. In addition, the mechanical properties of the annealed and unannealed samples are within error of each other, confirming that the structure and properties both remain unchanged with annealing.

**Table 3.6 Comparison of annealing conditions on selected polyurethane properties**

| Property | HT-29, Unannealed | HT-29, Annealed 130 °C | HM-29, Unannealed | HM-29, Annealed 130 °C |
|---|---|---|---|---|
| $T_{m,\,HS}$ (°C) | 161 | 162 | 163 | 163 |
| $\Delta H_{m,\,HS}$ (J/g HS) | 72 | 51 | 34 | 43 |
| Domain Spacing (nm) | 20 | 20 | 25 | 23 |
| Modulus (MPa) | 57 ± 5 | 61 | 66 ± 4 | 65 |
| Tensile Strength (MPa) | 30 ± 2 | 30 | 37 ± 2 | 30 |
| Extensibility (%) | 577 ± 11 | 624 | 652 ± 37 | 655 |
| Toughness (MPa) | 96 ± 7 | 108 | 121 ± 12 | 102 |

## 3.4 Conclusions

A series of segmented polyurethanes were synthesized with mixed diisocyanates within the hard segment. These "mixed hard segments" exhibited less crystallinity than pure HDI-BDO hard segments, as shown by DSC. Though the hard segment crystallinity is reduced, the polyurethanes with mixed hard segments have a similar degree of microphase segregation between the hard and soft segments, as indicated by DMA and SAXS. The suppressed crystallinity of the mixed hard segments allows the polyurethane

to form more well-organized hard domains seen in AFM imaging. The mixed hard segment domain formation is governed by the $\chi$-interaction between the hard and soft phases, and grows more continuous without being trapped by hard segment crystallinity. These more interconnected hard domains allow the polyurethane to deform to higher elongations and absorb more energy during tensile testing, without decreasing their initial modulus. The method of diisocyanate incorporation was also examined, and the hard domain crystallinity is further reduced by the addition of both diisocyanates simultaneously, instead of in a separate prepolymer step. The polyurethane with diisocyanates added in one step also exhibited improved mechanical properties, as expected from the reduction of hard segment crystallinity.

## 3.5 References


1. Meckel, W., W. Goyert, and W. Wieder, *Thermoplastic Polyurethane Elastomers*, in *Thermoplastic Elastomers*, G. Holden, et al., Editors. 1996, Hanser: Munich.
2. O'Brien, J.P., et al., *Nylons from Nature: Synthetic Analogs to Spider Silk.* Advanced Materials, 1998. **10**(15): p. 1185-1195.
3. Termonia, Y., *Molecular Modeling of Spider Silk Elasticity.* Macromolecules, 1994. **27**: p. 7378-7381.
4. Havens, J.R. and D.L. VanderHart, *Morphology of Poly(ethylene terephthalate) Fibers As Studied by Multiple-Pulse 1H NMR.* Macromolecules, 1985. **18**: p. 1663-1676.
5. Baker, A.M.E. and A.H. Windle, *Evidence for a partially ordered component in polyethylene from wide-angle X-ray diffraction.* Polymer, 2001. **42**: p. 667-680.
6. Oda, D.C. and G.C. Rutledge, *Molecular structure and orientation in processed polymers 1. Analysis of X-ray scattering data.* Polymer, 1999. **40**: p. 4635-4646.
7. Huy, T.A., et al., *Influence of interfacial structure on morphology and deformation behavior of SBS block copolymers.* Polymer, 2003. **44**: p. 1237-1245.

8. Flory, P.J., *Principles of Polymer Chemistry*. 1953, Ithaca: Cornell Univ. Press.
9. Lee, D.-K. and H.-B. Tsai, *Properties of Segmented Polyurethanes Derived from Different Diisocyanates.* Journal of Applied Polymer Science, 2000. **75**: p. 167-174.
10. Ng, H.N., et al., *Effect of segment size and polydispersity on the properties of polyurethane block polymers.* Polymer, 1973. **14**: p. 255-261.
11. Tyagi, D., J.E. McGrath, and G.L. Wilkes, *Small Angle X-ray Studies of Siloxane-urea Segmented Copolymers.* Polymer Engineering and Science, 1986. **26**(20): p. 1371-1398.
12. Li, Y., et al., *Multiphase Structure of Segmented Polyurethanes: Effects of Hard-Segment Flexibility.* Macromolecules, 1993. **26**: p. 612-622.
13. McLean, R.S. and B.B. Sauer, *Tapping-Mode AFM Studies Using Phase Detection for Resolution of Nanophases in Segmented Polyurethanes and Other Block Copolymers.* Macromolecules, 1997. **30**: p. 8314-8317.
14. Aneja, A. and G.L. Wilkes, *A systematic series of 'model' PTMO based segmented polyurethanes reinvestigated using atomic force microscopy.* Polymer, 2003. **44**: p. 7221-7228.
15. Quiram, D.J., G.R. Marchand, and R.A. Register, *Crystallization of Asymmetric Diblock Copolymers from Microphase-Separated Melts.* Macromolecules, 1997. **30**: p. 4551-4558.
16. Loo, Y.-L., A.J. Ryan, and R.A. Register, *Modes of Crystallization on Block Copolymer Microdomains: Breakout, Templated, and Confined.* Macromolecules, 2002. **35**: p. 2365-2374.
17. Prisacariu, C., et al., *The effect of hard segment ordering in copolyurethane elastomers obtained by using simultaneously two types of diisocyanates.* Polymer, 2003. **44**: p. 5407-5421.
18. Chu, B., et al., *Microphase Separation Kinetics in Segmented Polyurethanes: Effects of Soft Segment Length and Structure.* Macromolecules, 1992. **25**: p. 5724-5729.

# Chapter 4: Morphology of Segmented Polyurethanes with Mixed Hard Segments under Deformation

## 4.1 Introduction

The mechanical behavior of segmented polyurethanes is strongly related to the development of the microphase segregated polyurethane structure during deformation. As observed in chapter 3, polyurethanes with mixed hard segments exhibit a different mechanical response than pure HDI-BDO polyurethanes, which can be explained by an examination of the differences in their respective morphology development. It is desired to establish a correlation between the microstructure of polyurethanes with mixed hard segments and their improved mechanical properties, by understanding how their deformation mechanism differs from that of HDI-BDO polyurethanes.

Bonart *et al.* first examined the deformation of segmented polyurethanes using small-angle and wide-angle X-ray scattering, establishing that the hard segments form microphase segregated domains that function as physical crosslinks.[1],[2] As the domains are deformed at strains below 300%, the soft segments exert a torque on the hard domains, tilting them toward the strain direction. At higher strains, paracrystalline hard segments such as MDI-ethylene diamine or MDI-hydrazine can break apart from the domains and orient parallel to the strain direction, as the stress is transferred to strain-induced crystallites of the PTMO soft segments. For crystalline MDI-BDO hard segments, the hard domains behave more like inert fillers during deformation, and are

less capable of reorganizing at high strains. Bonart's proposed model for the deformation of a paracrystalline thermoplastic elastomer is reproduced in Figure 4.1.

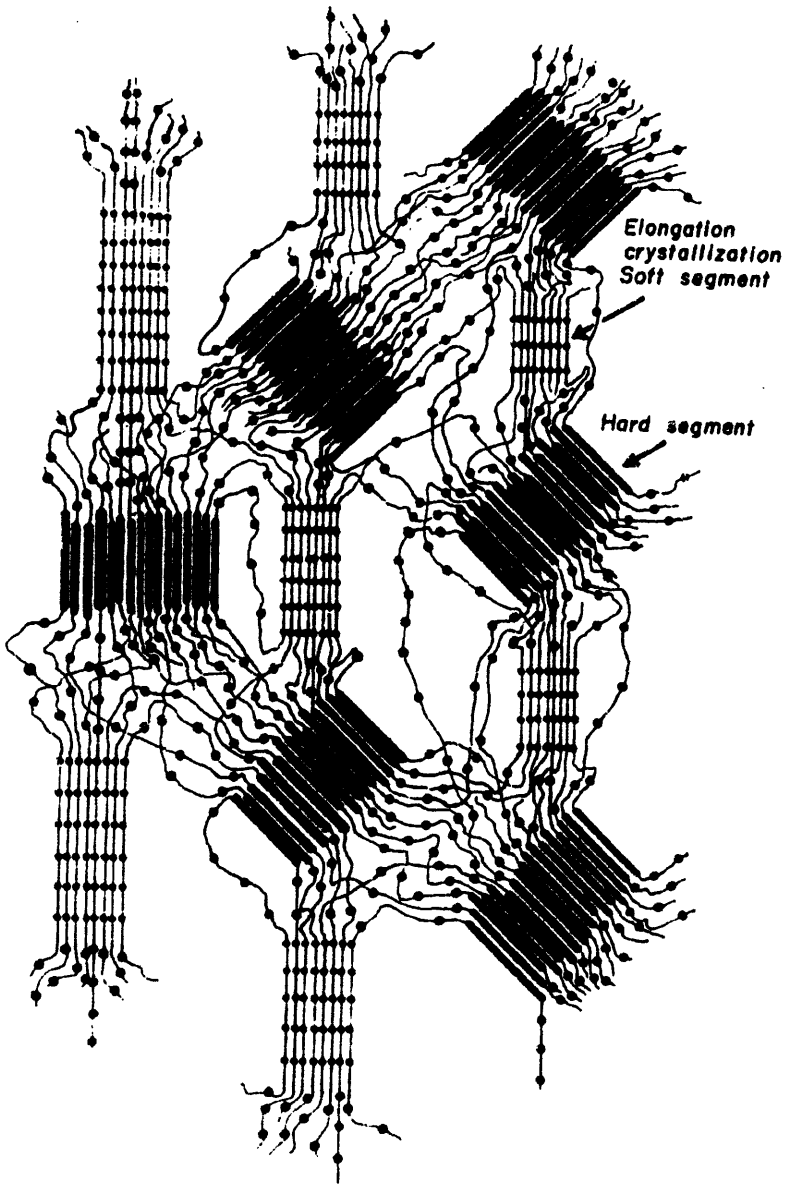


**Figure 4.1 Model of deformation behavior of a polyurethane with paracrystalline hard segments[1]**

Desper *et al.* also examined the deformation of segmented polyurethanes using SAXS, and discovered two dominant response mechanisms of the polyurethane network to tensile deformation, depending on the shape and structural rigidity of the hard domains, as depicted in Figure 4.2.[4] Hard domains with a high degree of structural

integrity and a high aspect ratio (L/D >> 1) deform through a shearing mechanism, due to a torque on the hard domains caused by the alignment of soft segment chains. This shearing mechanism tilts the hard domains at a preferred angle, resulting in a four-point scattering pattern, and induces a lower level of hysteresis, as the hard domains remain connected longer. In contrast, hard domains with a smaller aspect ratio and less ordered morphologies deform through a tensile mechanism, due to the separation of hard domains as the soft segments align. This tensile mechanism orients the hard segments parallel to the elongation, resulting in a two-point scattering pattern along the meridian, and induces a higher level of hysteresis. Blundell *et al.* also examined the deformation of thermoplastic polyurethanes using SAXS, and found deformation mechanisms similar to the work of Desper and coworkers.[5] For the interconnected hard domain morphologies, a four-point scattering pattern was observed due to structural reorganization. For the polyurethanes with fewer aggregated hard segments, affine deformation was observed, producing an elliptical scattering pattern on the meridian.

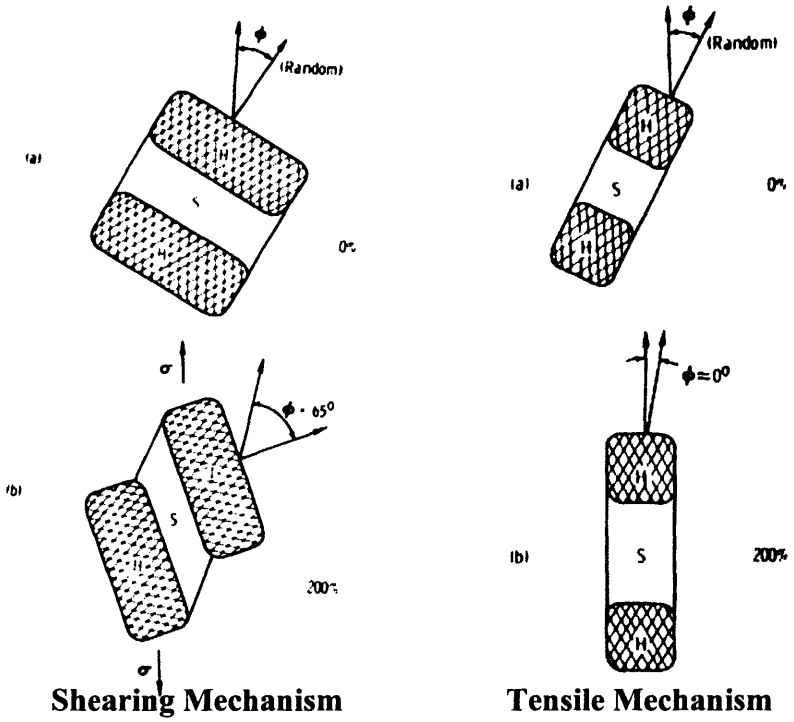


**Figure 4.2 Polyurethane deformation mechanisms based on hard segment rigidity and aspect ratio[4]**

Fourier transform infrared (FT-IR) dichroism has also been successfully utilized to study the relative orientation of polyurethane hard and soft segments during deformation.[3] This technique is based on tracking the dichroic ratio, or the ratio of polarized infrared absorption bands parallel and perpendicular to the strain direction. In these studies, it was observed that the orientation of the soft segment increased continuously during deformation. However, the orientation of the hard segments was observed to depend on whether the hard segments were crystalline or paracrystalline. The paracrystalline hard segments exhibited a positive dichroic ratio, aligning in the strain direction, while the crystalline hard segments exhibited a negative dichroic ratio at low strains. This negative orientation was interpreted as the rotation of rigid hard

domains, not individual hard segments, in the strain direction, in agreement with the scattering results of Bonart.

More recent studies of structural development in polyurethanes using simultaneous SAXS and WAXS, FT-IR dichroism, and AFM have expanded on these initial conclusions.[6],[7],[8] Lee *et al.* studied the deformation of polyurethanes with MDI-BDO hard segments using both FT-IR dichroism and SAXS, specifically examining the contribution of initial hard domain orientation on the mode of deformation.[7] Hard domain lamellae oriented perpendicular to the strain direction produced an increase in the average interdomain spacing under deformation, while lamellae aligned parallel to the strain direction decreased their interdomain spacing, due to shear compression, as shown in Figure 4.3. While the orientation of the soft segment increases linearly with strain, the orientation of the hard segment decreases initially, due to the rotation of the lamellar hard domain along the deformation direction. At high strains, the hard domains were broken up, and a fibril structure formed along the strain direction, in which the soft segments showed appreciable relaxation. AFM has also shown promise as a method for visual examination of morphology development, despite issues in reconciling the differences between surface and bulk morphology.[8]

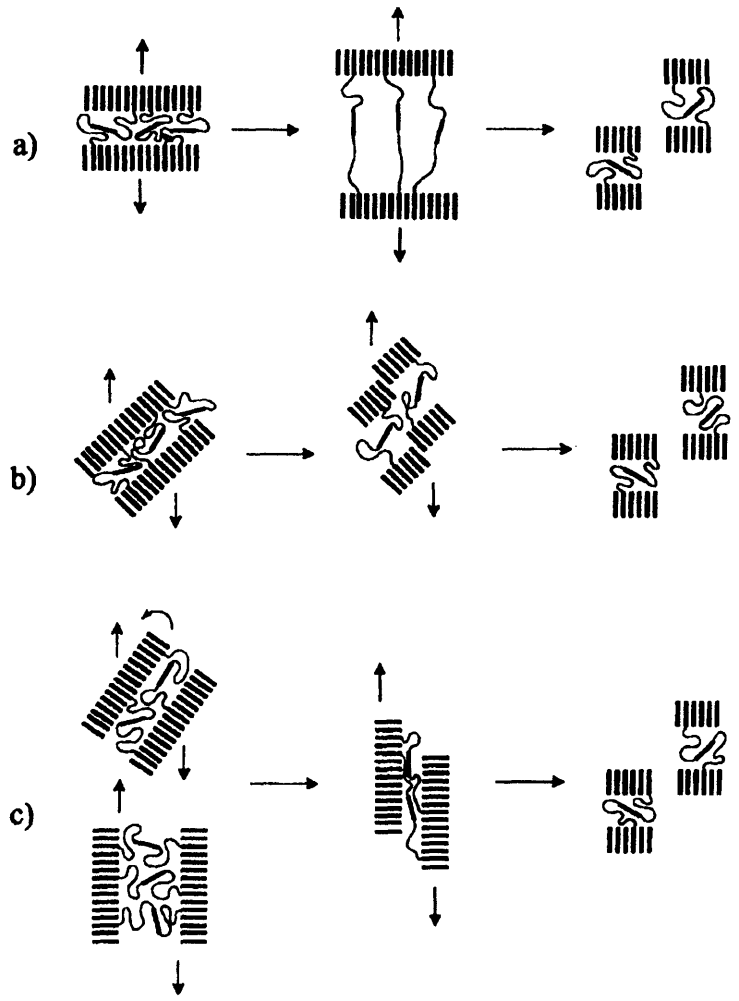


**Figure 4.3 Schematic model for the deformation of MDI-BDO hard domains at intermediate and high strains based upon initial orientation[7]**

## 4.2 Experimental

Small-angle X-ray scattering (SAXS) and wide-angle X-ray scattering were employed to examine the morphology of the segmented polyurethane films under tensile deformation. The synthesis of the segmented polyurethanes and the casting of thin films has already been described in Chapter 3.

### *4.2.1 Instrumentation*

#### 4.2.1.1 Synchrotron SAXS and WAXS

SAXS and WAXS data were simultaneous acquired for sample H-29 (HDI-BDO-PTMO, 29% hard segment) at the X27C beamline at the National Synchrotron Light Source (NSLS) at Brookhaven National Laboratory. The X-ray wavelength was 1.366 Å, which was monochromatized from the bending magnet using a double-multilayer (silicon/tungsten) monochromator. The typical flux was $9 \times 10^{11}$ photons/sec. The beam was collimated to a maximum spatial resolution of 100 nm using 3 pinholes. The relative X-ray intensity was measured before ($I_0$) and after ($I_1$) the sample using proportional counters. The scattered X-rays were detected using a Fuji BAS 2500 Imaging Plate System.

A home-built stretcher was used to elongate the ~0.1 mm thick films at a rate of 100% of their initial length per minute, which corresponds with the strain rate used to obtain the tensile data in Chapter 3. Scattering patterns were collected for 5 minutes at each strain position. A background pattern was also collected for 5 minutes within each sample environment. Each scattering pattern was then corrected using the formula:

$$\text{Corrected Pattern} = \text{Sample Pattern} - T^*(\text{Background Pattern}) \qquad (4.1)$$

T was taken to be the ratio $I_1(\text{sample})/I_1(\text{background})$ where $I_1$ was the measured beam intensity after the position of the sample or the sample environment.

#### 4.2.1.2 Optical Microscopy

A Carl Zeiss 2MAT Axioscope polarizing microscope equipped with crossed polarizers and a home-built static stretcher was used to visualize the anisotropy developed during deformation of the polyurethane films. All images were taken in transmission mode at 5x magnification.

### *4.2.2 Scattering Analysis*

SAXS and WAXS data were reduced from 2-D (Intensity vs. $2\theta,\chi$) to 1-D radial plots (Intensity vs. $2\theta$) or 1-D azimuthal plots (Intensity vs.$\chi$) by performing the appropriate integrations, where $2\theta$ is the scattering angle and $\chi$ is the azimuthal angle. Radial plots were generated at specific $\chi$ values (such as $0^o$ for an equatorial plot or $90^o$ for a meridional plot), by integrating over $\chi \pm 10^o$ for each value of $2\theta$. Azimuthal plots were generated at specific $2\theta$ values (corresponding to scattering peak positions) by integrating over $2\theta \pm 0.5^o$, for each value of $\chi$.

#### 4.2.2.1 WAXS Data Treatment

WAXS data are traditionally plotted as intensity versus scattering angle, $2\theta$. However, since the WAXS data being compared were from two sources with different wavelengths of radiation, the analysis was simplified by employing the use of a scattering vector. In this work the scattering vector s was defined as:

$$s = 2\sin(\theta)/\lambda \tag{4.2}$$

where Bragg's angle $\theta$ is one-half the radial scattering angle and $\lambda$ is the wavelength of the radiation, as previously specified. Bragg's Law thus specifies the crystalline d-spacing as the reciprocal of the peak position s.

4.2.2.2 SAXS Data Treatment

Similarly, SAXS data in this work were analyzed using the scattering vector s as previously defined. Note that the scattering vector s as defined here differs from the scattering vector q used in some SAXS literature:

$$q = 4\pi\sin(\theta)/\lambda = 2\pi * s \tag{4.3}$$

In analogy with Bragg's law, the average interdomain spacing, or long period between the hard and soft segments is thus given by the following relation:

$$L = 1/s = 2\pi/q \tag{4.4}$$

## 4.3 Results and Discussion

X-ray scattering is a powerful tool for analyzing the morphology development of segmented polyurethanes as a function of strain. SAXS provides information about the relative position of hard domains within the soft segment matrix, since the correlation length between hard domains gives rise to a scattering maximum in the small-angle region. Similarly, WAXS provides information about the relative position of crystalline or ordered hard segment and soft segment chains, as they both give rise to different crystalline reflections during deformation.

### *4.3.1 In-Situ SAXS*

To aid in the interpretation of 2-D SAXS results, Figure 4.3 shows the position of hard domains that give rise to various scattering positions. Hard segments are depicted as black rectangles, which organize in hard domains perpendicular to the long axis of the hard segments. The scattering peaks that occur in the small-angle regime are caused by the periodic spacing between the long axes of the hard domains, not the axes of the

individual hard segments. Samples were stretched vertically, so hard domains oriented perpendicular to the strain direction scatter along the meridian; conversely, hard domains oriented parallel to the strain direction scatter along the equator. Hard domains that tilt at a preferred angle produce a 4-point scattering pattern at their preferred angle. For example, in the cartoon in Figure 4.4, the hard domains aligned 30° from the strain direction produce scattering peaks at 30°, 150°, 210°, and 330°.

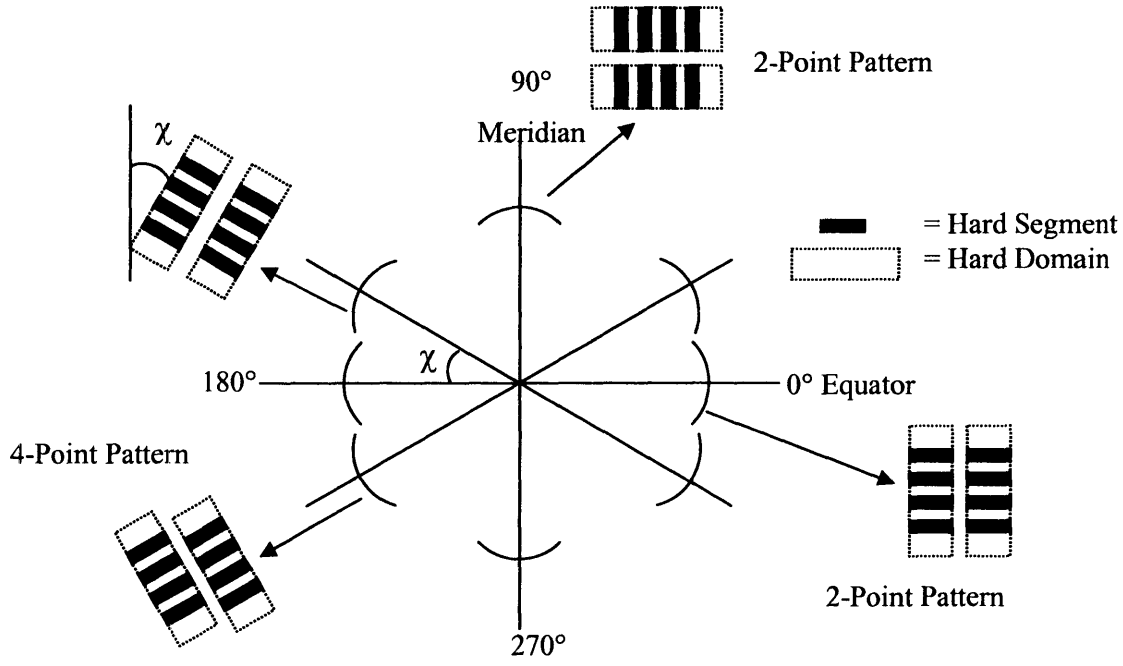


**Figure 4.4 Cartoon relationship between hard domain orientations and their corresponding scattering patterns**

The 2-D small-angle X-ray scattering patterns of polyurethane H-29 (HDI-BDO-PTMO, 29% hard segment) are shown as a function of time-averaged strain in Figure 4.5, along with cartoons representing the observed orientation behavior of the hard domains. As in Figure 4.4, the hard segments are depicted as black rectangles, and hard domains are indicated by dotted lines; the soft segments are omitted for clarity. Azimuthal scans at the average interdomain spacing are also shown in Figure 4.6 at various strain values. The isotropic scattering pattern at 0%, which indicates a random orientation of hard

domains, becomes increasingly anisotropic as a function of strain. Between 0% and 100%, scattering lobes appear at the equator, in a two-point pattern indicative of hard domains aligning in the direction of strain. Between 100% and 500%, the scattering lobes gradually sharpen into a six-point pattern, with the strongest peaks on the equator, and secondary peaks shifted from the equator by ±20°. This preferred tilt angle is caused by the torque exerted by the alignment of soft segment chains upon deformation.[1] Failure of the polyurethane occurs before the hard segments are able to completely rearrange in the strain direction, which would produce a sharp two-point pattern on the meridian. Unlike the segmented polyurethanes with MDI-BDO hard segments reported elsewhere[1], the HDI-BDO hard segments studied here are less able to break apart from existing hard domains and realign in a new domain during deformation, due to a stronger tendency for crystallization of the alkyl HDI hard segments and a greater degree of hydrogen bonding between hard segments.

The interdomain spacing of polyurethane H-29 was also measured as a function of strain in Figure 4.7, integrated over three directions of interest. When integrated over all azimuthal ($\chi$) angles, the average interdomain spacing increased from 17 nm to 22 nm, as most of the hard domains began to pull apart from each other during deformation. However, the hard domains oriented along the strain direction or at the preferred tilt angle both decreased their average spacing at high strain. The domains tilted at 20° from the strain direction decreased their spacing slightly, from 16.4 nm to 15.4 nm. This is consistent with the deformation of other hard domains that deform through a shearing mechanism.[4] The domains aligned along the strain direction exhibited the greatest decrease in average interdomain spacing, from 16.4 nm to 13 nm. This decrease is likely

due to the shear compression of hard domains that allows them to be spaced more closely at high strains, as illustrated in Figure 4.8.[7]

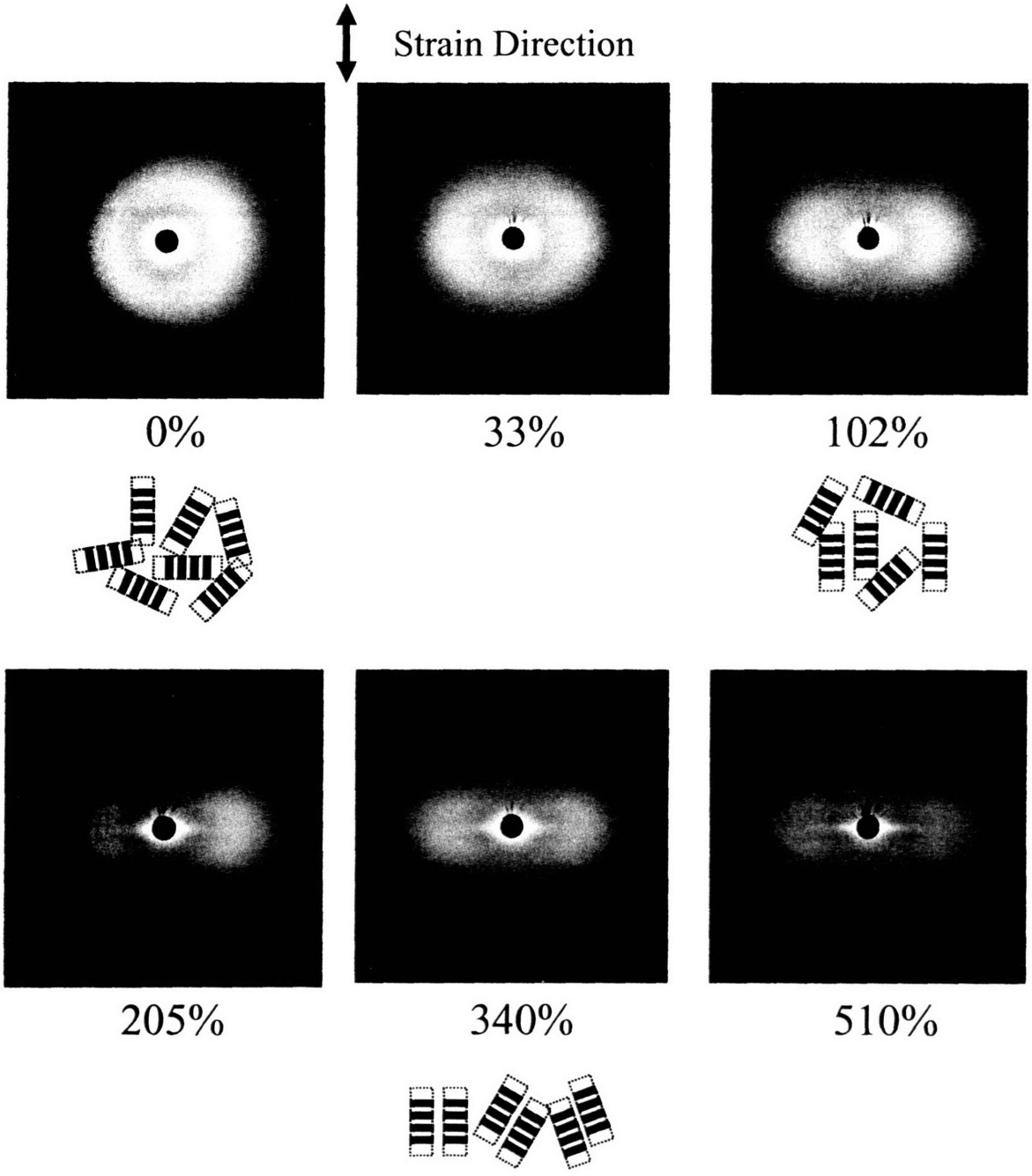


**Figure 4.5 Two-dimensional SAXS patterns of H-29 as a function of strain**

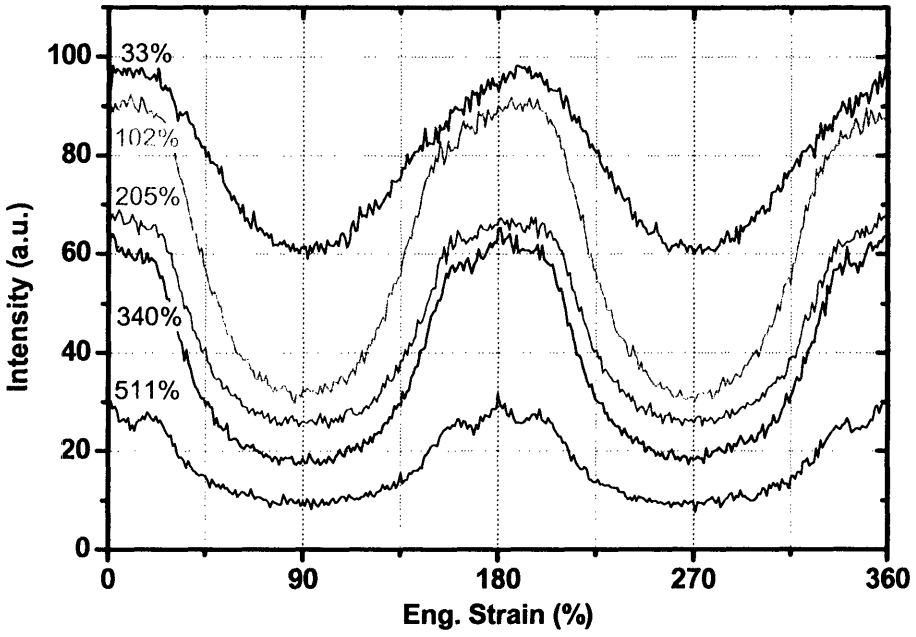


**Figure 4.6 Azimuthal plots of H-29 at the average interdomain spacing (17 nm) as a function of strain**

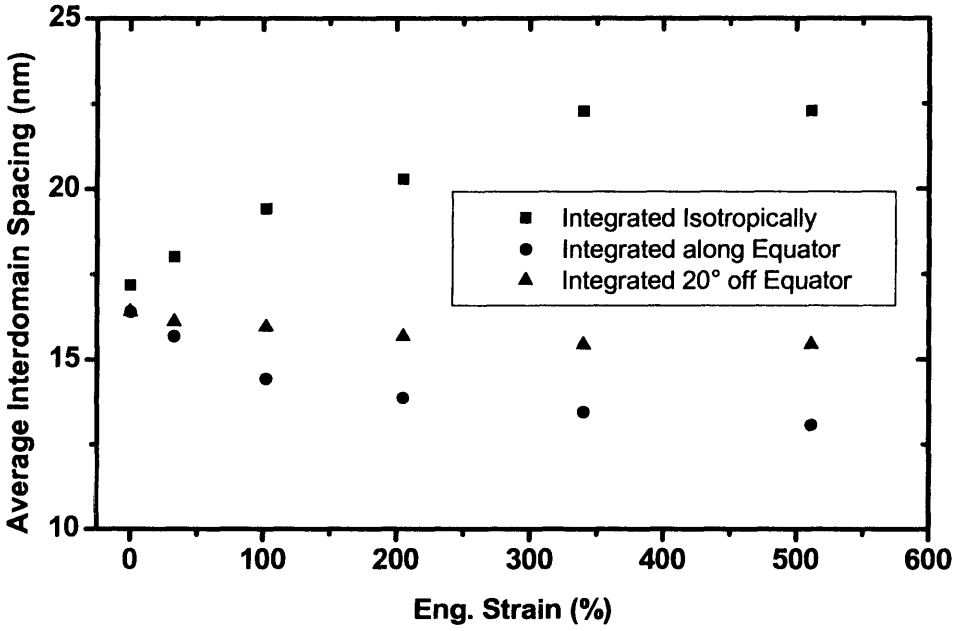


**Figure 4.7 Average interdomain spacing of H-29 integrated in several directions as a function of strain**

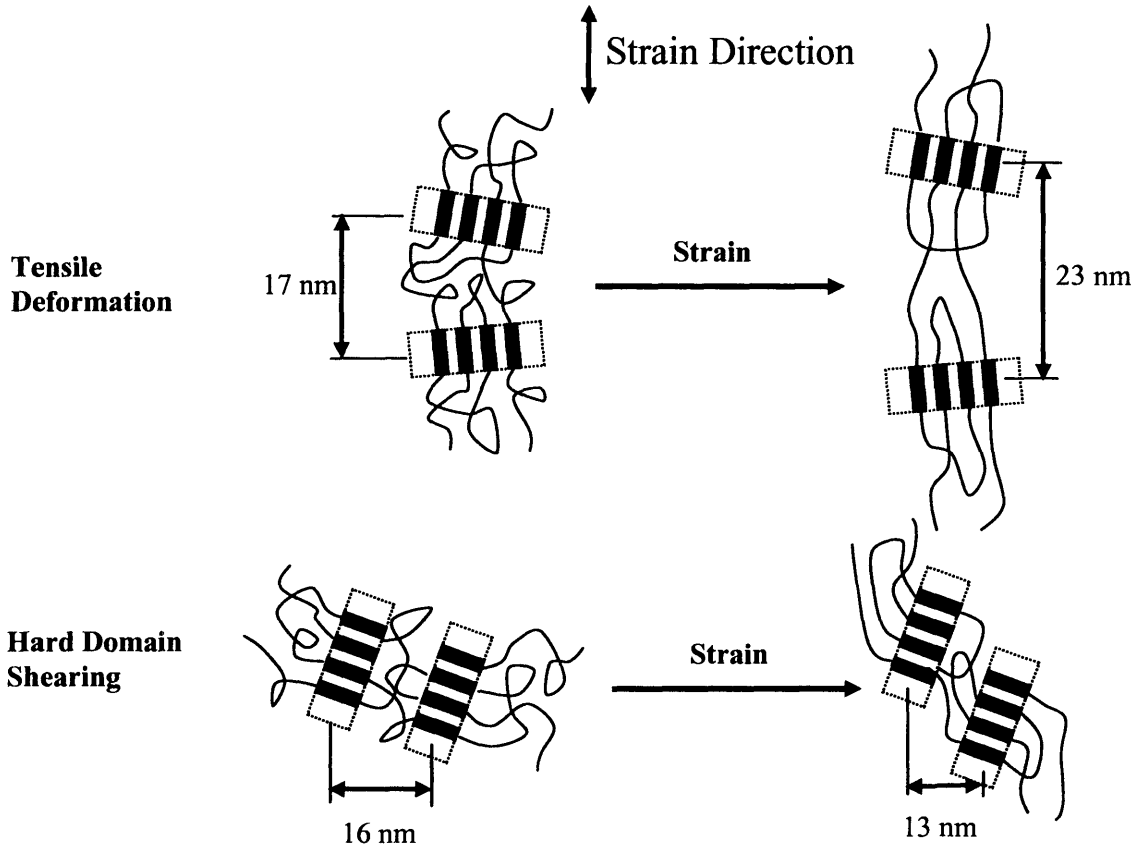


**Figure 4.8 Tensile deformation leads to an increase in the isotropic interdomain spacing, while the shearing of hard domains reduces the interdomain spacing along the equator and at ±20°.**

### *4.3.2 In-Situ WAXS*

The structural development under tensile deformation of the semicrystalline polyurethane H-29 was also examined by wide-angle X-ray, specifically observing the relative positions of crystalline hard and soft segments. The 2-D scattering patterns are shown as a function of strain in Figure 4.9, and these patterns are integrated in four different directions to give 1-D scattering profiles in Figure 4.10. To help assign scattering peaks to the hard segment or soft segment of this polyurethane, a special polyurethane was polymerized from HDI and 1,4-butanediol without any soft segment. This pure hard segment was also examined with WAXS, and its isotropic scattering

pattern is included in Figure 4.10(i). Initially, only three isotropic peaks are observed in H-29, which correspond with the three peaks identified in the HDI-BDO hard segment at d-spacings of 4.4 Å, 4.1 Å, and 3.7 Å, and are labeled A, B, and C, respectively. As the sample is deformed to 100% strain, two arcs appear along the equator at d-spacings of 4.4 Å and 3.7 Å. These two arcs resolve into clear spots by 500% strain, and correspond to the (002) and (202) reflections of PTMO crystallites, as observed in other multi-block copolymers with PTMO soft segments.[9],[10] The intensity of the PTMO reflections increases during deformation, as the sample undergoes strain-induced crystallization of the soft segment. Unfortunately, these two peaks partially overlap the crystalline or paracrystalline reflections from the HDI-BDO hard segments; however, the orientation of hard segments within hard domains can still be followed as a function of strain.

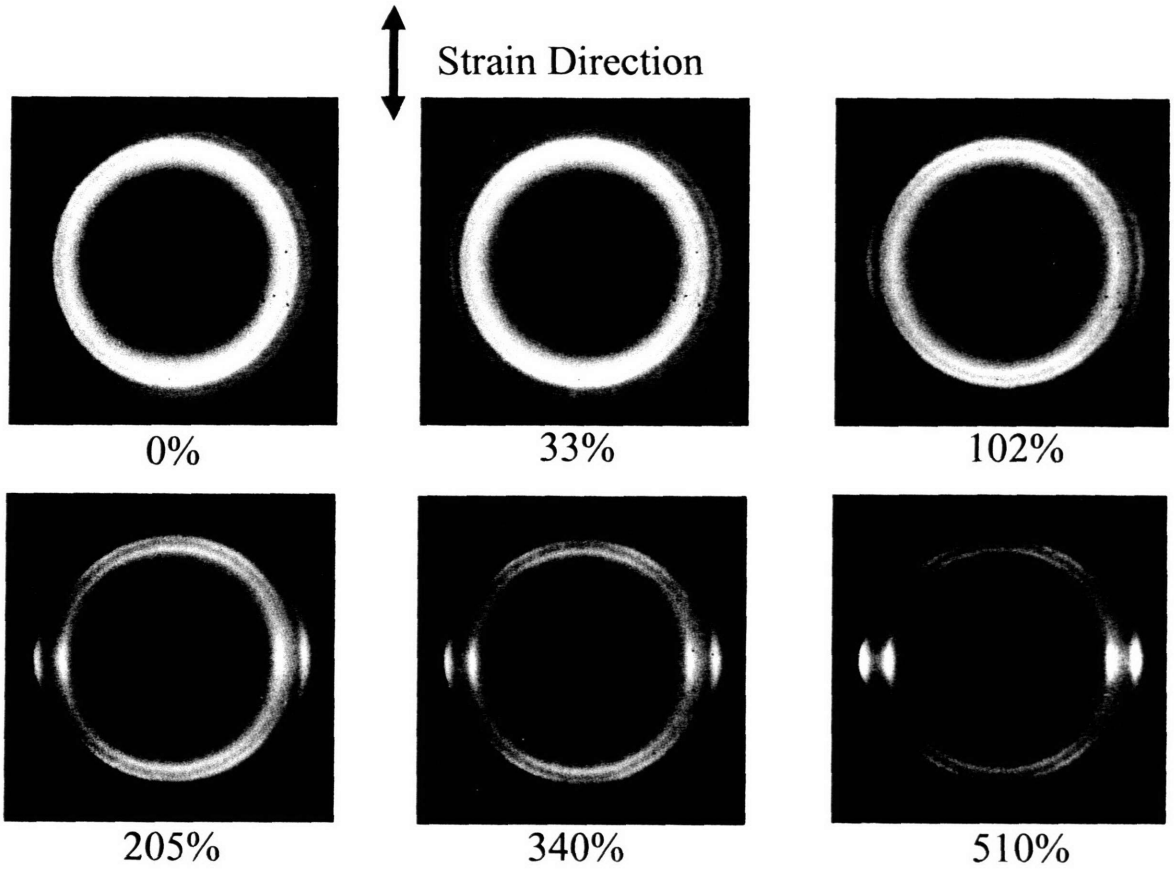


**Figure 4.9 Two-dimensional WAXS patterns of H-29 as a function of strain**

Azimuthal scans taken at each of the three HDI-BDO peak positions—A, B, and C—are presented in Figure 4.11. Peak A (4.4 Å) develops a preferred orientation of ±20° from the meridian, which suggests this reflection is related to the spacing of hard segments within hard domains that also adopt a preferred tilt angle of ±20°. The tilt angle for the individual hard segments is ±20° from the meridian, while the tilt angle for the hard domains is ±20° from the equator, due to the perpendicular orientation of hard segments within hard domains. According to Figure 4.11, peak B (4.1 Å) develops a preferred orientation of ±30° from the meridian. The increase in scatter along the equator that appears at high strain is caused by the strain-induced PTMO crystallites, though the intensity is far below the values for peaks A and C. The preferred orientation of peak B

at ±30° does not appear to be correlated with the orientation of sheared hard domains at ±20°. Instead, peak B is likely related to the correlation of hard segments that have broken free from the highly oriented hard domains and are now oriented along the strain direction. The ±30° orientation thus is not caused by the tilting of hard segments, but by the angular registration of hard segments as they separate from hard domains, as illustrated in Figure 4.12. It is important to note that while the intensity of peak B at a small azimuthal angle from the meridian does slightly increase at higher strains, there is still considerable scatter at peak A, even at 500% strain. This indicates that unlike polyurethanes with paracrystalline hard segments like MDI-BDO, the HDI-BDO hard domains persist at very high strains, and do not rearrange before tensile failure.[1],[7]

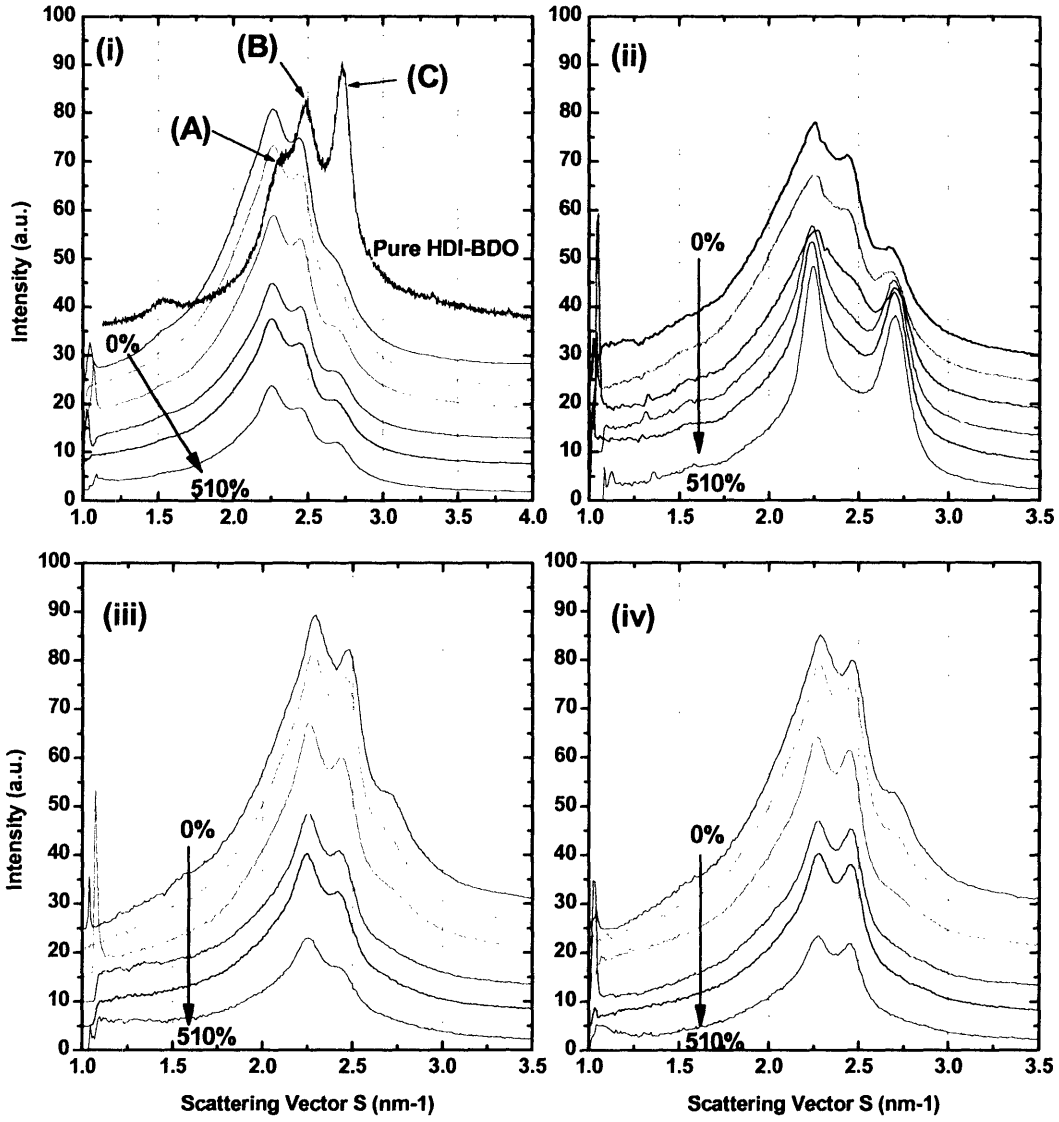


**Figure 4.10 One-dimensional WAXS patterns of H-29 integrated along four directions: (i) all directions (isotropically), (ii) the equator, (iii) the meridian, and (iv) 20° from the meridian**

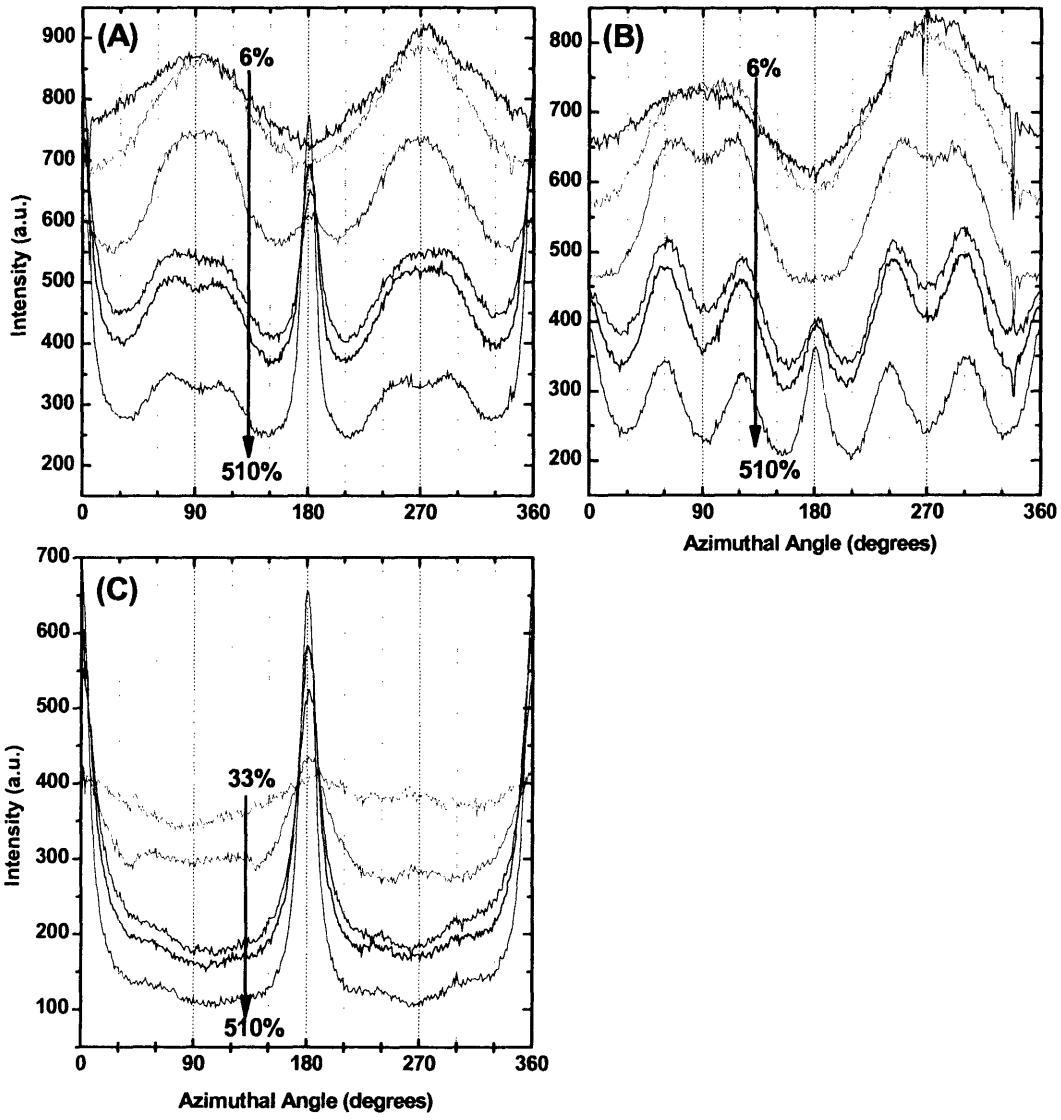


**Figure 4.11 Azimuthal WAXS plots of H-29 at peak positions A, B, and C indicated in Fig. 4.10 (4.4 Å, 4.1 Å, and 3.7 Å)**

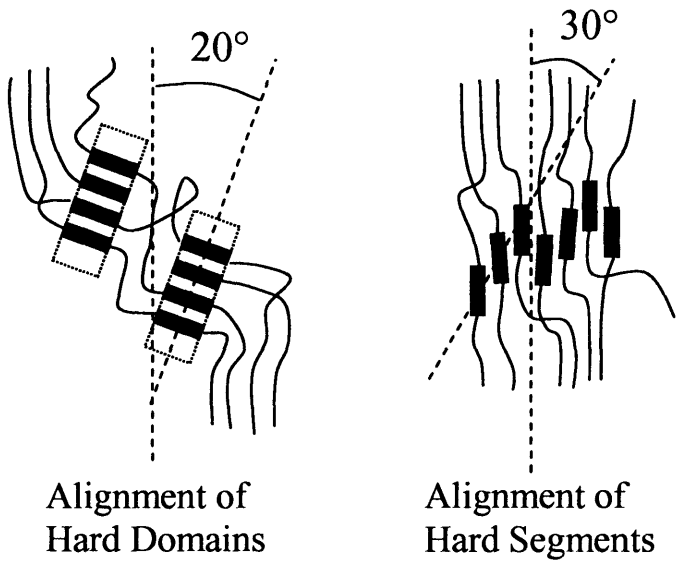


**Figure 4.12 Cartoon summary of the hard segment orientation behavior for H-29 at high strain observed by 2-D WAXS.**

*4.3.3 In-Situ Polarized Optical Microcopy*

The structural development of polyurethanes with mixed hard segments, specifically the presence and orientation strain-induced crystallization, was also examined using strain-controlled polarized optical microscopy. Figures 4.13, 4.14 and 4.15 show the anisotropy that develops during deformation of H-29, HT-29, and HM-29, respectively. In polyurethane H-29, a small number of crystallites are observed at 0% strain, but pronounced stress-whitening occurs around 100% strain due to strain-induced crystallization. This picture agrees well with the in-situ WAXS results presented in the previous section. The degree of crystallinity does not appreciably increase at strains above 100%, though the crystallites exhibit a stronger orientation in the strain direction, as evidenced by birefringence. Upon relaxation, the degree of crystallinity appears similar to the sample at 100% strain.

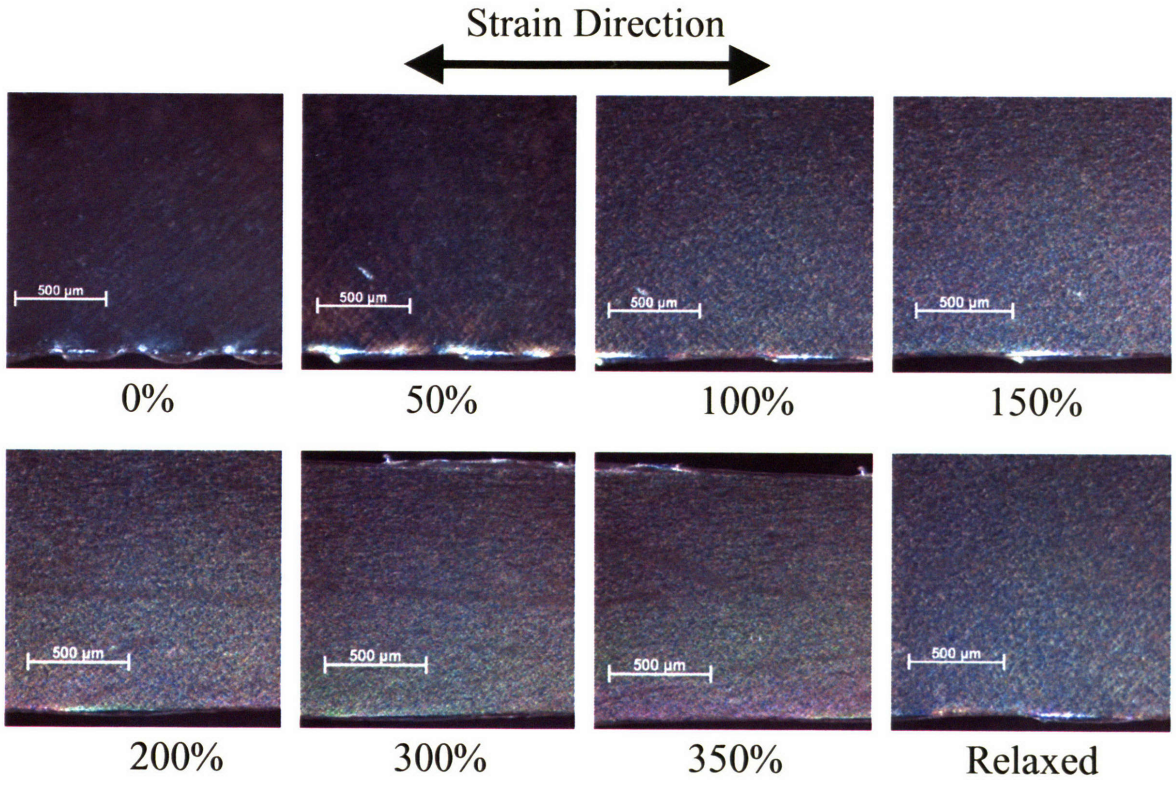


**Figure 4.13 Optical micrographs of H-29 under crossed polarizers as a function of strain**

In polyurethane HT-29, there are no crystallites observed at 0% strain, because the TDI units have interrupted the HDI-BDO hard segment crystallization, as explained in Chapter 3. However, HT-29 immediately exhibits stress-whitening under strain, as strain-induced crystallization occurs at lower strains than H-29. These crystallites exhibit a slight orientation in the strain direction by 200% strain. Upon relaxation, the stress-whitening increases even further, perhaps because the smaller crystallites combine to create larger crystallites that interact more strongly with the polarized light.

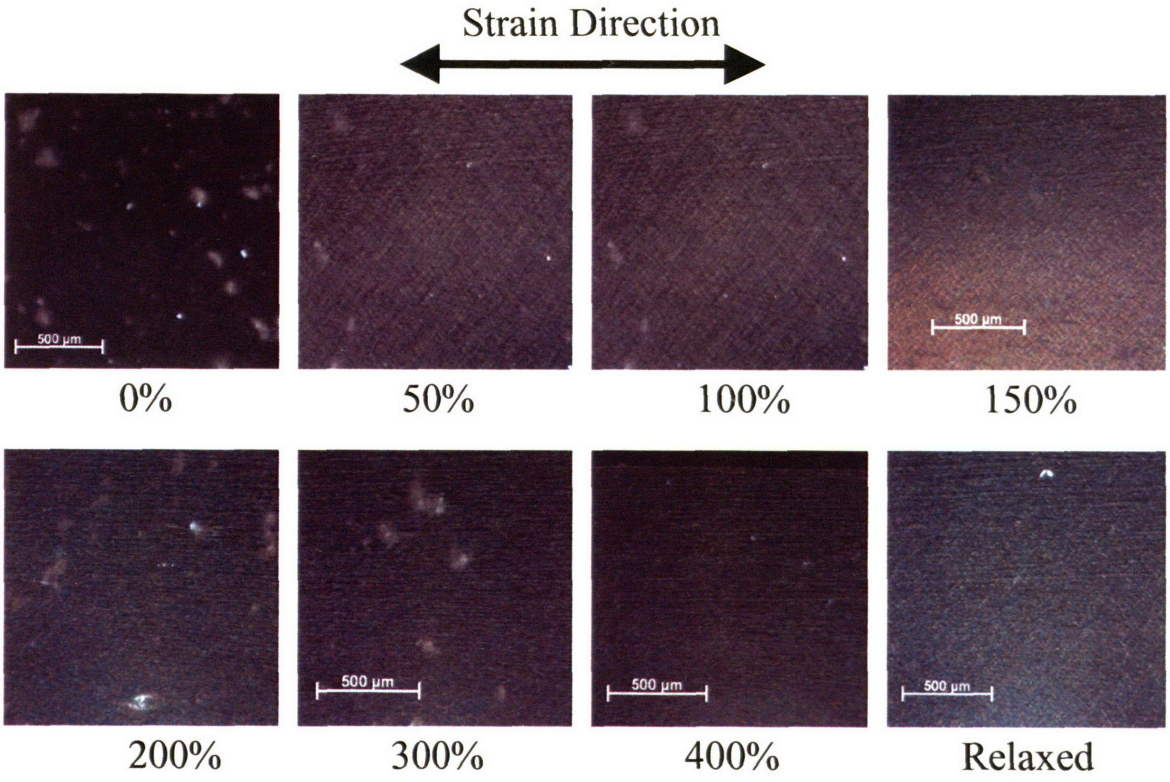


**Figure 4.14 Optical micrographs of HT-29 under crossed polarizers as a function of strain**

Polyurethane HM-29 exhibits a behavior that is very different from both H-29 and HT-29. There are no crystallites observed at 0% strain, but at strains of 20-25%, a large amount of birefringence is observed, not due to strain-induced crystallization but due to the orientation of the paracrystalline MDI groups within the hard segment. The sample exhibits an array of solid colors as the strain is increased, due to the changing thickness of the film through which the polarized light twists. However, the sample does not exhibit localized color change from crystalline structures such as spherulites. Upon relaxation, the polyurethane continues to show a strong orientation through birefringence, but not the degree of residual crystallization observed in H-29 or HT-29.

Polarized optical microscopy was also used to study polyurethane samples with similar hard segments to the observed samples, but with shorter soft segments (samples

H-20, HT-20, and HM-20 from Chapter 3). These polyurethane films exhibited the same trends based on hard segment type, but for brevity the data are not pictured here.

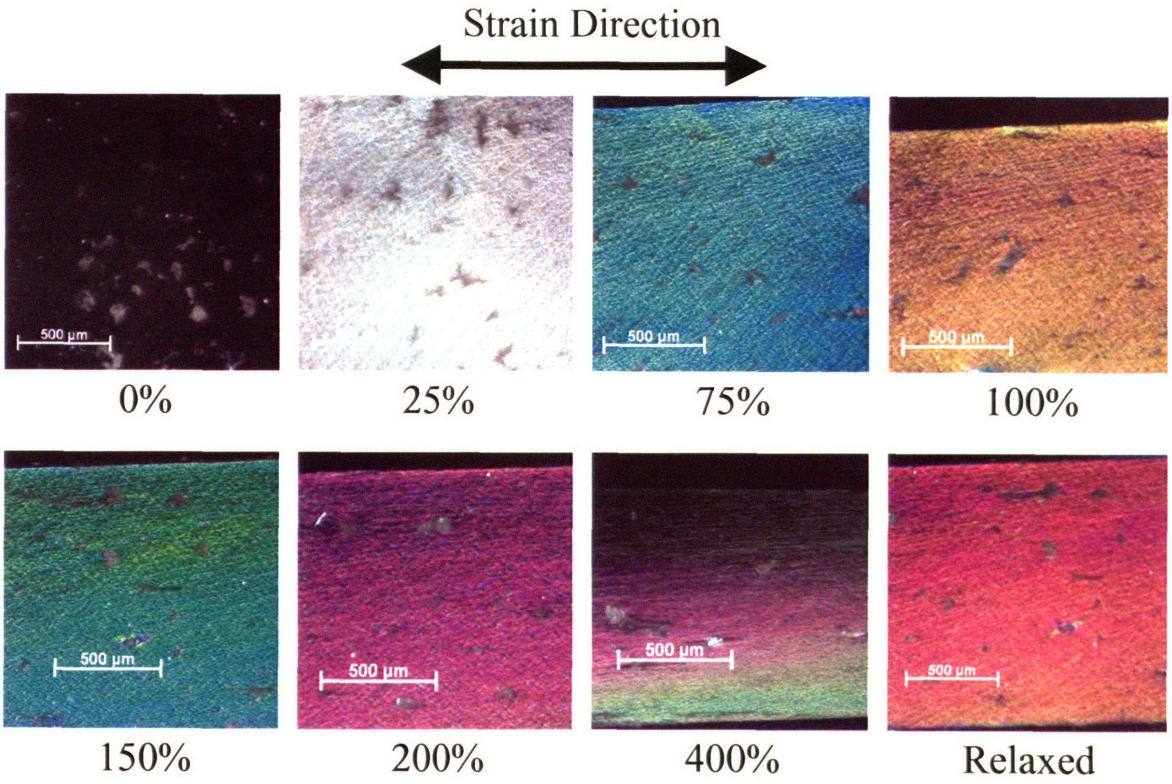


**Figure 4.15 Optical micrographs of HM-29 under crossed polarizers as a function of strain**

## 4.4 Conclusions

The structural development of several segmented polyurethanes was analyzed during tensile strain by a combination of SAXS, WAXS, and polarized optical microscopy. A segmented polyurethane with HDI-BDO hard segments and a PTMO soft segment (H-29) was deformed with simultaneously collecting synchrotron SAXS and WAXS data. The polyurethane hard domains are initially isotropic at an average interdomain spacing of 17 nm. As the sample is deformed, the hard domains orient along the strain direction and at a preferred tilt angle of ±20° from the strain direction. While

the average spacing of all hard domains increases from 17 to 22 nm during deformation, the spacing of hard domains aligned with the strain decreases from 16 to 13 nm, and the spacing of hard domains shearing at ±20° decreases slightly from 16 to 15 nm. The HDI-BDO-PTMO polyurethane exhibits a large amount strain induced crystallization of PTMO, evidenced by WAXS crystalline peaks aligned along the equator at high strain. The crystalline HDI-BDO hard segments also align under strain in agreement with the hard domain orientation observed by SAXS. Polyurethane films with mixed diisocyanates in the hard segment were also compared to the HDI-BDO polyurethane using polarized optical microscopy. The polyurethanes with mixed diisocyanates initially exhibited less crystallinity, but had more overall orientation of chain segments at higher strains, due to the ability of the less crystalline hard segments to align and reinforce the polyurethane.

## 4.5 References


1. Bonart, R., L. Morbitzer, and G. Hentze, *X-Ray Investigations Concerning the Physical Structure of Cross-Linking in Urethane Elastomers. II. Butanediol as Chain Extender.* Journal of Macromolecular Science - Physics, 1969. **B3**(2): p. 337-356.
2. Bonart, R., L. Morbitzer, and E.H. Muller, *X-Ray Investigations Concerning the Physical Structure of Crosslinking in Urethane Elastomers. III. COmmon STructure Principles for Extensions with Aliphatic Diamines and Diols.* Journal of Macromolecular Science - Physics, 1974. **B9**(3): p. 447-461.
3. Seymour, R.W., A.E. Allegrezza, and S.L. Cooper, *Segmental Orientation Studies of Block Copolymers: 1. Hydrogen-Bonded Polyurethanes.* Macromolecules, 1973. **6**(6): p. 896-902.

4. Desper, C.R., et al., *Deformation of Microphase Structures in Segmented Polyurethanes.* Macromolecules, 1985. **18**: p. 2755-2761.
5. Blundell, D.J., et al., *Real-time SAXS/stress-strain studies of thermoplastic polyurethanes at large strains.* Polymer, 2002. **43**: p. 5197-5207.
6. Yeh, F., et al., *In-Situ Studies of Structure Development during Deformation of a Segmented Poly(urethane-urea) Elastomer.* Macromolecules, 2003. **36**: p. 1940-1954.
7. Lee, H.S., S.R. Yoo, and S.W. Seo, *Domain and Segmental Deformation Behavior of Thermoplastic Elastomers Using Synchrotron SAXS and FTIR Methods.* Journal of Polymer Science - Polymer Physics, 1999. **37**: p. 3233-3245.
8. McLean, R.S. and B.B. Sauer, *Tapping-Mode AFM Studies Using Phase Detection for Resolution of Nanophases in Segmented Polyurethanes and Other Block Copolymers.* Macromolecules, 1997. **30**: p. 8314-8317.
9. Chu, L.-Z. and B. Chu, *Crystalline structure and morphology of microphases in compatible mixtures of poly(tetrahydrofuran-methyl methacrylate)diblock copolymer and polytetrahydrofuran.* Journal of Polymer Science - Polymer Physics, 1999. **37**: p. 779-792.
10. Lee, D., et al., *Micro-phase separation behavior of Amphiphilic Polyurethanes Involving Poly(ethylene oxide) and poly(tetramethylene oxide).* Journal of Polymer Science - Polymer Physics, 2003. **41**: p. 2365-2374.

# Chapter 5: Polyurethane/Clay Nanocomposites

## 5.1 Introduction

The incorporation of nano-scale filler particles has shown promise for the improvement of mechanical properties of segmented polyurethanes.[1],[2] The mechanical property improvements observed in nanocomposite structures are directly related to the nanoparticle surface to volume ratio, which in turn depends on the degree of particle dispersion. For polymer-clay nanocomposites, four thermodynamically stable structures are obtainable, as represented in Figure 5.1.[2] In Figure 5.1(a), the clay platelets are miscible with the polymer but the clay spacing remains at its normal interlayer spacing. As the attractions between the polymer and clay increase, the polymer chains begin to disrupt the clay layers, creating an intercalated structure depicted in Figure 5.1(b). The clay still exhibits some periodicity in WAXD, but the spacing is greater than that of the undispersed particles, independent of the clay loading.[1],[5] Two types of exfoliated states, ordered and disordered, are depicted in Figure 5.1(c) and (d). In both exfoliated states, the clay sheets are fully separated, and the interparticle distance depends only on the overall degree of clay loading; however, the ordered exfoliated state can be detected by X-ray diffraction, while the disordered exfoliated state cannot. The exfoliated state maximizes the surface-to-volume ratio of the clay particles and creates the greatest potential improvement to mechanical properties. Most polyurethane nanocomposites exhibit a mixture of the intercalated and exfoliated states of clay dispersion.[6] TEM and WAXD are the primary tools for observing the nanocomposite morphology.

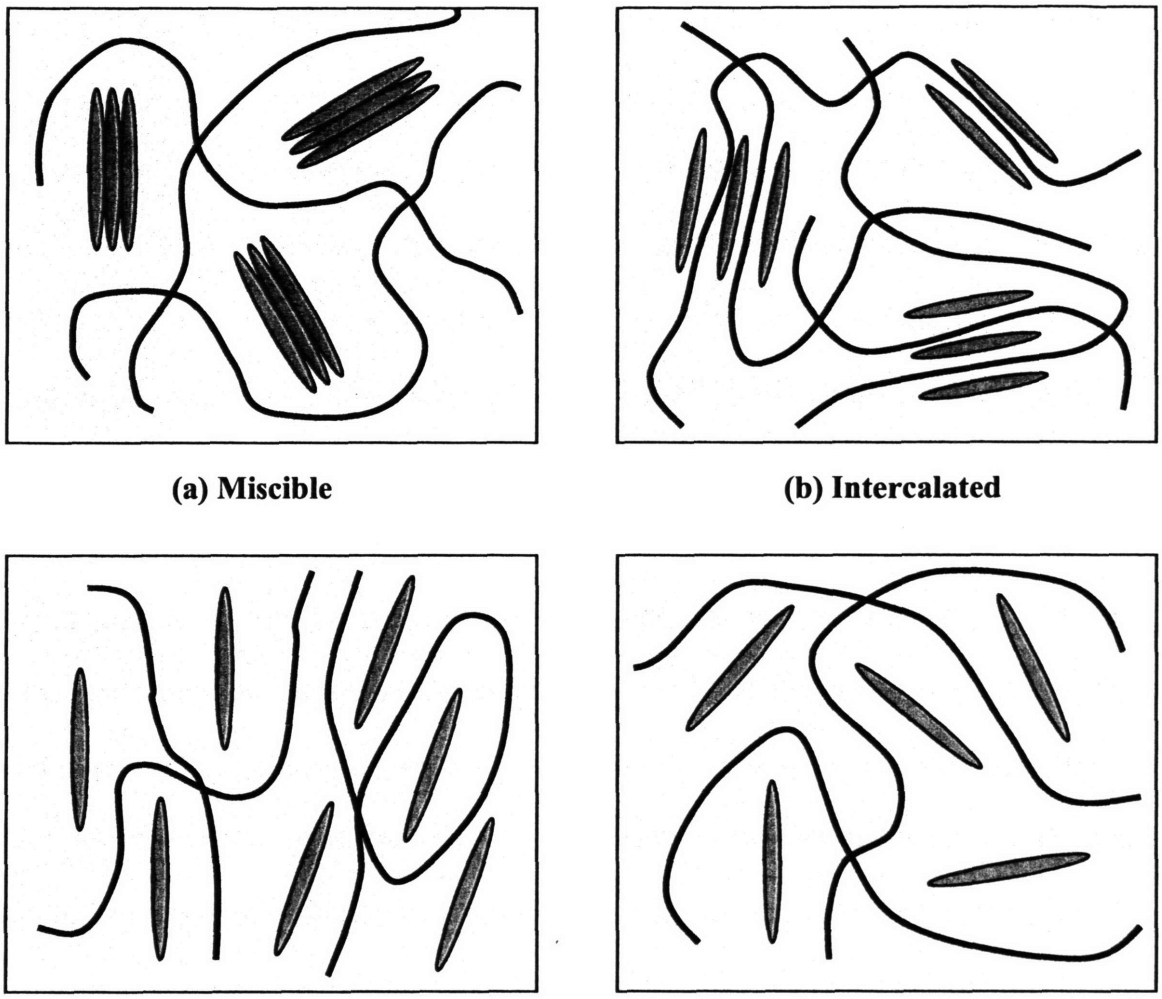

**(a) Miscible** **(b) Intercalated**

**(c) Ordered Exfoliated** **(d) Disordered Exfoliated**

**Figure 5.1 Polymer-clay nanocomposite morphologies**

Laponite, a synthetic layered silicate clay, has shown potential in the reinforcement of polyurethanes with polar blocks, due to the hydrophilic nature of the clay. Unlike previous attempts at dispersing clay nanoparticles, McKinley and co-workers have discovered a novel solvent-exchange method to create exfoliated and/or intercalated polyurethane nanocomposite structures. McKinley *et al.* have reported the exfoliation of Laponite nanoparticles in Elasthane, a segmented thermoplastic

polyurethane composed of PTMO soft segments and MDI-BDO hard segments (40 wt%).[3] The Elasthane/Laponite nanocomposites with 20 wt% clay loading exhibited a 23-fold increase in initial modulus and a 4-fold increase in toughness at 30% deformation, without a decrease in extensibility or tensile strength. TEM and WAXD confirmed that the Laponite is fully exfoliated in the polyurethane matrix. An increase in the heat distortion temperature and the disruption of hard domain melting peaks were also reported for the Laponite nanocomposites, suggesting the clays discs are preferentially associated with the hard domains. A second study examined the dispersion of Laponite into segmented polyurethanes with PEO or PEO-PPO-PEO soft segments and HDI-BDO hard segments.[4] The Laponite nanoparticles dispersed in these new matrices exhibited a mixture of intercalated and exfoliated structures by TEM and WAXD. However, the nanocomposite experienced a degradation of mechanical properties, including a three-fold reduction in tensile strength and a five-fold reduction of elongation. The reduction of tensile properties was attributed to preferential interactions between the PEO-containing soft segments and the Laponite platelets, which restricted the mobility of the soft segments. To further test this hypothesis, it was desired to examine the structure and properties of a segmented polyurethane that also includes HDI-BDO hard segments, but instead has a more hydrophobic PTMO soft segment.

## 5.2 Experimental

### *5.2.1 Materials*

Polyurethane H-20, which contains a HDI-BDO hard segment (37 wt%) and a PTMO soft segment, was the segmented polyurethane elastomer chosen for this

reinforcement study. The morphological and mechanical properties of this polyurethane were described in Chapters 3 and 4. Laponite RD, a discotic, smectic synthetic clay, was obtained from Southern Clay Products. N,N-dimethylacetamide (DMAc) was ordered from Sigma-Aldrich and used as received.

### *5.2.2 Solvent-Exchange Method and Film Casting*

A novel approach was employed to disperse Laponite into the H-20 polyurethane matrix. In this method, Laponite was well-dispersed in deionized water at a concentration of 1g / 100mL by stirring at room temperature for one day. To that mixture, 100 – 200 g of DMAc as added and stirred for one day. The water was then removed from the Laponite/water/DMAc mixture via vacuum distillation at 75 °C. The removal of water was monitored by measuring the mass loss; the distillation was stopped when the loss of solution mass exceeded that of the added water. This step is critical due to the strong affinity of water to Laponite.

H-20 polyurethane was then dissolved in the Laponite/DMAc dispersion, at a concentration of 1.5 wt%, and the amount of Laponite/DMAc dispersion was adjusted to produce a clay loading of 10 wt%. The mixtures were then cast into Teflon molds described in Section 3.2.3. Thin films (80-100 μm thick) of the polyurethane nanocomposites were obtained by slow evaporation of the DMAc in an oven at 60 °C, controlled via a regulated $N_2$ purge.

### *5.2.3 Instrumentation*

#### 5.2.3.1 Differential Scanning Calorimetry

Thermal phase behavior was examined with a TA Instruments Q1000 Differential Scanning Calorimeter (DSC), operated at a heating rate of 10°C/min under a 50 mL/min nitrogen purge. Polyurethane films were subjected to two heating and cooling cycles from -90 to 250 °C. Transitions were recorded from the first heating and cooling scans, to observe phase behavior in the cast films, using a linear extrapolation method for $T_m$ and midpoint inflection method for $T_g$.

#### 5.2.3.2 Dynamic Mechanical Analysis

Dynamic mechanical analysis (DMA) was performed on a TA Instruments Q800 DMA equipped with a film/fiber clamp, operated at a frequency of 1 Hz and heating rate of 3 °C/min from -100 to 170 °C.

#### 5.2.3.3 Tensile Testing

The tensile properties of polyurethane nanocomposites were determined using a Zwick/Roell Z010 with a 500N load cell and convex jaw grips with aluminum and flat polyurethane faces to minimize tearing at the grips. The sample was deformed at a crosshead speed of 100% gauge length/minute. A minimum of three samples were examined for statistical analysis.

#### 5.2.3.4 Wide-Angle X-ray Diffraction

The clay dispersal mechanism in the polyurethane nanocomposites was investigated using a Rigaku RU300 rotating anode X-ray generator with a 185 mm

diffractometer and a scintillation counter. Scattered CuKα radiation with wavelength of 1.54 Å was detected at a scan rate of 5°/min and a 0.5° sample interval.

5.2.3.5 Transmission Electron Microscopy

TEM lamellas were prepared in a JEOL JEM9310 Focused Ion Beam (FIB) instrument. The polyurethane composite samples were first sputter coated with ~200 nm of gold then a localized ~1 micron thick carbon protective film was deposited over the area selected for lamella preparation. The samples were milled and polished in the FIB to ultimately give 10 by 10 microns by ~80 nm thick lamella. The lamellas were transferred to TEM grids using a micromanipulation system. A micromanipulator position controlled polished glass rod was used to pick up the lamellas (electrostatically) under an observation microscope. The lamellas were then gently placed on TEM grids. Unstained samples were observed with a JEOL 200CX electron microscope operating at 200 kV.

## 5.3 Mechanical Behavior

Composite thin films of H-20 polyurethane with 0% and 10% Laponite clay loadings were obtained from the slow evaporation of solutions in DMAc. A representative stress-strain curve for each sample is plotted in Figure 5.2, and the tensile properties from all tested samples are summarized in Table 5.1. The uncertainty figure represents the standard deviation for three films at each composition. Similar to the results for the Elasthane nanocomposites, the H-20 nanocomposite with 10% Laponite exhibits a distinct increase in tensile modulus, tensile strength, and toughness. Furthermore, the ultimate elongations of the loaded and unloaded polyurethane films are within error of each other. The improvement in mechanical properties of H-20 is not as

dramatic as the 23-fold increase in modulus and 4-fold increase in toughness reported for Elasthane at 20% Laponite loading; however, Elasthane with 10% Laponite loading exhibited only a four-fold increase in modulus and 60% increase in toughness, which is more consistent with the results for H-20. [3] It should also be noted that the mechanical properties of the unloaded H-20 film, especially the tensile modulus, are better than those reported for H-20 in Chapter 3. This property difference is attributed to the change in film casting procedure. The extremely slow evaporation under a $N_2$ purge creates more ordered polyurethane structures. However, within each set of experiments, the film casting conditions were kept constant to enable property comparison.

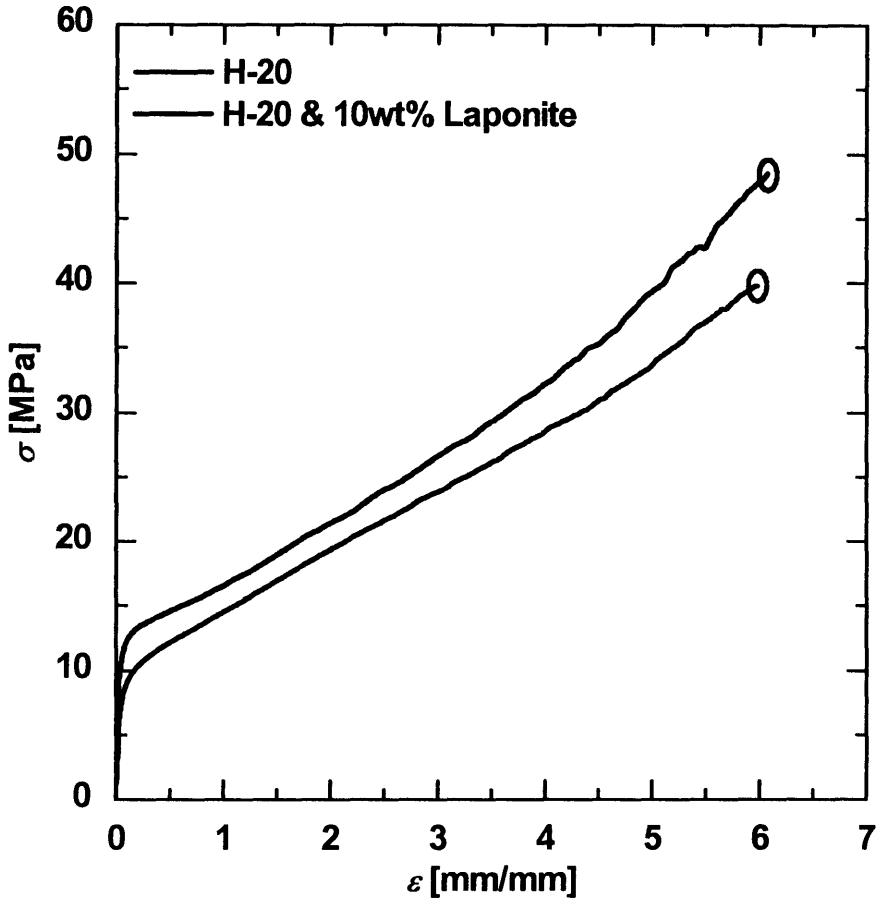


**Figure 5.2 Comparison of the stress-strain behavior of H-20 with and without 10% Laponite loaded**

**Table 5.1 Tensile properties of H-20 with and without 10 wt% Laponite loaded**

| Property | H-20 | H-20 w/ 10% Laponite |
|---|---|---|
| Elastic Modulus (MPa) | 260 ± 18 | 473 ± 26 |
| Ultimate Tensile Strength (MPa) | 40 ± 5 | 48 ± 2 |
| Ultimate Elongation (%) | 628 ± 35 | 617 ± 26 |
| Toughness (MPa) | 149 ± 21 | 170 ± 13 |

The dynamic mechanical properties of the polyurethane nanocomposites were also examined. Figure 5.3 shows the storage modulus, loss modulus and tan(δ) curves for both the loaded and unloaded H-20 polyurethane. The plateau modulus of the nanocomposite is distinctly increased, accompanied by an increase in the heat distortion

temperature from 162 °C to 167 °C. For this work, the heat distortion temperature is defined as the temperature at which the storage modulus drops to 8 MPa. At lower temperatures, the shape of the loss modulus and tan(δ) curves remains similar for the loaded and unloaded polyurethane. The absence of any effect on the soft segment glass transition suggests that the Laponite particles are associated with the polyurethane hard segments, as also observed in Elasthane/Laponite nanocomposites. This hypothesis will be explored further in the following section.

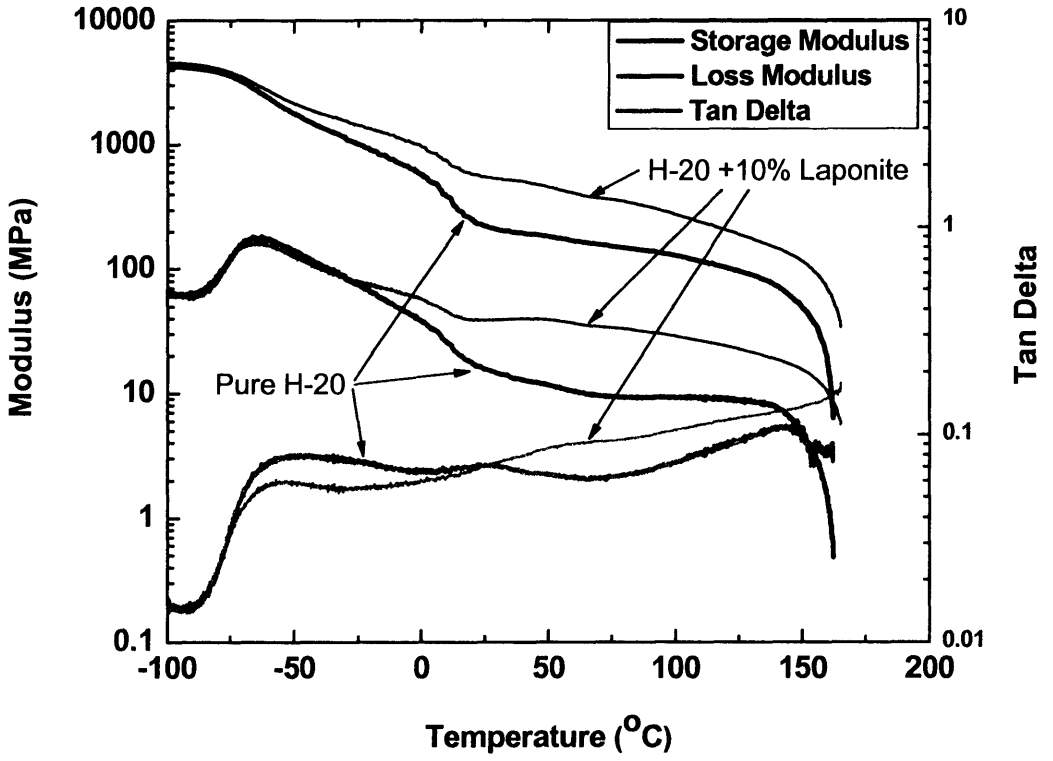


**Figure 5.3 Dynamic mechanical behavior of H-20 segmented polyurethane with and without 10% Laponite loaded**

## 5.4 Morphological Behavior

The mechanical property improvements observed in nanocomposites are directly related to the nanoparticle morphology within the polymer matrix. As explained in Section 5.1, the fully exfoliated state creates the highest surface to volume ratio of dispersed nanoparticles. This increased interaction between the clay disks and the polymer matrix produces the greatest improvement in mechanical properties. Therefore, to fully understand the property improvement of the H-20/Laponite nanocomposite, the interparticle arrangement should be examined by TEM and WAXD.

TEM images of the H-20/Laponite nanocomposite are shown in Figure 5.4. In both images, the clear majority of the clay nanoparticles are exfoliated, showing no periodic spacing with one another. However, a small fraction of nanoparticles in each image are observed to be in small intercalated stacks of 3-4 clay discs with a periodic spacing. The spacing of these discs is best examined by WAXD to confirm that the clay stacks are no longer at their initial crystal spacing, and thus intercalated by polyurethane chains.

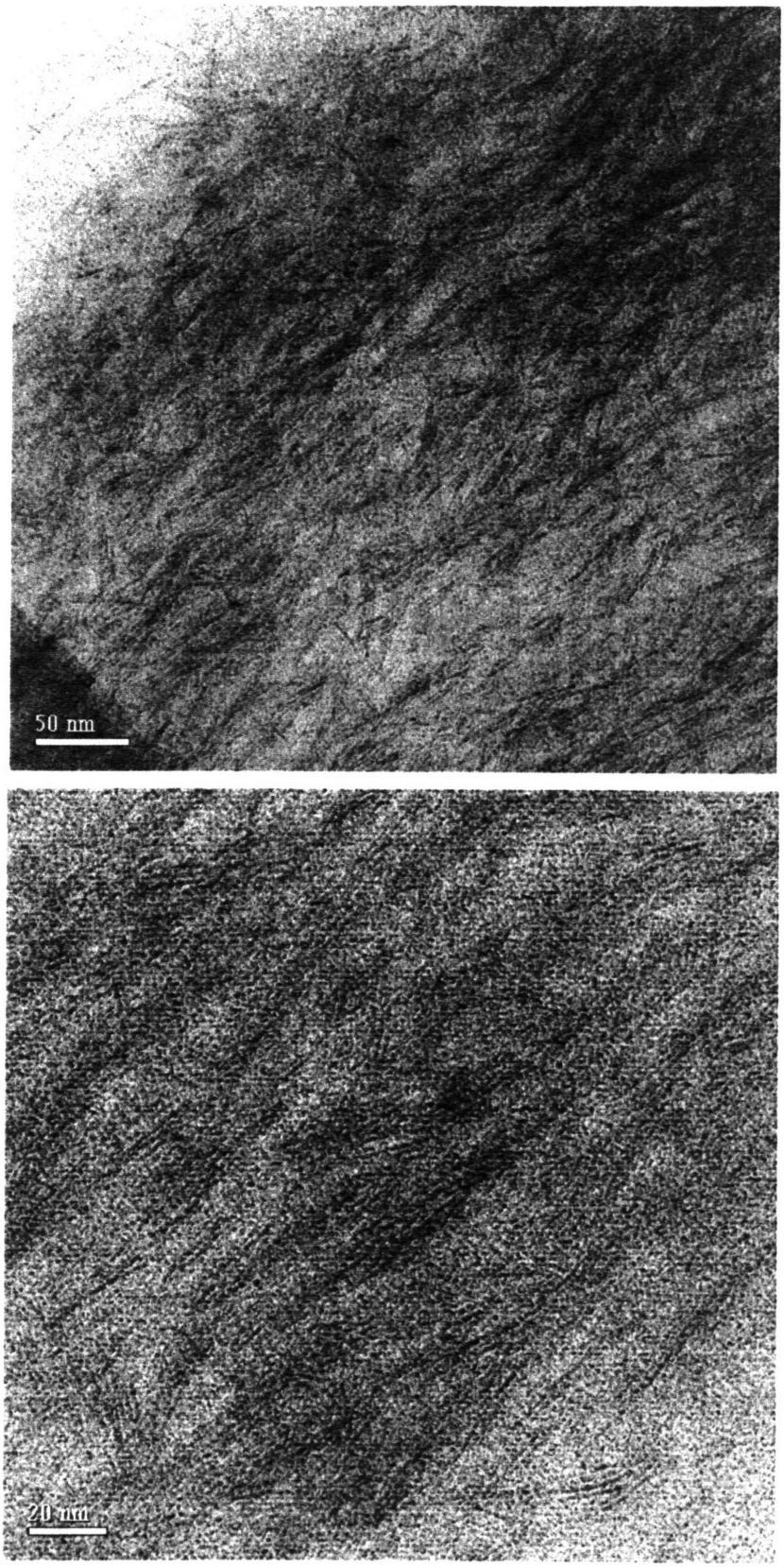


**Figure 5.4 TEM images of 10 wt% Laponite/H-20 nanocomposites showing clay exfoliation with some intercalated structure**

The WAXD spectra of the loaded and unloaded H-20 polyurethane are shown in Figure 5.5. To enable peak identification, the diffraction patterns of undispersed Laponite crystals and a pure HDI-BDO hard segment are also included for comparison. Comparing the diffraction patterns of the Laponite crystals and the H-20/Laponite nanocomposite, it is clear that the dispersed Laponite loses all its higher order crystal reflections. In addition, the (001) Laponite reflection, which is directly related to the inter-disc spacing in the crystal structure, shifts from 7° in the undispersed Laponite to 5° in the H-20/Laponite nanocomposite. This suggests the formation of at least some intercalated structure, in which the polyurethane chains coordinate between the Laponite discs, resulting in a less ordered structure that still exhibits slight periodicity.

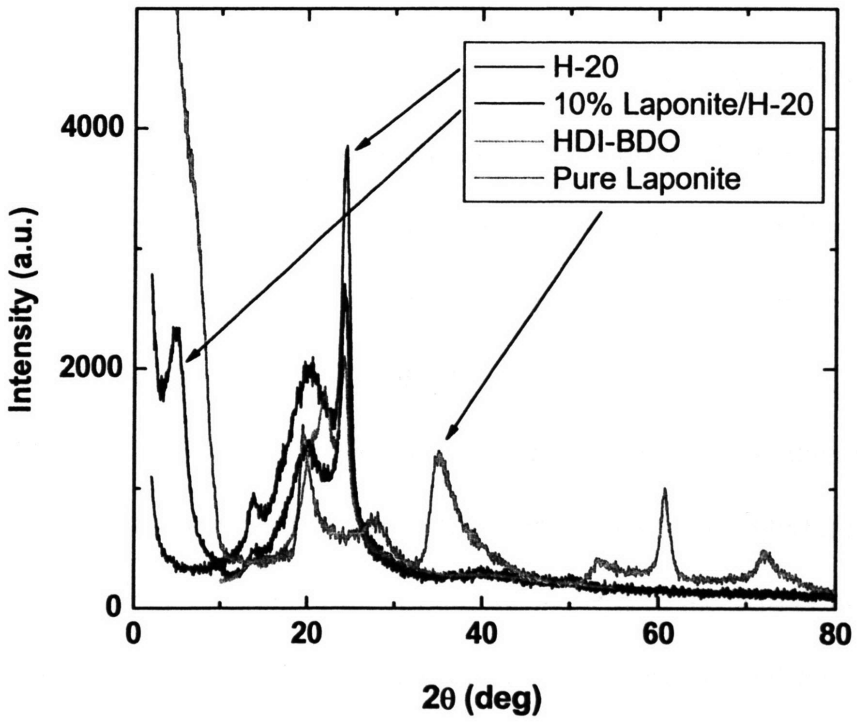


**Figure 5.5 WAXD patterns of H-20 polyurethane with and without 10 wt% Laponite loaded. (Laponite and HDI-BDO are included for comparison.)**

In addition to the clay nanoparticle morphology, the nanocomposite mechanical properties are related to the polyurethane phase association of the clay particles.[6] The hydrophilic nature of Laponite clay particles suggests a preferential association with the HDI-BDO hard segments, which are more polar than the PTMO soft segments. This phase association was alluded to by the DMA results, and is explored more fully using DSC. The DSC traces of the loaded and unloaded H-20 polyurethane are shown in Figure 5.6; the top curve is the first heating and cooling cycle, while the lower curve is the second heating and cooling cycle. The neat H-20 polyurethane and nanocomposite have similar heating curves in the first cycle; however, their difference becomes apparent during the first cooling. The neat H-20 polyurethane exhibits a sharp exotherm at 125 °C, which indicates the formation of crystalline hard domains. This hard domain formation is suppressed in the H-20/Laponite nanocomposite, because the Laponite disks are associated with the hard segments in the phase mixed state, and prevent the hard segments from crystallizing to form hard domains upon cooling. This phenomenon is similar to the interruption of HDI-BDO crystallinity by the additional bulky TDI and MDI units in polyurethanes with mixed hard segments observed in Chapter 3. The interruption of hard domain formation is also reflected in the second heating of the nanocomposite, which exhibits a smaller hard segment endotherm than the neat H-20 polyurethane. It should be noted that Laponite nanoparticles do not interfere with hard domain formation during the initial film casting, since the hard the hard domain endotherm is a similar size during the first heating. Rather, the association of the clay disks with the hard segments only prevents the formation of hard domains during bulk film cooling at the relatively fast rate of 10 °C/min.

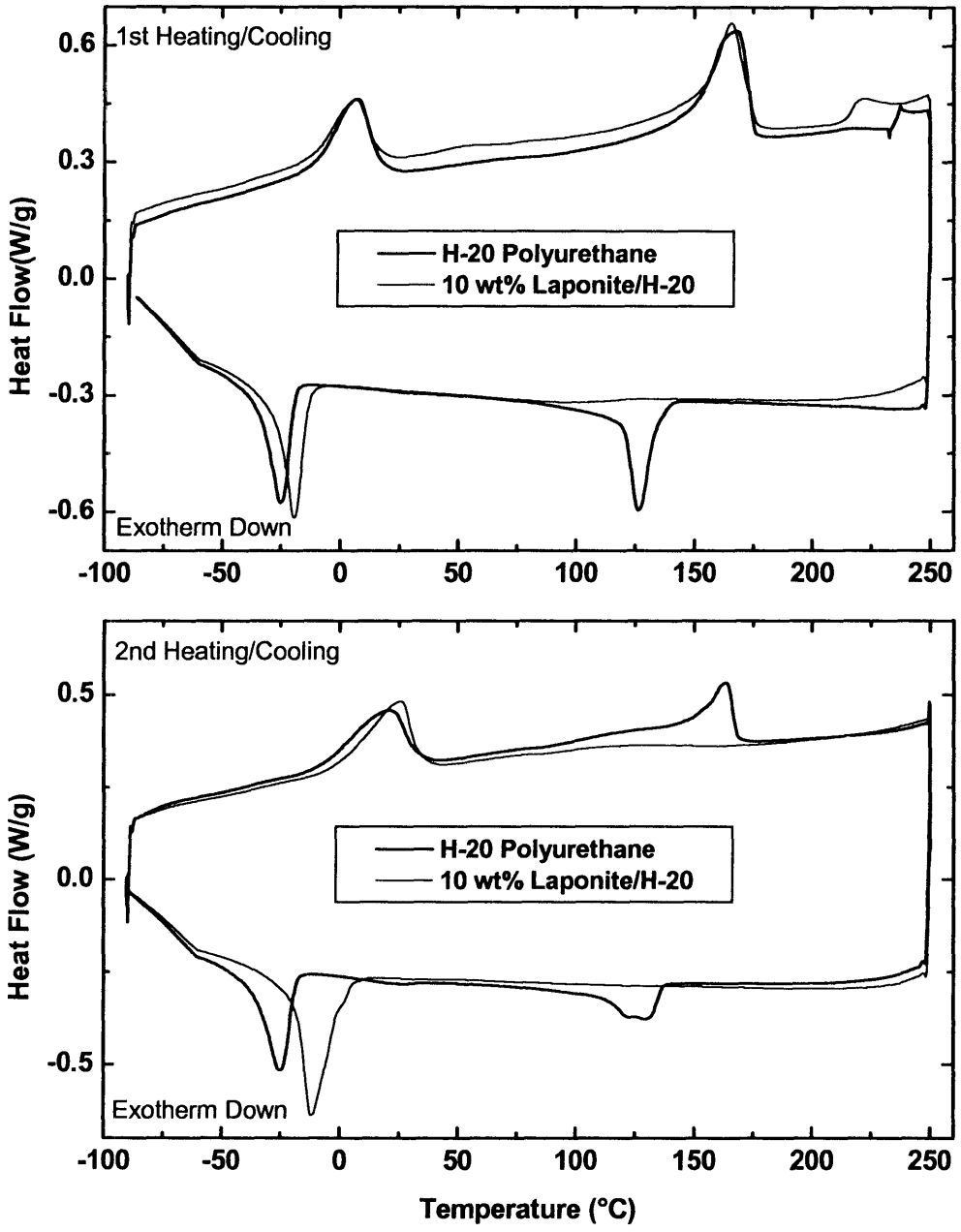


**Figure 5.6 DSC traces of H-20 segmented polyurethane with and without 10 wt% Laponite loaded, showing particle association with hard segments**

## 5.6 Conclusions

A HDI-BDO-PTMO polyurethane/Laponite nanocomposite was created using a novel solvent exchange process, in order to enhance the mechanical properties of the polyurethane matrix and examine the phase association of the nanoparticles. The polyurethane nanocomposite exhibited an improvement in tensile modulus and strength, without sacrificing the extensibility. TEM images and WAXD patterns confirmed exfoliation of most nanoparticles, with the remainder in an intercalated structure. DSC and DMA results both indicated association of Laponite particles with the hydrophilic HDI-BDO hard segments. The improvement in mechanical properties is thus attributed to the reinforcement of polyurethane hard domains by the Laponite clay discs, which in turn improves the integrity of the polyurethane network structure without sacrificing the mobility of the soft segment chains.

## 5.7 References


1. Ray, S.S. and M. Okamoto, *Polymer/layered silicate nanocomposites: a review from preparation to processing.* Progress in Polymer Science, 2003. **28**(11): p. 1539-1641.
2. LeBaron, P.C., Z. Wang, and T. Pinnavaia, *Polymer-layered silicate nanocomposites: an overiew.* Applied Clay Science, 1999. **15**(1): p. 11-29.
3. Kumar, N., S. Liff, and G.H. McKinley, To Be Submitted, 2005.
4. James-Korley, L.T., et al., To Be Submitted, 2005.
5. Thostenton, E.T., C. Li, and T.-W. Chou, *Nanocomposites in context.* Composites Science and Technology, 2005. **65**: p. 491-516.
6. Finnigan, B., et al., Morphology and properties of thermoplastic polyurethane nanocomposites incorporating hydrophilic layered silicates. Polymer, 2004. **45**: p. 2249-2260.

# Chapter 6: Polyurethane/Siloxane Nanocomposites

## 6.1 Introduction

As indicated in the previous chapter, the incorporation of nanoscale clay particles is a promising technique for the improvement of mechanical properties of segmented polyurethanes. The hydrophilic clay discs associate closely with the hard segments to provide hard domain templates and reinforcement. Conversely, the dispersion of most nanoparticles within the soft matrix of a polyurethane may lead to undesired restriction of the soft segment elasticity.[1] However, if the nanofillers are small enough, closer to the molecular scale, they may provide the soft segment reinforcement desired for the spider silk analogs. Siloxane resins such as polyhedral oligomeric silsesquioxanes (POSS) exist as small cages 1-4 nm in size, on a size scale intermediate between conventional nanoparticles and simple molecules. These nanofillers may be incorporated either covalently through a tethering linkage to the polymer backbone, or noncovalently through hydrophobic interactions with the soft segment.[2] The covalent linkage of such cages is beyond the scope of this thesis; however, the non-covalent incorporation of a series of POSS cages and a POSS-like MQ siloxane resin into polyurethane soft segments is the subject of this chapter.

Polyhedral oligomeric silsesquioxanes (POSS) are a class of siloxanes with the general repeat structure $SiO_{1.5}R$.[2] They are capable of forming random, ladder or cage structures and can be functionalized at the corners of the cages with non-reactive or reactive groups, the latter enabling their grafting onto polymer matrices. The first

oligomeric organosilsesquioxanes were isolated by Scott in 1946,[3] but interest in them increased drastically when a large scale process for POSS monomer synthesis was developed by a group at Edwards Air Force Base in the late 1990s.[4] POSS monomers are now available in a multitude of structures and functionalities from Hybrid Plastics Company in Fountain Valley, CA. POSS has been tested as a nanoscale filler in many polymer matrices, both covalently attached and non-covalently dispersed.[5-13] Fu *et al.* covalently tethered cyclohexyl-POSS into the hard segments of a polyurethane with MDI and bisphenol A, and found significant mechanical reinforcement of the polyurethane due to the formation of nanoscale POSS crystals within the hard domain.[5, 6] However, there is no literature currently available on the dispersion of POSS cages within a polyurethane soft segment.

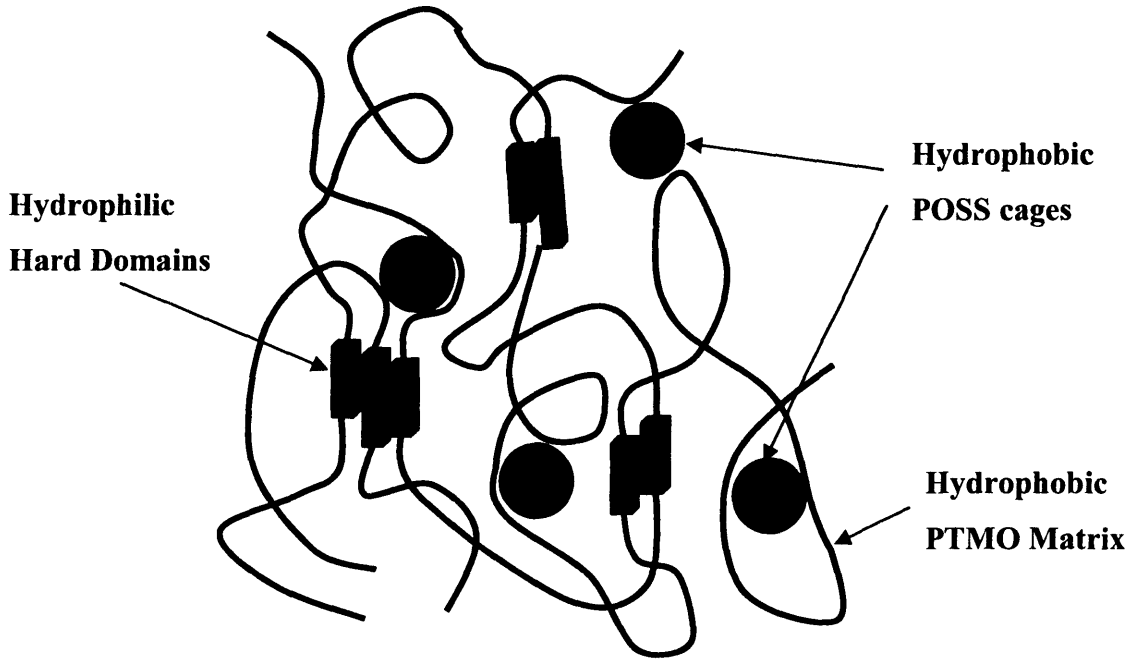


**Figure 6.1 Segmented polyurethane/POSS nanocomposite structure**

## 6.2 Experimental

### *6.2.1 Materials*

Polyurethanes H-20, H-29, and HT-20 were the segmented polyurethane elastomers chosen for this reinforcement study. The morphological and mechanical properties of this polyurethane were described in Chapters 3 and 4, but a summary of the composition and molecular weights is reproduced in Table 6.1. MQ-resin was obtained from Dow Corning and used as received. Octa-isobutyl-POSS and isooctyl-POSS (cage mixture) were ordered from Hybrid Plastics and used as received. N,N-dimethylacetamide (DMAc) and tetrahydrofuran (THF) were ordered from Sigma-Aldrich and used as received.

**Table 6.1 Compositions and molecular weights of selected polyurethanes used for siloxane resin dispersion study**

| Sample | Soft Segment | Hard Segment | HS wt% | $M_w$ (kDa) | $M_w/M_n$ |
|---|---|---|---|---|---|
| H-20 | PTMO-2000 | HDI-BDO | 37 | 233 | 2.13 |
| H-29 | PTMO-2900 | HDI-BDO | 29 | 79 | 2.11 |
| HT-20 | PTMO-2000 | HDI-TDI-BDO | 38 | 140 | 2.97 |

### *6.2.2 Siloxane Resin Dispersion*

Polyurethane mixtures with MQ-resin were obtained by solution processing in DMAc. The polyurethane was dissolved in DMAc at a concentration of 5 wt% and refluxed at 120 °C for 1 hour. The specified portion of resin was separately dissolved in DMAc at room temperature. The resin solution was then added to the polyurethane solution and mixed on a roll mixer overnight.

Polyurethane mixtures with POSS were obtained by solution processing in a DMAc/THF mixture, since the POSS had limited solubility in DMAc alone. The DMAc/THF ratio was 1:1 for the isooctyl-POSS mixtures and 1:4 for the isobutyl-POSS

mixtures. The polyurethane was dissolved in DMAc at a concentration of 10-20 wt%, and refluxed at 120 °C for 1 hour, after which it was cooled, and THF was added. The POSS was first dissolved in THF at room temperature, after which the DMAc was added. The resin solution was then added to the polyurethane solution and mixed on a roll mixer overnight.

Solutions of the polyurethane/resin mixtures were free cast into custom-made Teflon® dishes 4 cm x 6 cm x 4 cm deep. The solvent mixture was allowed to evaporate in a fume hood at room temperature for 2-3 days until the film appeared completely dry, after which the films were placed in a vacuum oven at 60 °C and dried for 1 hour. Final film thicknesses varied from 0.08 mm to 0.12 mm, depending on the total amount of sample. Strips of polyurethane film for tensile testing were cut from the cast film using a custom-built cutter consisting of 2 straight razors held at a fixed width of 5.4 mm.

### *6.2.3 Instrumentation*

#### 6.2.3.1 Differential Scanning Calorimetry

Thermal phase behavior was examined with a TA Instruments Q1000 Differential Scanning Calorimeter (DSC), operated at a heating rate of 10°C/min under a 50 mL/min nitrogen purge. Polyurethane films were subjected to two heating and cooling cycles from -90 to 250 °C. Transitions were recorded using a linear extrapolation method for $T_m$ and midpoint inflection method for $T_g$ from the first heating and cooling scans to observe phase behavior in the cast films.

6.2.3.2 Dynamic Mechanical Analysis

Dynamic mechanical analysis (DMA) was performed on a TA Instruments Q800 DMA equipped with a film/fiber clamp, operated at a frequency of 1 Hz and heating rate of 3 °C/min from -100 to 170 °C.

6.2.3.3 Tensile Testing

The tensile properties of polyurethane nanocomposites were determined using a Zwick/Roell Z010 with a 500N load cell and convex jaw grips with aluminum and flat polyurethane faces to minimize tearing at the grips. The sample was deformed at a crosshead speed of 100% gauge length/minute. A minimum of three samples was examined for statistical analysis.

## 6.3 Results and Discussion

### *6.3.1 Mechanical Characterization*

The mechanical properties of three different sets of polyurethane siloxane composites were measured. The first set consisted of H-20 with various loadings of MQ-resin; the second set consisted of HT-20 with 3 wt % loadings of MQ-resin and isooctyl-POSS; the third set consisted of HT-20 with various loadings of isobutyl-POSS. Within each set, an unloaded polyurethane film was cast from the same solvent mixture in a parallel process, to enable mechanical property comparison. The property modification of each set will be discussed separately.

Transparent thin films of H-20 with MQ-resin loadings of 1 wt%, 3 wt%, 5 wt%, and 0 wt% were obtained by solution casting from DMAc. A representative stress-strain

curve for each sample is plotted in Figure 6.2, and the average tensile properties from all tested samples are summarized in Table 6.2. The uncertainty figure represents the standard deviation for three films at each composition. At all MQ-resin loadings, the modulus increased by about 60%; however, the tensile strength, elongation and toughness of the 1% and 5% loaded polyurethanes all decreased. While the properties of the 3% loaded sample were more similar to the unloaded polyurethane, the variation between repeated samples was much higher, such that within error, the tensile properties may have also slightly deteriorated for the 3% loading. In any case, the mechanical property variations with MQ-resin loaded into an HDI-PTMO polyurethane were not dramatic.

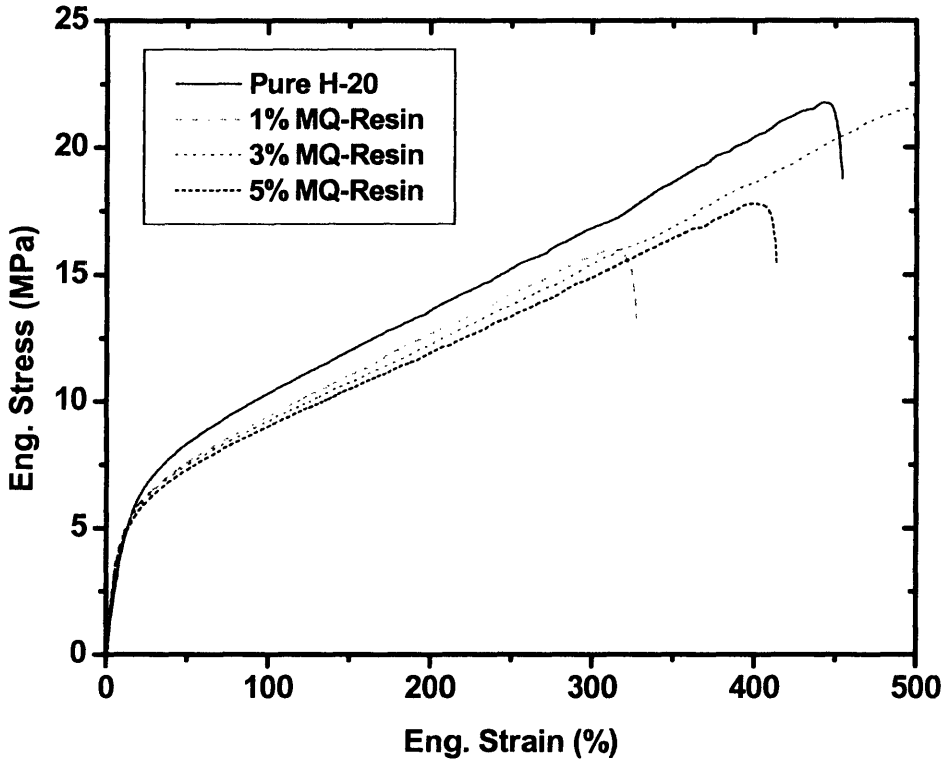


**Figure 6.2 Comparison of the stress-strain behavior of H-20 various with various loadings of MQ-resin**

**Table 6.2 Tensile properties of H-20 with various loadings of MQ-resin**

| Sample | Modulus (MPa) | Tensile Strength (MPa) | Extensibility (%) | Toughness (MPa) |
|---|---|---|---|---|
| Pure H-20 film | 50 ± 2 | 21 ± 2 | 456 ± 26 | 64 ± 8 |
| + MQ-Resin (1%) | 84 ± 8 | 15 ± 1 | 304 ± 19 | 33 ± 4 |
| + MQ-Resin (3%) | 78 ± 2 | 20 ± 4 | 460 ± 107 | 62 ± 21 |
| + MQ-Resin (5%) | 81 ± 1 | 19 ± 3 | 422 ± 78 | 54 ± 16 |

Transparent thin films of HT-20 with 3 wt % loadings MQ-resin and isooctyl-POSS were obtained by solution casting from a 1:1 DMAc/THF mixture. A switch was made from the HDI-polyurethane (H-20) to the HDI-TDI polyurethane (HT-20) for the creation of POSS composites because of better solubility of the polyurethane in the DMAc/THF mixture, as well as improved properties of the native polyurethane. A representative stress-strain curve for each sample is plotted in Figure 6.3, and the average tensile properties from all tested samples are summarized in Table 6.3. The mechanical properties of the various HT-20 composites are all within uncertainty of the pure HT-20 polyurethane processed in the same manner. At high strains, the HT-20/isoctyl-POSS composite exhibited a slight sawtooth pattern in all tested samples; this is most likely due to slippage at the grip, as the POSS resin tends to diffuse toward the free surface and act as a lubricant.

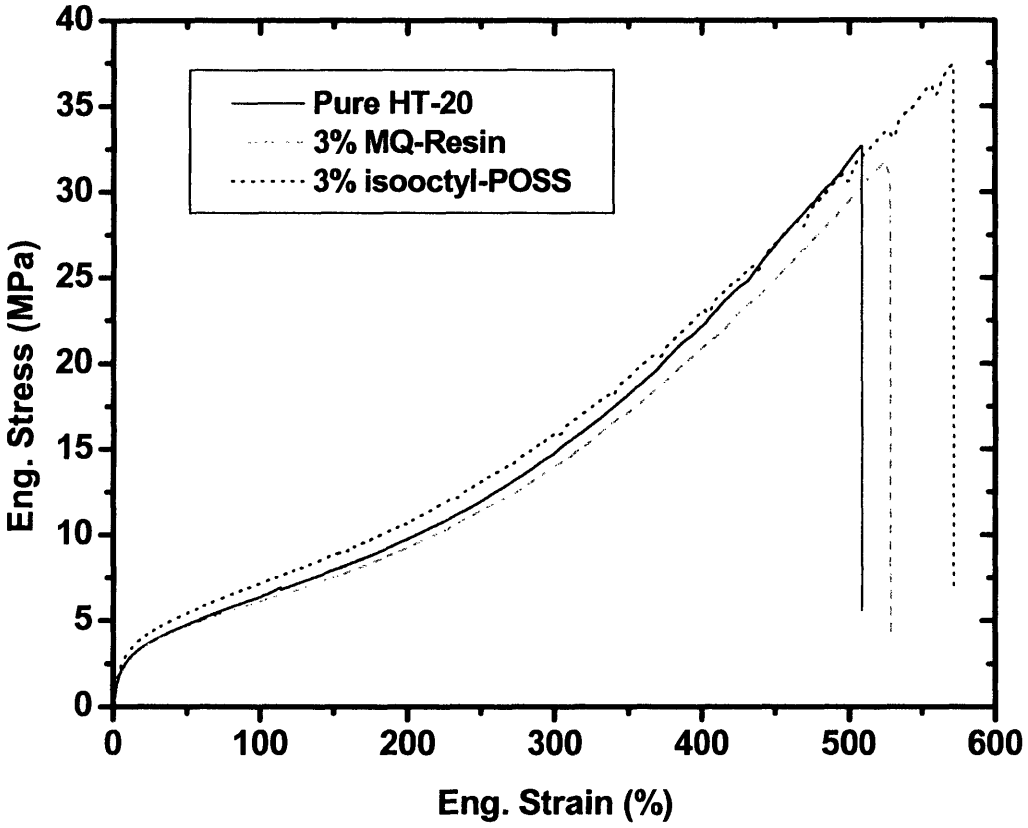


**Figure 6.3 Comparison of the stress-strain behavior of HT-20 with 3% loadings of MQ-resin and isooctyl-POSS**

**Table 6.3 Tensile properties of HT-20 with 3% loadings of MQ-resin and isooctyl-POSS**

| Sample | Modulus (MPa) | Tensile Strength (MPa) | Extensibility (%) | Toughness (MPa) |
|---|---|---|---|---|
| HT-20 (from DMAc) | 46 ± 6 | 35 ± 5 | 498 ± 73 | 55 ± 6 |
| HT-20 (from DMAc/THF) | 44 ± 5 | 33 ± 4 | 509 ± 26 | 51 ± 1 |
| + 3% MQ-Resin (from DMAc/THF) | 41 ± 5 | 36 ± 5 | 559 ± 30 | 50 ± 5 |
| + 3% i-octyl-POSS (from DMAc/THF) | 48 ± 1 | 36 ± 5 | 565 ± 71 | 53 ± 1 |

Transparent thin films of HT-20 with various loadings of isobutyl-POSS were also obtained by solution casting from a 1:4 DMAc/THF mixture. The higher concentration of THF was necessary to preserve the solubility of the isobutyl-POSS, which has a stronger tendency to crystallize. A representative stress-strain curve for each sample is plotted in Figure 6.4, and the average tensile properties from all tested samples are summarized in Table 6.4. The initial shape of stress strain curve for all the prepared composites remained the same, including moduli that were within uncertainty of each other. However, the composite samples all broke at an elongation around 430%, resulting in a 25% reduction in toughness when compared to the pure polyurethane, which extended to around 510%. The presence of the isobutyl-POSS does not seem to show a reinforcing effect; instead, the presence of undispersed, crystalline POSS may contribute to the premature failure of the polyurethane elastomer.

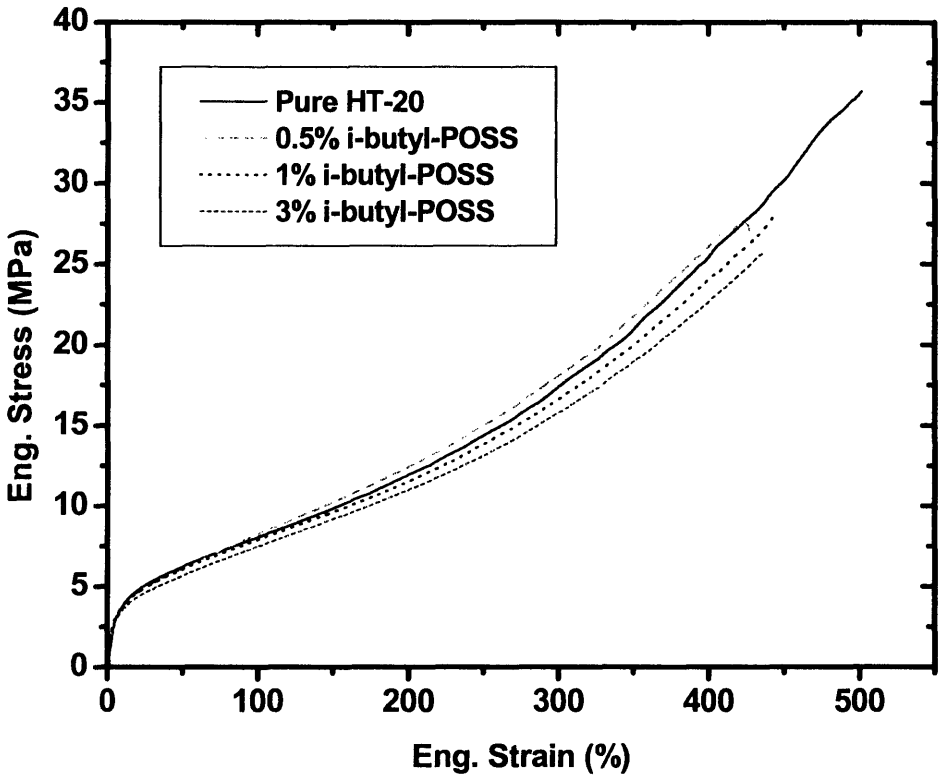


**Figure 6.4 Comparison of the stress-strain behavior of HT-20 with various loadings of isobutyl-POSS, cast from THF/DMAc (80%/20%)**

**Table 6.4 Tensile properties of HT-20 with various loadings of isobutyl-POSS, cast from THF/DMAc (80%/20%)**

| Sample | Modulus (MPa) | Tensile Strength (MPa) | Extensibility (%) | Toughness (MPa) |
|---|---|---|---|---|
| HT-20 | 67 ± 2 | 36 ± 7 | 514 ± 39 | 86 ± 17 |
| 0.5% i-butyl-POSS | 68 ± 4 | 29 ± 4 | 422 ± 78 | 65 ± 10 |
| 1% i-butyl-POSS | 65 ± 10 | 31 ± 4 | 476 ± 26 | 66 ± 4 |
| 3% i-butyl-POSS | 65 ± 9 | 27 ± 1 | 433 ± 4 | 60 ± 3 |

### *6.3.2 Siloxane Phase Association*

The design of the siloxane/polyurethane composites called for association of the resin with the soft segment of the polyurethane to provide mechanical reinforcement. While the reinforcing effect of these resins is minimal, if existing at all, an understanding of the polyurethane phase association of the various resins is still desired. Differential scanning calorimetry (DSC) is a good technique for observing the association of the resins, since the hard and soft phases each exhibit unique transitions in DSC, and the modification of a phase transition partially indicates resin association with that phase. The first heating and cooling of H-29 loaded with 1 wt% and 3 wt% MQ-resin is presented in Figure 6.5. In the cooling curve, the recrystallization of HDI-BDO hard segments at 130 °C is partially suppressed by the presence of the MQ-resin. In contrast, the recrystallization of PTMO at -20 °C is unaltered by the MQ-resin. This suggests that the MQ-resin is more closely associated with the hard segments at equilibrium, and thus only reinforces the hard domain. However, the resin association with the hard domains is not as dramatic as that for the Laponite particles reported in Chapter 5. This is likely due to both the higher loading (10 wt%) of Laponite, as well as the stronger hydrophilic character of the Laponite surface.

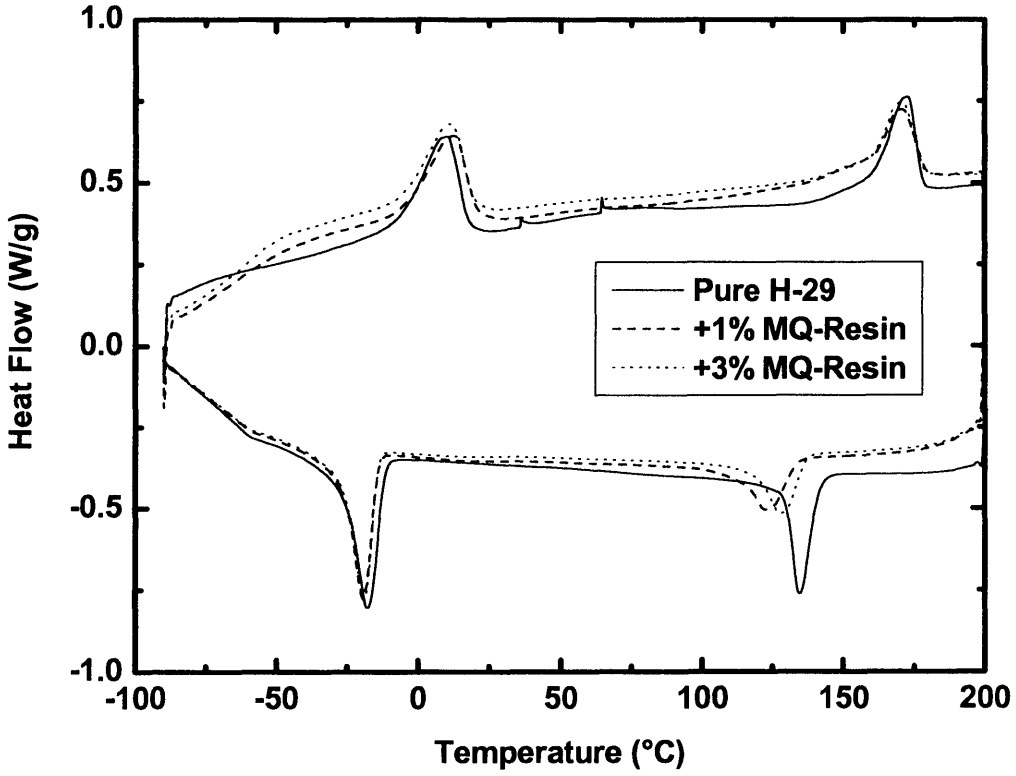


**Figure 6.5 DSC traces of H-29 segmented polyurethane with various loadings of MQ-resin, indicating depression of hard segment crystallization**

Samples of HT-20 loaded with 3 wt% MQ resin and isooctyl-POSS were also analyzed by DSC. However, the heating and cooling curves (not pictured) for the composites were identical to the pure polyurethane, indicating no preferential association with either phase. In Chapter 3, it was demonstrated that HT-20 is even more phase segregated than H-20; however, the presence of TDI units may lower the hydrophilic character of the HDI hard segments, such that a weaker phase preference exists for the MQ-resin. The weak phase association also corresponds with the mechanical property effect, which is minimal between HT-20 and the resins.

The samples of HT-20 loaded with isobutyl-POSS all failed at lower strains than the pure HT-20 polyurethane, which was blamed in part on the formation of POSS crystals within the matrix that contributed to early failure. To observe the formation of isobutyl-POSS crystals within the PTMO soft segment, a separate series of isobutyl-POSS mixtures was prepared with pure PTMO-2900. Isobutyl-POSS was added to solutions of PTMO-2900 in THF at concentrations of 1 wt%, 5 wt%, and 10 wt% relative to PTMO. Oligomeric films were cast from each of the solutions and analyzed via DSC. All samples showed a melting point for the isobutyl-POSS around 58 °C, as indicated in Table 6.5. The ratio of melting enthalpies can be used to estimate the percent crystallinity of isobutyl-POSS within the PTMO by assuming the pure isobutyl-POSS is completely crystalline, using the following relation:

$$\chi_c \approx \frac{\Delta H_m(mixture)}{\Delta H_m(POSS) * c} \tag{6.1}$$

where $\chi_c$ represents the percent crystallinity and c is the measured concentration of POSS in PTMO. As the POSS loading decreases, the solubility in POSS increases; however, even at a relatively low loading of 1 wt% there is still a considerable fraction of POSS left as small crystallites within the PTMO matrix. This large fraction of untethered POSS crystals may contribute to the early failure of crystalline POSS composites.

**Table 6.5 Melting temperature and enthalpy of isobutyl-POSS dispersed in PTMO-2900 at various loadings.**
**(The percent crystallinity is estimated from the melting enthalpies.)**

| Isobutyl-POSS Loading in PTMO-900 | Melting Point (°C) | Melting Enthalpy (J/g) | % Crystallinity of POSS |
|---|---|---|---|
| 1 wt% | 57.6 | 0.11 | 63% |
| 5 wt% | 57.8 | 0.75 | 86% |
| 10 wt% | 57.9 | 1.61 | 92% |
| Pure isobutyl-POSS | 58.1 | 17.41 | 100% (assumed) |

## 6.4 Conclusions

A series of polyurethane/siloxane resin composites were created by solution processing in DMAc and DMAc/THF mixtures. Composites of an HDI-polyurethane with MQ-resin indicated association of the resin with the hard segments, producing a 60% increase in modulus with a small loss of toughness. Composites of HDI-TDI polyurethanes exhibited no strong phase association with either the MQ-resin or isooctyl-POSS via DSC, and no substantial change in properties. However, composites of HDI-TDI polyurethanes with isobutyl-POSS exhibited formation of POSS crystals at all loadings, which resulted in tensile failure at strains 80-100% lower than the pure polyurethane. The non-covalent dispersion of POSS and MQ-resin into segmented polyurethanes attempted here does not appear to be a viable technique for substantial property improvement, perhaps due to ineffective dispersion of cages on the molecular scale and weak interactions with the polyurethane matrix. The covalent attachment of POSS cages within the soft segment, may provide both a more effective dispersion as well as stronger bonding with the polyurethane during deformation.[13]

## 6.5 References


1. James-Korley, L.T., et al., Advanced Materials, 2005. **To Be Submitted.**
2. Li, G., et al., *Polyhedral Oligomer Silsesquioxane (POSS) Polymers and Copolymers: A Review.* Journal of Inorganic and Organometallic Polymers, 2001. **11**(3): p. 123-154.
3. Scott, D.W., *Thermal Arrangement of Branched-Chain Methylpolysiloxanes.* Journal of the American Chemical Society, 1946. **68**: p. 356.
4. Lichtentan, J.D., et al., *Method of functionalizing polycyclic silicones and the resulting compounds*. 1999: U.S. Patent 5942638.

5. Fu, B.X., et al., *Structural development during deformation of polyurethane containing polyhedral oligomeric silsesquioxane (POSS) molecules.* Polymer, 2001. **42**: p. 599-611.
6. Fu, B.X., et al., *Nanoscale reinforcement of polyhedral oligomeric silsesquioxane (POSS) in polyurethane elastomer.* Polymer International, 2000. **49**: p. 437-440.
7. Fu, B.X., et al., *Physical gelation in ethylene-propylene copolymer melts induced by polyhedral oligomeric silsesquioxane (POSS) molecules.* Polymer, 2003. **44**: p. 1499-1506.
8. Romo-Uribe, A., et al., *Viscoelastic and Morphological Behavior of Hybid Styryl-Based Polyhderal Oligomeric Silsesquioxane (POSS) Copolymers.* Journal of Polymer Science: Part B: Polymer Physics, 1998. **36**: p. 1857-1872.
9. Mather, P.T., et al., *Mechanical Relaxation and Microstructure of Poly(norbornyl-POSS) Copolymers.* Macromolecules, 1999. **32**: p. 1194-1203.
10. Pan, G., J.E. Mark, and D.W. Schaefer, *Synthesis and Characterization of Fillers of Controlled Structure Based on Polyhedral Oligomeric Silsesquioxane Cages and Their Use in Reinforcing Siloxane Elastomers.* 2003.
11. Waddon, A.J., et al., *Nanostructured Polyethylene-POSS Copolymers: Control of Crystallization and Aggregation.* Nano Letters, 2002. **2**(10): p. 1149-1155.
12. Zhang, W., et al., *Effect of Methyl Methacrylate/Polyhedral Oligomeric Silsesquioxane Random Copolymers in Compatabilization of Polystyrene and Poly(methyl methacrylate) Blends.* Macromolecules, 2002. **35**: p. 8029-8038.
13. Kopesky, E.T., et al., *Thermomechanical properties of poly(methyl methacrylate)s containing tethered and untethered polyhedral oligomeric silsesquioxanes.* Macromolecules, 2004. **37**(24): p. 8992-9004.

# Chapter 7: Liquid Crystalline Polyurethane Soft Segments

## 7.1 Introduction

Previous research in our group on segmented polyurethanes with side chain liquid crystalline (LC) soft segments has shown that the LC mesogens align cooperatively with the hard segments during deformation.[1, 2] While in a side-chain LC polymer the mesogens are not load bearing, the incorporation of a main-chain LC mesogen into a segmented polyurethane creates an orientable unit capable of soft segment reinforcement. This LC mesogen should have a degree of orientation intermediate between the polyurethane hard segment and soft segment, just as spider silk contains sequences that are of intermediate order between the alanine-rich crystals and the glycine-rich amorphous matrix.[3] A cartoon of the liquid crystalline polyurethane design is drawn in Figure 7.1.

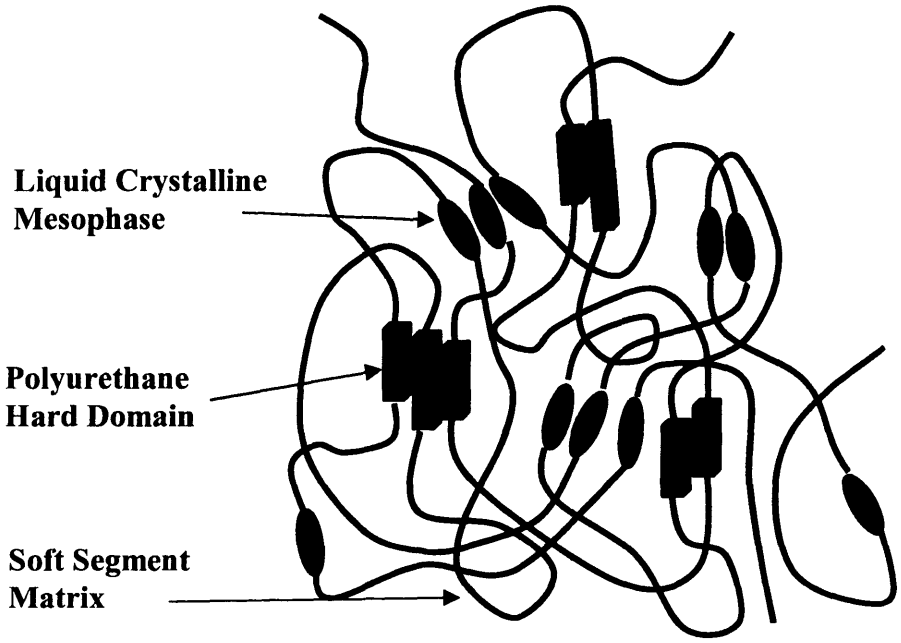


**Figure 7.1 Cartoon representation of main-chain liquid crystalline (LC) mesogens as reinforcing units within the polyurethane soft segment.**

The superior mechanical properties of main-chain LC polymers is well documented.[4, 5] However, these rod-like polymers do not fit the requirements for a flexible polyurethane soft segment; instead, longer spacers are required between the LC mesogens to provide soft segment flexibility. For this initial investigation, intermediate PTMO molecular weights ($M_n$ = 650 and $M_n$ = 1000) will be copolymerized with a simple LC mesogen, 4,4'-biphenyl. The use of this difunctional aromatic mesogen has been well-documented in the literature.[6-10] In order to be successfully incorporated into a polyurethane, the liquid crystalline soft segment must remain oligomeric. The overall molecular weight of the copolymer soft segment is controlled through the addition of excess PTMO; this also creates primary alcohol functionalities at the soft segment endgroups, enabling reaction with the polyurethane hard segment. The biphenyl mesogen can be incorporated into the soft segment through an ester or ether linkage. The advantage of the ether linkage is suppressed hydrogen bonding with the hard segment, to maintain polyurethane microphase segregation, as explained in Section 1.3.2. The advantage of the ester linkage is the ease of synthetic addition to the PTMO soft segment. Both approaches to biphenyl incorporation within PTMO are explored in this chapter.

## 7.2 Experimental

The synthesis of the biphenyl-PTMO soft segments, using both the ether and ester linkages, are described separately here, as well as their incorporation into a segmented polyurethane. Afterward, the techniques used for soft segment and polyurethane characterization are described.

### *7.2.1 Materials*

Poly(tetramethylene oxide) (PTMO, $M_n$ = 650 and $M_n$ = 1000), was purchased from Polysciences, and Terethane® 250 (PTMO, $M_n$ = 250) was purchased from Sigma-Aldrich. All other materials were purchased from Sigma-Aldrich. PTMO samples were dried under vacuum for 3 days at 60 °C. N,N-dimethylacetamide (DMAc), dichloromethane ($CH_2Cl_2$), triethylamine (TEA) and pyridine were dried over calcium hydride ($CaH_2$) and distilled under $N_2$. 4,4'-biphenol was sublimed under vacuum at 200 °C. 1,4-butanediol and 1,6-diisocyanatohexane (HDI) were vacuum distilled. Biphenyl-4,4'-dicarboxylic acid (DBA), methanesulfonyl chloride, benzyltriethylammonium chloride, and stannous octoate were used as received.

### *7.2.2 Biphenyl-PTMO Copolyether Synthesis*

A copolyether of biphenol and PTMO was synthesized using the two-step method outlined in Figure 7.2, which is adapted from the method of Hong *et al.*[6] In the first step, methanesulfonyl chloride was slowly added to an alcohol-terminated PTMO oligomer in $CH_2Cl_2$, at 0 °C under $N_2$, with TEA to neutralize the HCl byproduct. After addition, the solution was allowed to warm to room temperature and react for 12-18 hours. The reaction mixture was then added to ice-cold dilute HCl, and the organic layer was separated and washed with HCl and water, respectively. Finally, the mesylate-terminated PTMO product was recovered by evaporation of the solvent.

In the second step, the PTMO-mesylate was reacted with 4,4'-biphenol in a base-catalyzed condensation reaction to form a polyether of alternating PTMO and biphenyl units. This reaction was conducted in DMAc under $N_2$, with a potassium carbonate ($K_2CO_3$) catalyst, and was held at 120 °C under refluxing DMAc for 24 hours. Finally,

the product was precipitated into a ten-fold excess of methanol, collected via filtration, and dried under vacuum at 60-80 °C for at least one week.

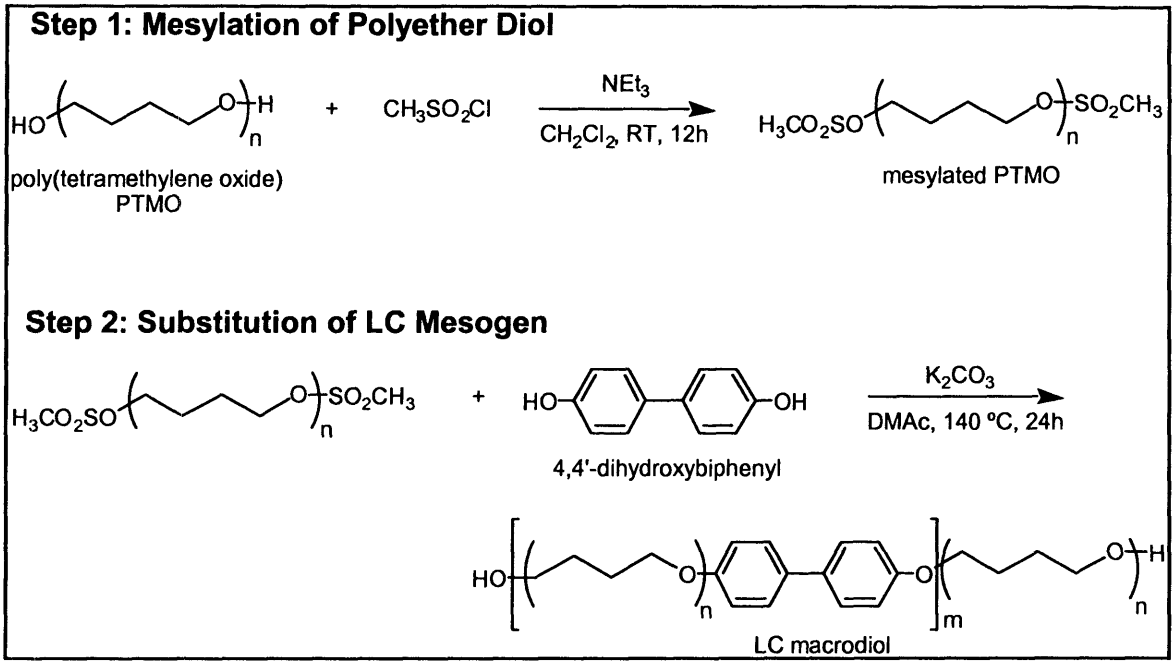


**Figure 7.2 Synthesis of biphenyl-PTMO co-polyether oligomer for use as liquid crystalline polyurethane soft segment.**

### *7.2.3 Biphenyl-PTMO Copolyester Synthesis*

A copolyester of biphenol and PTMO was synthesized using the two-step method outlined in Figure 7.3, which is adapted from the method of Burdett.[11] In the first step, 15g of biphenyl-4,4'-dicarboxylic acid (DBA) and 0.066g of benzyltriethylammonium chloride catalyst was dissolved in 75 mL $CH_2Cl_2$ and refluxed under $N_2$ at 85 °C. 9 mL sulfonyl chloride was then added to the solution and refluxed overnight. While still hot, the solution was pressure filtered through a Size C ceramic filter. Crystals of biphenyl diacid chloride (Melting Pt = 186 – 189 °C) were filtered, washed with ethanol, and dried under vacuum overnight.

In the second step, 330 mg biphenyl diacid chloride was dissolved in toluene at a concentration of 2 wt%, which was limited by solubility. 1.4 mL pyridine was added to the solution, and a stoichiometric equivalent of PTMO was slowly dripped into the solution over 30 minutes. As the reaction proceeded, pyridinium salts fell out of solution; the mixture was stirred under $N_2$ overnight at room temperature. The mixture was then filtered to remove precipitated salts, and rotovapped to pull off most of the toluene. The concentrated oligomer solution was then precipitated into cold diethyl ether, filtered, washed with ether, and dried under vacuum overnight.

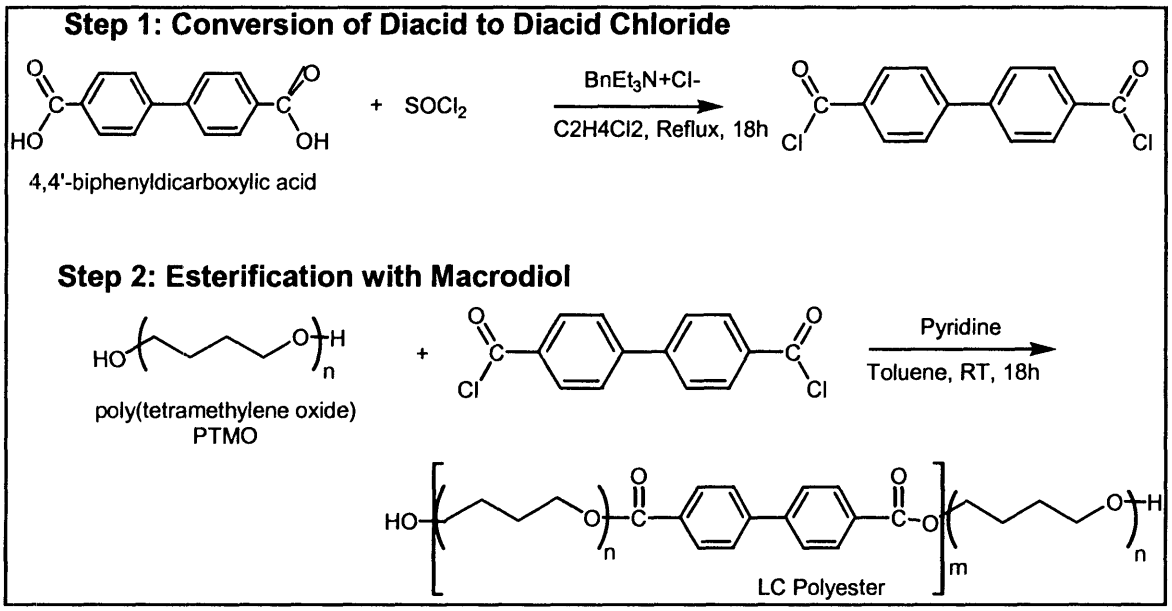


**Figure 7.3 Synthesis of biphenyl-PTMO co-polyester oligomer for use as liquid crystalline polyurethane soft segment.**

### *7.2.4 Segmented Polyurethane Synthesis*

The biphenyl-PTMO copolyether and copolyester were converted to a segmented polyurethane, using the same two-step approach outlined in Figure 7.4. In the first step, the LC soft segment was endcapped with excess HDI, in DMAc under a $N_2$ atmosphere with a stannous octoate catalyst, and the solution was held at 60 °C for 3 hours. In the

second step, the endcapped macromonomer was polymerized to high molecular weight through the stoichiometric addition of 1,4-butanediol at 60 °C for 12-18 hours. Progress of the reaction was monitored via FTIR by observing the free isocyanate peak at 2250 $cm^{-1}$, and adding extra charges of 1,4-butanediol until the isocyanate peak disappeared. Finally, the polyurethane was precipitated into a ten-fold excess of methanol, collected via filtration, and dried under vacuum at room temperature for >24 hours.

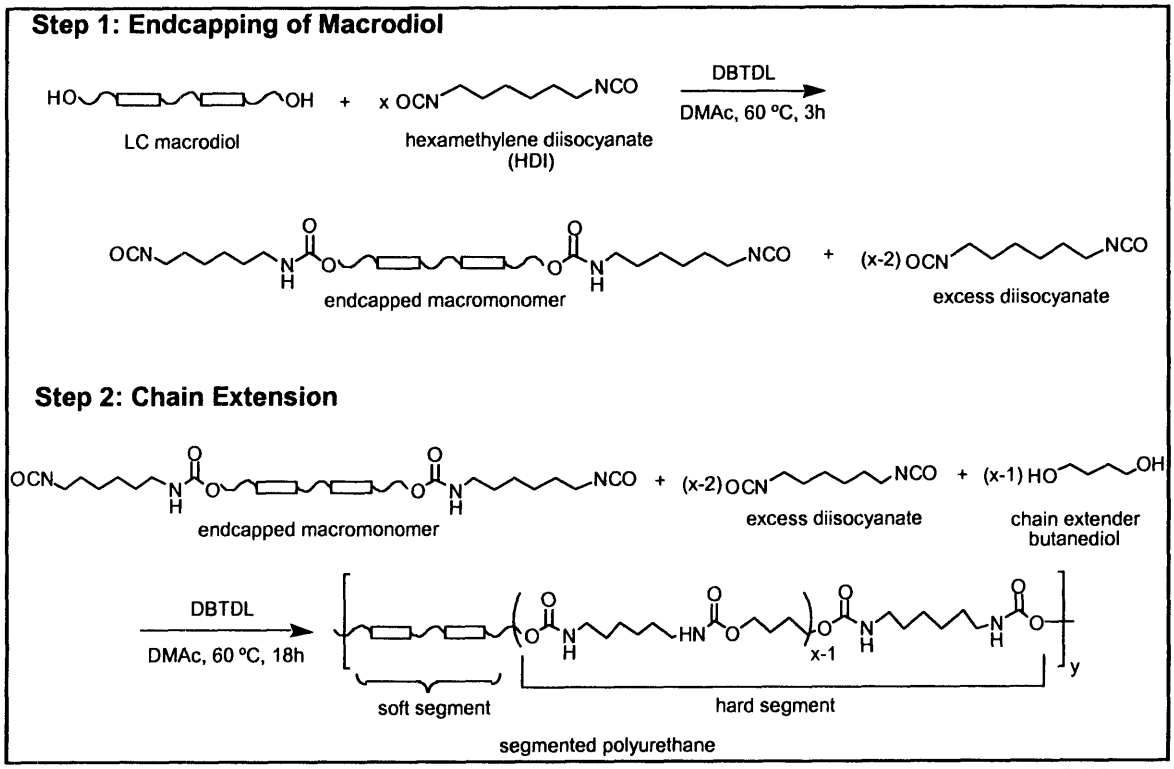


**Figure 7.4 Synthesis of segmented polyurethane with biphenyl-PTMO copolymer soft segment.**

### *7.2.5 Instrumentation*

#### 7.2.5.1 Gel Permeation Chromatography

Molecular weights and molecular weight distributions of copolyethers were determined relative to polystyrene standards by a Waters Gel Permeation Chromatograph

(GPC) equipped with a UV-absorption detector, a refractive index detector, two PL Gel 5μm MIXED-C columns from Polymer Laboratories, and a THF eluent. Molecular weights and molecular weight distributions of copolyesters and segmented polyurethanes were determined relative to poly(ethylene oxide) standards by a Waters Gel Permeation Chromatograph (GPC) equipped with a refractive index detector, two PL Gel 5μm MIXED-C columns from Polymer Laboratories, and a DMAc eluent.

#### 7.2.5.2 Differential Scanning Calorimetry

Thermal phase behavior of copolyethers was examined with a Perkin-Elmer Differential Scanning Calorimeter (DSC 7 AMB), operating at a heating rate of 20°C/min from -30°C to 200°C under nitrogen atmosphere. Thermal phase behavior of copolyesters and polyurethanes was examined with a TA Instruments Q1000 Differential Scanning Calorimeter (DSC), operated at a heating rate of 10°C/min under a 50 mL/min nitrogen purge. As-precipitated polyurethane samples were subjected to two heating and cooling cycles from -90 to 200 °C. Transitions were recorded from the second heating and cooling scans, using a linear extrapolation method for $T_m$ and midpoint inflection method for $T_g$.

#### 7.2.5.3 Small-angle X-Ray Scattering (SAXS)

Small-angle X-ray scattering experiments were performed on a Molecular Metrology SAXS equipped with CuKα radiation and a two-dimensional, gas proportional multi-wire Gabriel detector. Variations in beam intensity were corrected by normalizing with a photodiode placed on the beam stop when subtracting background radiation.

## 7.3 Results and Discussion

The analysis of polyurethanes made from biphenyl-PTMO copolymers using the ether and ester linkages is discussed in separate sections, followed by commentary on the synthesis and properties of liquid crystalline polyurethane soft segments in general.

### *7.3.1 Biphenyl-PTMO Copolyether Soft Segments*

Copolymers of biphenol and PTMO were synthesized using PTMO blocks with $M_n$=250 and $M_n$=650 (referred to as BP-PTMO-250 and BP-PTMO-650), which translates to 3.5 and 9 repeat units of PTMO between each biphenyl unit, respectively. GPC results indicated $M_n$=950 for BP-PTMO-250 and $M_n$=5200 for BP-PTMO-650, relative to polystyrene standards. DSC results (not pictured) indicated a single endotherm at 102 °C for BP-PTMO-250 shows, and two closely spaced endotherms at 45 °C and 65 °C for BP-PTMO-650. The larger spacing between biphenyl units lowered the clearing point and generally increased the overall copolymer mobility. The BP-PTMO-650 copolymer also exhibited nematic LC behavior between 60 and 75 °C in hot-stage optical microscopy.

Both copolymers were used as soft segments in polyurethanes with HDI-BDO hard segments. Although BP-PTMO-650 demonstrated more promising properties as a soft segment, the polyurethane from BP-PTMO-650 did not polymerize to high molecular weight, due to problems purifying the BP-PTMO product and regulating the stoichiometry during polyurethane synthesis. However, the polyurethane made with BP-PTMO-250 soft segments exhibited strong phase segregation, as demonstrated in Figure 7.5. This figure compares the DSC traces from three different materials: a polyurethane with a pure PTMO-2900 soft segment (PU-PTMO), a biphenyl-PTMO-250 copolyether

(BP-PTMO), and a HDI-polyurethane containing the copolymer as its soft segment (PU-BP-PTMO). The endotherm at 155 °C in the PU-PTMO and PU-BP-PTMO traces associated with the breakup of the polyurethane hard domains does not shift appreciably when the biphenyl units are incorporated into the soft segment, indicating strong phase segregation between the hard domains and the biphenyl-containing soft segment. The endotherm at 102 °C in the PU-BP-PTMO and BP-PTMO traces is associated with the breakup of the biphenyl units in the soft segment. This endotherm also does not shift appreciably when the macrodiol (BP-PTMO) is converted to a polyurethane (PU-BP-PTMO), which further indicates strong phase segregation between the hard domains and the biphenyl units.

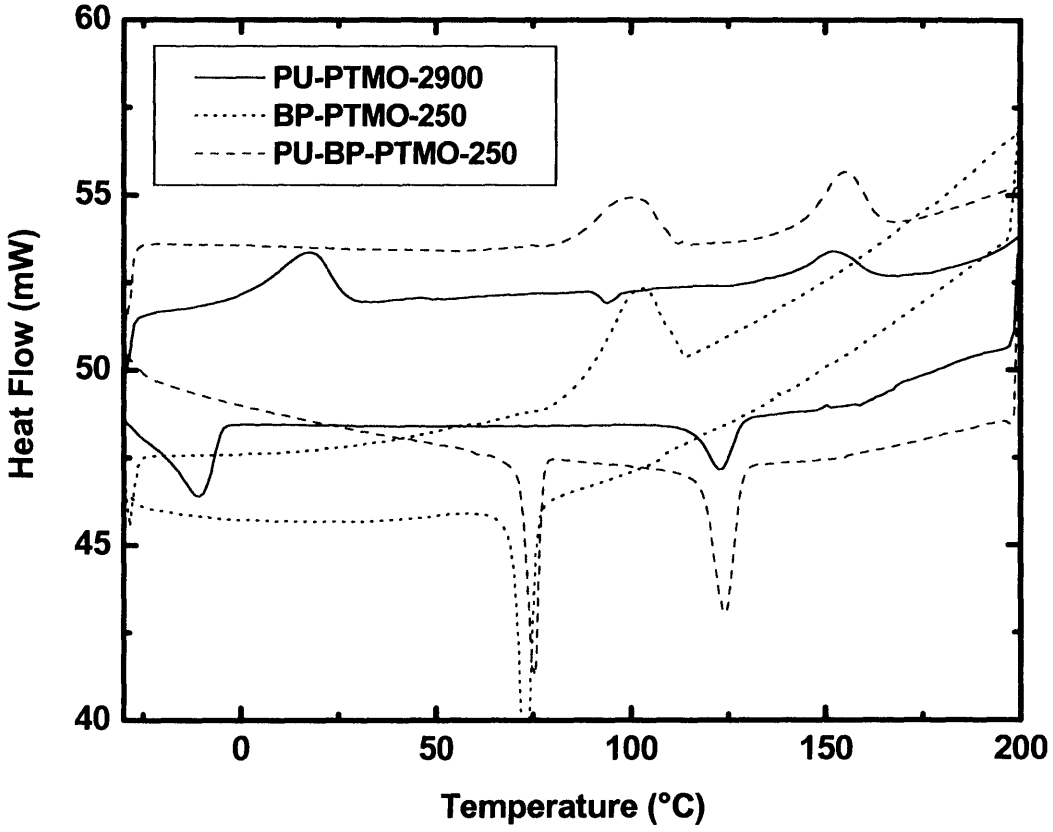


**Figure 7.5 DSC Comparison of a biphenyl-PTMO-250 polyether soft segment to a HDI-polyurethane made with the BP-PTMO soft segment (PU-BP-PTMO) and a HDI-polyurethane made with a pure PTMO-2900 soft segment.**

*7.3.2 Biphenyl-PTMO Copolyester Soft Segments*

Copolymers of biphenyldicarboxylic acid and PTMO were synthesized using PTMO blocks with $M_n$=650 and $M_n$=1000 (referred to as BP-PTMO-650 and BP-PTMO-1000), which translates to 9 and 14 repeat units of PTMO between each biphenyl unit, respectively. The buildup of molecular weight is shown through the GPC results in Table 7.1. The buildup indicates the incorporation of one biphenyl until on average into BP-PTMO-650, and three biphenyl units into BP-PTMO-1000. These GPC results also agreed with endgroup analysis by NMR. The molecular weights of segmented

polyurethanes made from both these biphenyl-PTMO polyesters were low, and the polyurethanes consequently did not form elastomeric films for mechanical characterization. However, samples of the pure PTMO, BP-PTMO and polyurethanes were analyzed by DSC for both the PTMO-650 and PTMO-1000 series, and are presented in Figures 7.6 and 7.7, respectively. In both series, the presence of the biphenyl unit depresses the melting point and crystallization point of PTMO. The glass transition of both the PTMO and BP-PTMO is not observable by DSC; however, the glass transitions of PU-BP-PTMO-650 and PU-BP-PTMO-1000 are -60 °C and -65 °C, respectively. This pronounced elevation of $T_{g,ss}$ is due to the incorporation of the biphenyl mesogen, which partially restricts the chain mobility. In chapter 3, the elevation of $T_{g,ss}$ was taken as an indication of phase mixing between the hard and soft segments; however, that analysis is only valid with pure PTMO soft segments, as indicated by a comparison of biphenyl-PTMO polyurethanes with pure PTMO polyurethanes.

**Table 7.1 Molecular weight buildup of biphenyl-PTMO polyesters and polyurethanes, and hard segment composition of polyurethanes. (GPC data taken in DMAc relative to PEO standards)**

| Sample | PU HS% | $M_n$ (Da) | $M_w$ (Da) | $M_w/M_n$ |
|---|---|---|---|---|
| PTMO-650 | | 490 | 610 | 1.24 |
| BP-PTMO-650 | | 1,060 | 2,020 | 1.90 |
| PU-BP-PTMO-650 | 31 | 5,380 | 10,320 | 1.92 |
| BP-PTMO-1000 | | 1,472 | 2,905 | 1.97 |
| PU-BP-PTMO-1000 | 24 | 8,754 | 24,330 | 2.78 |
| PU-PTMO-2900 | 29 | 26,570 | 52,930 | 1.99 |

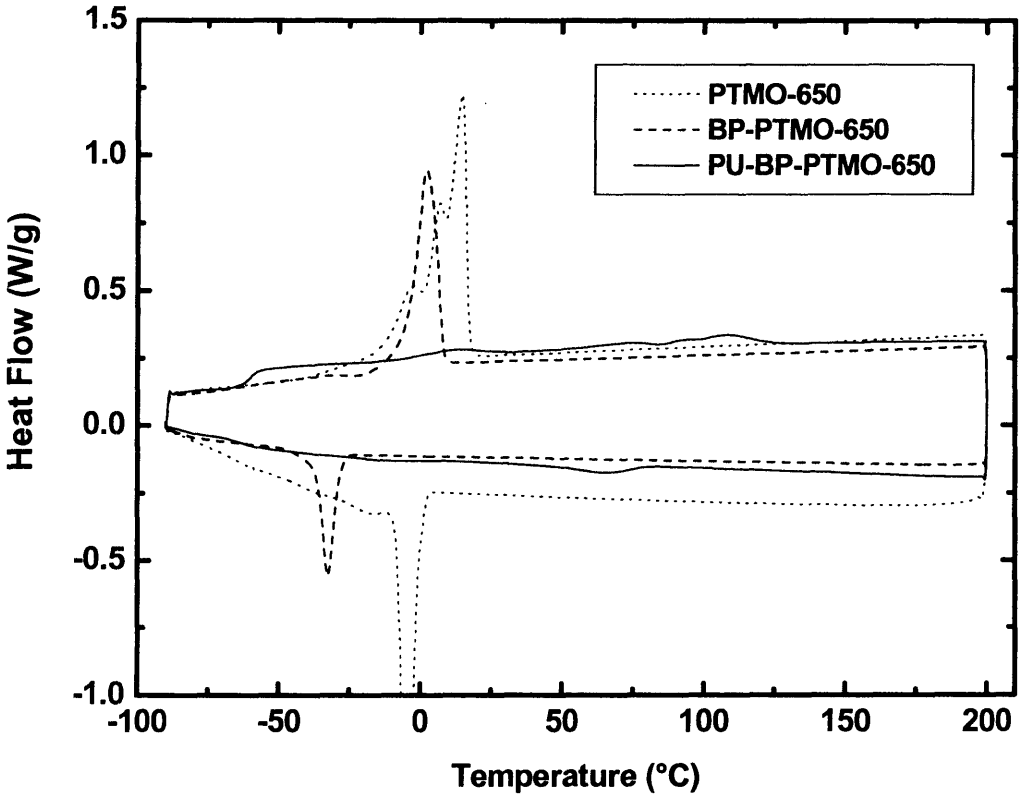


**Figure 7.6 DSC Comparison of (A) PTMO-650 macrodiol, (B) Biphenyl-PTMO-650 polyester soft segment, and (C) HDI-polyurethane made with the BP-PTMO soft segment.**

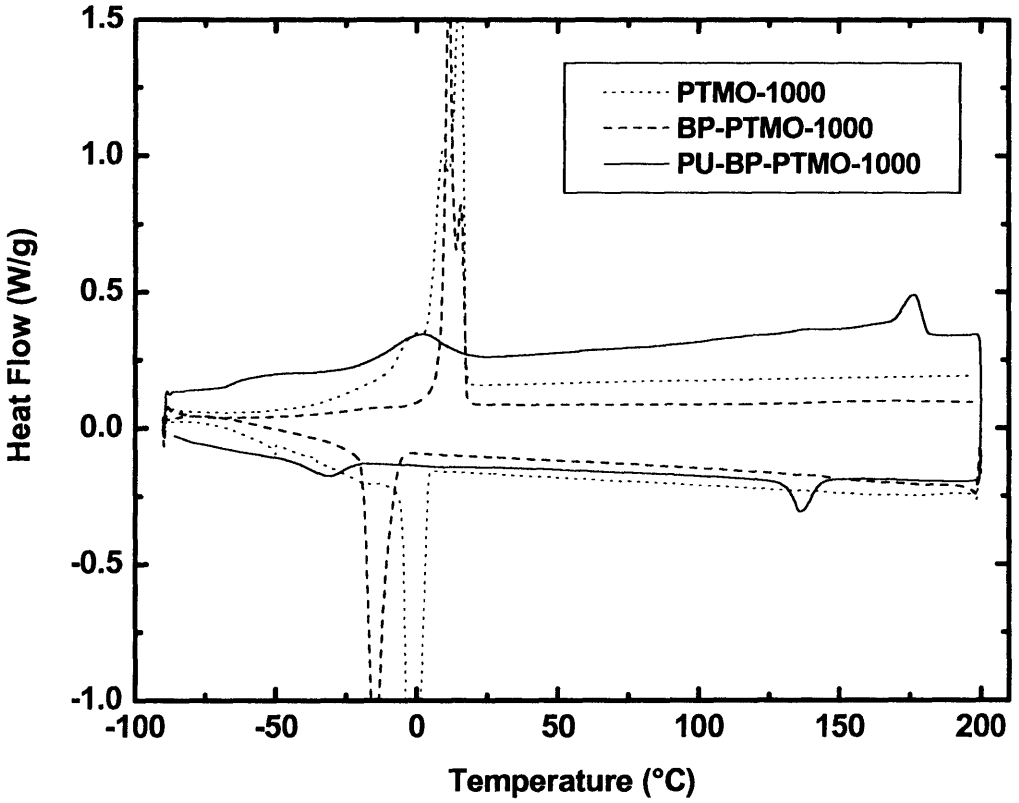


**Figure 7.7 DSC Comparison of (A) PTMO-1000 macrodiol, (B) Biphenyl-PTMO-1000 polyester soft segment, and (C) HDI-polyurethane made with the biphenyl-PTMO soft segment.**

Figures 7.8 and 7.9 compare the DSC and DMA traces from PU-BP-PTMO-1000 with those from an HDI-BDO polyurethane with a pure PTMO hard segment, PU-PTMO-2900 (named H-29 in previous chapters). The primary differences between these two samples are the length of the soft segment and its ability to crystallize. From the DMA results, the $T_g$ of the soft segment is elevated 15 °C by the presence of the biphenyl unit. The melting point and enthalpy of the PTMO soft segment crystallites are reduced by the shorter segments of PTMO that are capable of crystallization. The DSC hard segment transitions of both polyurethanes are similar, indicating a strong microphase

separated structure in both samples. However, the DMA indicates mechanical failure of the BP-PTMO polyurethane 20 °C lower than the PTMO polyurethane, most likely due to the lower overall molecular weight and mechanical integrity of the polyurethane.

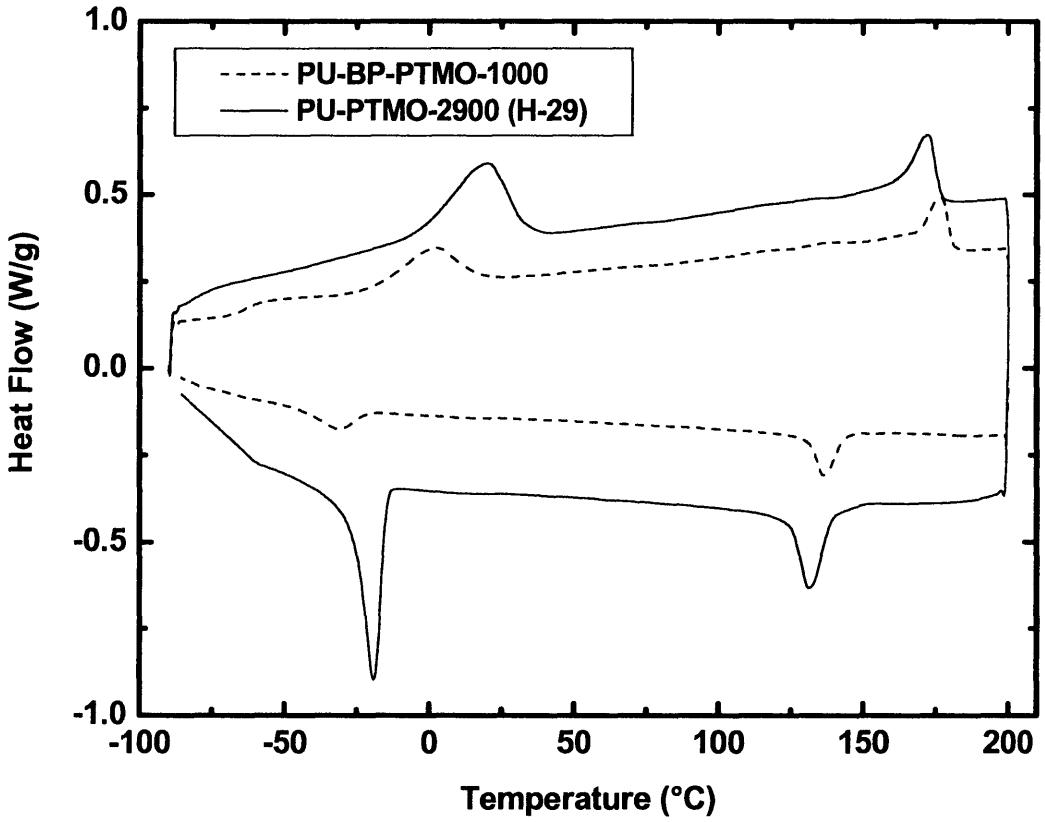


**Figure 7.8 DSC Comparison of (A) Polyurethane made with the biphenyl-PTMO soft segment to (B) polyurethane with pure PTMO-2900 soft segment.**

Due to the synthetic challenges in creating high molecular weight polyurethanes with liquid crystalline soft segments, it remains unclear whether the incorporation of main-chain LC mesogens into the soft segment can provide mechanical reinforcement during deformation. The primary obstacles are proper purification of the BP-PTMO polyester or polyether, and characterization of their molecular weight and end-group

functionality before their subsequent use in polyurethane synthesis. Since polyurethane synthesis is sensitive to water, it is critical that the BP-PTMO be purified and properly dried before reaction with diisocyanates to eliminate side reactions. Polyurethane chemistry is also sensitive to the stoichiometry of the reaction mixture, so it is critical to have a correct characterization of the BP-PTMO molecular weight to ensure proper charges of diisocyanates and chain extender during polyurethane synthesis.

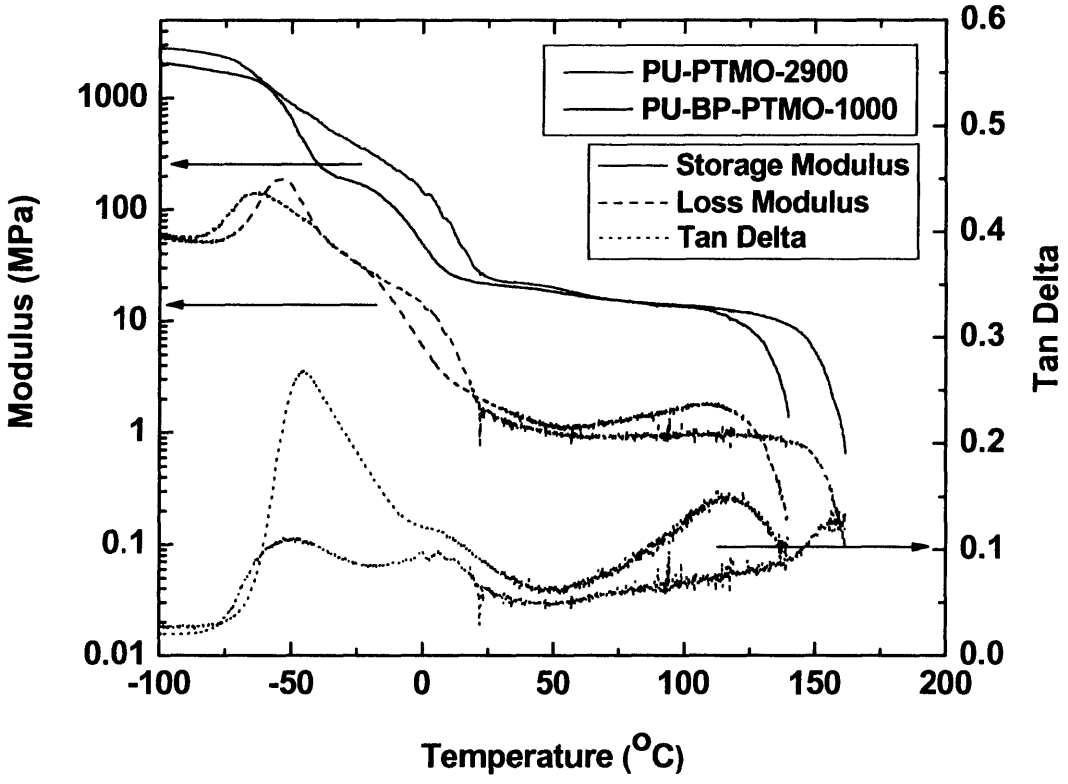


**Figure 7.9 DMA Comparison of (A) Polyurethane made with the biphenyl-PTMO soft segment to (B) polyurethane with pure PTMO-2900 soft segment.**

## 7.4 Conclusions

A series of oligomeric polyesters and polyethers were synthesized from a biphenyl mesogen and PTMO of various molecular weights, and incorporated as the soft

segment of a segmented polyurethane. The copolyesters with biphenyl units spaced between 9 and 14 PTMO repeat units exhibited glass transitions of -60 °C and -65 °C, respectively, which are low enough to maintain flexibility as a soft segment macrodiol. The biphenyl units spaced between four PTMO repeat units exhibited a crystalline transition at 100 °C, and the copolymer is unsuitable as a polyurethane soft segment. Segmented polyurethanes made from the biphenyl-PTMO copolymers and HDI-BDO hard segments were strongly microphase segregated, though limited by low overall molecular weight. Due to synthetic limitations in the development of high molecular weight polyurethanes, the question of whether the soft segment may be reinforced by the incorporation of liquid crystalline mesogens remains unanswered.

## 7.5 References


1. Nair, B.R., V.G. Gregoriou, and P.T. Hammond, *FT-IR Studies of Side Chain Liquid Crystalline Thermoplastic Elastomers.* Polymer, 2000. **41**(8): p. 2961-2970.
2. Nair, B.R., *Synthesis, Characterization, and Infrared Dichroism of Novel Side-Chain Liquid Crystalline Polyurethane Systems*, in *Materials Science and Engineering*. 2000, Massachusetts Institute of Technology: Cambridge.
3. Knight, D.P. and F. Vollrath, *Liquid Crystals and Flow Elongation in a Spider's Silk Production Line.* Proceedings of the Royal Society of London, 1999. **266**: p. 519-523.
4. Northholt, M.G. and D.J. Sikkema, *Lyotropic Main Chain Liquid Crystal Polymers.* Advances in Polymer Science, 1990. **98**: p. 115-177.
5. Collings, P.J., *Liquid Crystals: Nature's Delicate Phase of Matter.* 1990, Princeton: Princeton University Press.

6. Hong, K.-C., J. Kim, and J.-Y. Bae, *Synthesis and characterization of oxyethylene copolymers with phenyl and/or 4,4'-biphenyl structural units in the backbone.* Polymer Bulletin, 2000. **44**: p. 115-122.
7. Asrar, J., et al., *Thermotropic Homopolyesters. I. The Preparation and Properties of Polymers Based on 4,4'-Dihydroxybiphenyl.* Journal of Polymer Science: Part B: Polymer Physics, 1983. **21**: p. 1119-1131.
8. Krigbaum, W.R., J. Watanabe, and T. Ishikawa, *Thermoptropic Polyesters. 2. Investigation of the Mesophase Properties of Polymers Based on 4,4'-dihydroxybiphenyl.* Macromolecules, 1983. **16**: p. 1271-1279.
9. Maeda, Y., K. Osada, and J. Watanabe, *Phase Behavior of Crystal Polymorphs of Thermotropic Poly(hexamethylene 4,4'-biphenyldicarboxylate) under Hydrostatic Pressure.* Macromolecules, 2000. **33**: p. 2456-2461.
10. Kricheldorf, H.R., O. Struve, and G. Schwarz, *Whiskers: 13. Polyesters based on 4,4'-biphenyldiol and biphenyl-4,4'-dicarboxylic acid.* Polymer, 1996. **37**(19): p. 4311-4320.
11. Burdett, K.A., *An Improved Acid Chloride Preparation via Phase Transfer Catalysis.* Synthesis, 1991. **1991**(6): p. 441-442.

# Chapter 8: Conclusions and Future Directions

## 8.1 Summary

This thesis explores the design, synthesis, and characterization of segmented polyurethane elastomers and composites with hierarchical microstructures similar to the multiple levels of order found in spider silk. Three such systems were investigated: polyurethanes with mixed isocyanates in the hard segment, polyurethane nanocomposites with clay and siloxane particles, and polyurethanes with liquid crystalline soft segments.

A series of segmented polyurethanes containing two different diisocyanates in the hard segment was synthesized, with the bulkier diisocyanates preferentially located at the interphase between the hard and soft domains. The mixed diisocyanates disrupted the crystallinity of the HDI-BDO hard segments while retaining a strong degree of phase segregation between the hard and soft microphases. The disruption of crystallinity within the mixed hard segments allowed the hard domains formed during film casting to become more interconnected, as observed through AFM imaging. In turn, this interconnected hard domain structure provided improved elongation and tensile strength, thereby increasing the toughness without a reduction of the initial modulus. The method of diisocyanate incorporation was also examined, and the hard domain crystallinity is further reduced by the addition of both diisocyanates simultaneously, instead of in a separate prepolymer step. The polyurethane with diisocyanates added in one step also exhibited improved mechanical properties, as expected from the reduction of hard segment crystallinity.

The deformation of segmented polyurethanes with pure and mixed hard segments was also investigated using *in-situ* SAXS, WAXS, and optical microscopy. A polyurethane film with pure HDI-BDO hard segments and a PTMO-2900 soft segment exhibited an initial interdomain spacing of 17 nm. As the sample was deformed under tension, the hard domains adopted a preferred tilt angle of ±20° from the strain direction, due to shearing of the hard domains. The average interdomain spacing increased to 23 nm during deformation, while the spacing of hard domains aligned in the strain direction decreased to 13 nm, and the spacing of hard domains aligned at the preferred tilt angle remained constant. The HDI-BDO-PTMO polyurethane also exhibited a large amount of strain induced crystallization of PTMO, evidenced by WAXS crystalline peaks aligned along the equator at high strain. Polyurethane films with mixed diisocyanates in the hard segment were also compared to the HDI-BDO polyurethane using polarized optical microscopy. The polyurethanes with mixed diisocyanates initially exhibited less crystallinity, but had more overall orientation of chain segments at higher strains, due to the ability of the less crystalline hard segments to align and reinforce the polyurethane.

Several polyurethane nanocomposite structures were created using nanoparticles that preferentially associate with the hard or soft segments. An HDI-PTMO polyurethane/Laponite nanocomposite exhibited a modest improvement in tensile modulus and strength, without sacrificing the extensibility. The Laponite discs exhibited an exfoliated structure, associating with and reinforcing the hydrophilic polyurethane hard segments. Composites of the HDI-PTMO polyurethane with MQ-resin also indicated association of the resin with the hard segments, producing a 60% increase in modulus with a small loss of toughness. Composites of an HDI-TDI polyurethane

exhibited no strong phase association with either the MQ-resin or isooctyl-POSS, and no substantial change in mechanical properties. However, composites of HDI-TDI polyurethanes with isobutyl-POSS exhibited formation of POSS crystals at all loadings, which resulted in tensile failure at strains 80-100% lower than the pure polyurethane.

A series of oligomeric polyesters and polyethers were synthesized from a biphenyl mesogen and PTMO of various molecular weights, and incorporated as the soft segment of a segmented polyurethane. The copolyesters with biphenyl units spaced between 9 and 14 PTMO repeat units exhibited glass transitions of -60 °C and -65 °C, respectively, which are low enough to maintain flexibility as a soft segment macrodiol. Segmented polyurethanes made from the biphenyl-PTMO copolymers and HDI-BDO hard segments were strongly microphase segregated, though limited by low overall molecular weight due to difficulties in purifying the biphenyl soft segments. The low molecular weight of the polyurethanes precluded sufficient mechanical characterization to establish the effectiveness of the biphenyl units at reinforcing the polyurethane.

## 8.2 Future Directions

### *8.2.1 Polyurethanes with Mixed Hard Segments*

This thesis established the ability of mixed diisocyanates to disrupt the crystallinity of a polyurethane hard segment. The literature on such systems is relatively limited[1], and this work represents the first research to note the improvement of hard domain connectivity and ordering as a result of the reduction of crystallinity in mixed hard segments. More work is needed to develop this hypothesis, including systematic variation of film casting and annealing conditions to monitor the growth of the

microphase separated structure. The kinetics of HDI hard domain formation has already been studied with time-resolved synchrotron X-ray scattering[2]; however, the expansion of these kinetic studies to the mixed hard segment polyurethanes would capture the competing roles of $\chi N$ interactions and crystallization on hard domain formation.

The deformation of polyurethanes with mixed hard segments was only partially characterized in this thesis. Specifically, synchrotron SAXS and WAXS were only collected during the deformation of pure HDI-BDO polyurethanes, due to limitations on beam-time. The SAXS and WAXS behavior of mixed hard segment polyurethanes under deformation will further examine the enhanced hard segment alignment and suppression of strain-induced crystallization observed via optical microscopy. While the library of mixed hard segment systems could also be broadened through the incorporation of several more diisocyanates, the improvement in mechanical properties was observed to be modest at best. Therefore, the mixed hard segment systems probably do not warrant sufficient investigation beyond the fundamental mechanisms of microphase separation and deformation noted above.

### *8.2.2 Polyurethane Nanocomposites*

The investigation into polyurethane nanocomposites confirmed a correlation between property improvement and the phase association of the dispersed nanoparticle. For both the Laponite and siloxane particles, modest property improvements were reported for particles that associated with the HDI-polyurethane hard segments in Chapters 5 and 6. In addition, siloxane particles associated with the soft segments led to the deterioration of mechanical properties, due to the constraints on the flexible soft segment matrix. These conclusions appear to be in conflict with the original design of

nanoparticles that associate with the soft segment, in order to mimic the hierarchical structure of spider silk. However, the limitation of these nanocomposite systems is most likely related to incomplete dispersion of the particles, which was unable to be characterized. Large clumps of nanoparticles would tie together many soft segment chains, destroying the elastomeric nature of the polyurethane nanocomposite.

For future work in this area, we propose to covalently link individual POSS cages to a polyurethane soft segment, as shown in Figure 8.1. While POSS cages have been covalently attached within a polyurethane hard segment, it has not been attempted within a soft segment.[3] The covalent attachment and subsequent purification of a PTMO-POSS soft segment would ensure molecular-level dispersion of the POSS cages, which should provide non-covalent secondary interactions between POSS cages, without overly constraining the flexibility of the PTMO matrix.

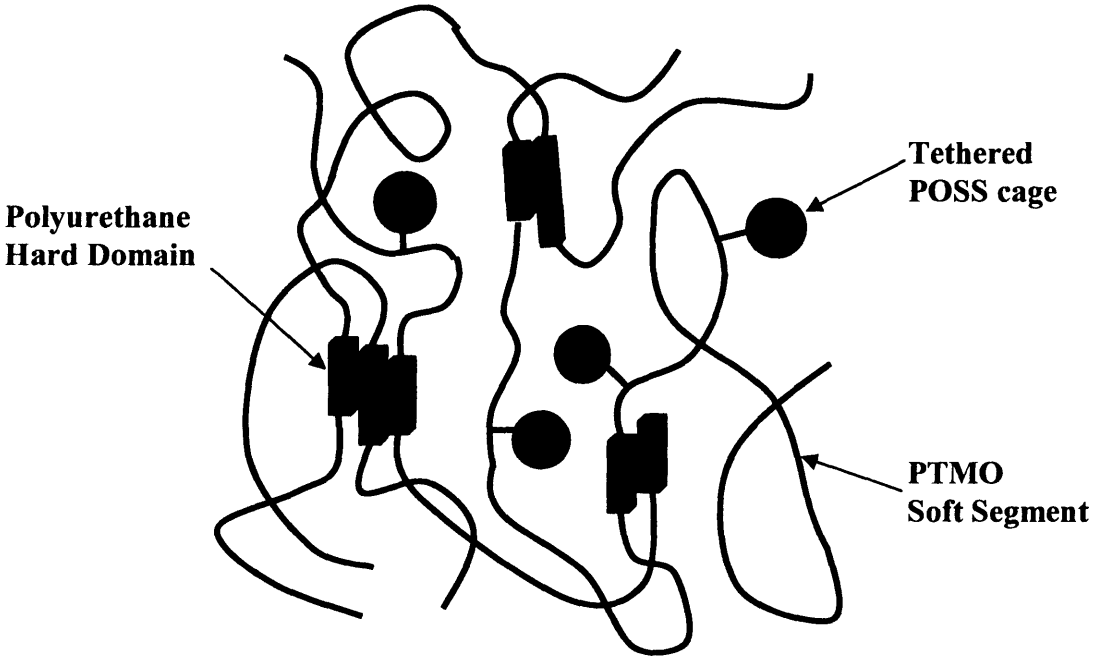


**Figure 8.1 Cartoon representation of covalently linked-POSS cages within a polyurethane soft segment**

Finally, the incorporation of Laponite particles into an HDI-PTMO polyurethane produced modest improvements in mechanical properties, but not as dramatic as those for Elasthane.[4] However, the loading of Laponite was not optimized for the HDI-PTMO polyurethane, so a systematic study at various loading levels could produce a more substantial property improvement. In addition, the strong phase segregation observed in polyurethanes with mixed hard segments suggests that Laponite may be a suitable nanoparticle for reinforcing those systems as well.

## 8.3 References


1. Prisacariu, C., et al., *The effect of hard segment ordering in copolyurethane elastomers obtained by using simultaneously two types of diisocyanates.* Polymer, 2003. **44**: p. 5407-5421.
2. Li, Y., et al., *Effect of Hard Segment Flexibility on Phase Separation of Segmented Polyurethanes.* Macromolecules, 1994. **27**: p. 612-614.
3. Fu, B.X., et al., *Structural development during deformation of polyurethane containing polyhedral oligomeric silsesquioxane (POSS) molecules.* Polymer, 2001. **42**: p. 599-611.
4. Kumar, N., S. Liff, and G.H. McKinley, *New Method to Make High Performance Polymer Nanocomposites.* Nature Materials, 2005. **Submitted**.